Structure and fault rock sequences of the Moonlight Fault Zone, West Otago: constraints on fault reactivation during basin inversion

Simon Alder

a thesis submitted for the degree of

Masters of Science

at the University of Otago, Dunedin,

New Zealand

January 26, 2016

Abstract

Large normal faults are often reactivated as high-angle reverse faults during compressional basin inversion. Although a common situation worldwide, basin inversion is poorly understood from a mechanical perspective, as high-angle reverse faults are severely misoriented for reactivation (frictional 'lock-up' should occur at dips of c. 60°). Prevailing models of failure on high-angle reverse faults rely on fluid overpressure, however such models are calculated on the assumption of Byerlee-type friction (friction coefficient of 0.6 – 0.85).

The Moonlight Fault Zone in New Zealand, is a >200 km long Oligocene basin-bounding normal fault that reactivated in the Miocene as a high-angle reverse fault during basin inversion (present dip angle 65°-77°). Excellent exposures of the fault zone exhumed from c. 4-10 km depth are found in creek sections along the entire strike length. This thesis presents field and microstructural observations concerning the structure and fault rock assemblages found in five creek sections within the MFZ, and aims to provide some of the first observational constraints on the structure and possible mechanical properties of reactivated normal faults.

In the MFZ wall rocks are mainly quartz-albite-muscovite-chlorite schists with a strong foliation that is everywhere sub-parallel to the Moonlight Fault (i.e. dip angle 65°-75°), with deformation varying in response to host rock composition. Where the hanging wall consists of well foliated, intact greenschist or quartzofeldspathic gneiss, pseudotachylyte is present lying largely sub-parallel to the foliation. Where the hanging wall consists of fissile greyschist it is host to foliation-parallel fault breccias. The footwall is mainly greyschist where fault movements resulted in the formation of meso to macro scale folds whose fold axial planes lie parallel to the orientation of the Moonlight Fault. Where folding has not accommodated all reverse-slip, Moonlight Fault-parallel breccias are present.

Although the overall structure of the fault zone changes significantly along strike in response to wall rock composition, the fault core always contains

interconnected layers of foliated cataclasite or gouge rich in authigenically-grown chlorite and muscovite which is regionally significant and, critically, interconnected on a regional scale. The fault core is regularly flanked by a zone of breccia which at times shows a strain transition into the <5 metre thick fault core. Microstructural evidence suggests deformation in the fault core was accommodated by a combination of cataclasis, frictional slip along phyllosilicate seams and dissolution-precipitation.

Published frictional strength measurements for chlorite and muscovite (friction coefficient of 0.32-0.38) are used to explore mechanical models of frictional reactivation along high-angle reverse faults. Results show that low-friction fault cores increase the frictional lock-up angle to 71˚, allowing for easier reactivation of faults that initially formed at 60˚. These results indicate that low frictional strength may play an important role in slip on high-angle reverse faults during basin inversion.

Acknowledgements

Many thanks are required for everyone who assisted in the production of this thesis. Firstly I would like to acknowledge and thank Steve Smith for his guidance and supervision. I would also like to thank Brent Pooley for thin section production; Gemma Kerr for XRD assistance; Mark Raven and Peter Self of CSIRO for quantitative XRD analysis; Jordan Crase for fieldwork assistance and discussion of ideas; John and Ginny Foster, Bruce Douglas and the Aspinall family for granting land access and the University of Otago, American Association of Petroleum Geologists and Royal Society of New Zealand for financial assistance.

Contents

1. INTRODUCTION 1

1.1 GEOLOGICAL SETTING AND PREVIOUS WORK 2
1.1.1 Regional Geology 2
1.1.2 Geological History of basement terranes 3
1.1.3 The Aspiring Lithological Association 6
1.1.4 The Moonlight Fault Zone 7
1.2 THE MOONLIGHT FAULT IN FAN CREEK 11
1.2.1 Hanging wall 11
1.2.2 Fault core 12
1.2.3 Footwall 12

2. MATUKITUKI VALLEY 15

2.1 OVERVIEW 15
2.2 HOST ROCKS 16
2.2.1 Hanging wall greenschists 16
2.2.2 Footwall greyschists 18
2.3 FAULT ZONE STRUCTURE AND DEFORMATION 19
2.3.1 Hanging wall pseudotachylyte 19
2.3.2 Small cataclasite bearing faults in the hanging wall 25
2.3.3 Breccias and foliated cataclasites in the footwall and fault core 26
2.4 FAULT ROCK MICROSTRUCTURES 29
2.4.1 Pseudotachylytes 29
2.4.2 Mixed pseudotachylyte – brittle fault vein 37
2.4.3 Deformation along the main trace of the Moonlight Fault 39
2.4.4 Small-scale faults 47

3. STONY CREEK 49

3.1 OVERVIEW 49
3.2 HOST ROCKS 50
3.2.1 Hanging wall 50
3.2.2 Footwall 51
3.3 FAULT ZONE STRUCTURE AND DEFORMATION 54
3.3.1 Fault core 54
3.3.2 Hanging Wall 55
3.3.3 Footwall 56
3.4 FAULT ROCK MICROSTRUCTURES 59
3.4.1 Hanging Wall 59
3.4.2 Footwall 60

4. MOONLIGHT CREEK 63

4.1 OVERVIEW 63
4.2 HOST ROCKS 63
4.2.1 Hanging wall 63
4.2.2 Footwall 64

4.3 FAULT ZONE STRUCTURE AND DEFORMATION 66
4.3.1 Fault core *66*
4.3.2 Hanging wall *67*
4.3.3 Footwall *69*
4.4 FAULT ROCK MICROSTRUCTURES 74
4.4.1 Pseudotachylyte *74*
4.4.2 Foliated cataclasites in the hanging wall *75*
4.4.3 Stylolites within the sedimentary package *76*
4.4.4 Fault core *78*

5. TWELVE MILE CREEK 81

5.1 OVERVIEW 81
5.2 HOST ROCKS 82
5.2.1 Hanging wall *82*
5.2.2 Footwall *83*
5.3 FAULT ZONE STRUCTURE AND DEFORMATION 87
5.3.1 Moonlight Fault ultracataclasite *87*
5.3.2 Foliated fault gouge *88*
5.3.3 Shear zones *88*
5.4 FAULT ROCK MICROSTRUCTURES 90
5.4.1 Moonlight Fault ultracataclasite *90*

6. DISCUSSION 93

6.1 NEOGENE EXHUMATION AND OFFSET 93
6.1.1 Offset along the Moonlight Fault *94*
6.2 KINEMATICS OF THE MOONLIGHT FAULT ZONE 94
6.3 FAULT ZONE DEFORMATION 95
6.3.1 Hanging wall deformation *95*
6.3.2 Footwall deformation *99*
6.3.3 Fault core deformation *100*
6.4 ALONG STRIKE VARIATION IN FAULT ZONE STRUCTURE 102
6.5 FRICTIONAL STRENGTH MEASUREMENTS 103
6.6 MECHANICS OF INVERSION 107
6.7 IMPLICATIONS 111
6.7.1 Failure along the Moonlight Fault Zone *111*
6.7.2 Basin inversion *113*

7. CONCLUSIONS 115

REFERENCES 117

APPENDIX 129

A. FIELD ACCESS 129
B. SCANNING ELECTRON MICROSCOPY 130
C. X-RAY DIFFRACTION 130

List of Tables

TABLE 2.1. QUANTITATIVE XRD ANALYSIS ON THE FOLIATED CATACLASITE 42
TABLE 6.1. EXPERIMENTALLY-MEASURED FRICTION COEFFICIENTS 106

List of Figures

1.1. EXTENSION AND INVERSION OF A SEDIMENTARY BASIN 1
1.2. GEOLOGICAL MAP OF THE OTAGO REGION. 4
1.3. CROSS SECTION OF THE OTAGO SCHIST 5
1.4. CROSS-SECTION OF NEW ZEALAND'S TECTONO-STRATIGRAPHIC TERRANES 7
1.5. THE MOONLIGHT FAULT IN RELATION TO THE MAXIMUM COMPRESSIVE STRESS 9
1.6. TRACE OF THE MOONLIGHT FAULT 10
1.7. CROSS SECTION OF THE MOONLIGHT FAULT ZONE IN FAN CREEK 11

2.1. CROSS SECTION OF THE MOONLIGHT FAULT ZONE IN THE MATUKITUKI VALLEY. 15
2.2. OVERVIEW OF THE MOONLIGHT FAULT ZONE IN THE WEST MATUKITUKI VALLEY 16
2.3. FOLDED GREENSCHISTS IN DOWNS CREEK 17
2.4. INTERNAL FOLIATION OF GREENSCHIST. 18
2.5. CHEVRON FOLDED FOOTWALL GREYSCHIST 20
2.6. MINERAL SEGREGATIONS IN THE GREYSCHIST 20
2.7. ORIENTATION OF PSEUDOTACHYLYTE FAULT VEINS 22
2.8. PSEUDOTACHYLYTE FAULT VEIN 22
2.9. PSEUDOTACHYLYTE FAULT VEINS SHOWING A COMPLEX STEPOVER REGION 23
2.10. PSEUDOTACHYLYTE INJECTION VEINS EMANATING FROM A FAULT VEIN 23
2.11. DEFORMATION ASSOCIATED WITH MIXED PSEUDOTACHYLYTE – BRITTLE FAULT 24
2.12. SMALL SCALE OFFSET ON CATACLASITE BEARING FAULT IN DOWNS CREEK. 25
2.13. ORIENTATION OF SMALL CATACLASITE-BEARING FAULTS. 26
2.14. TRANSITION FROM HANGING WALL GREYSCHIST INTO THE CENTRAL FAULT CORE 28
2.15. ALTERATION OF REMNANT CLAST IN A PSEUDOTACHYLYTE 30
2.16. HOST GREENSCHIST FRAGMENTS WITHIN A PSEUDOTACHYLYTE VEIN 30
2.17. REWORKED ULTRACATACLASITE CLASTS WITHIN A PSEUDOTACHYLYTE. 31
2.18. AMPHIBOLE SPHERULITES IN PSEUDOTACHYLYTE 32
2.19. FLOW BANDING IN A PSEUDOTACHYLYTE VEIN 32
2.20. KAERSUTITE SPHERULITES FORMING AROUND ILMENITE MICROLITES 33
2.21. TITANITE GRAINS AS CLUSTERS WITHIN A CHLORITE MATRIX. 34
2.22. FE-OXIDES FORM SEAMS AROUND QUARTZ AND ALBITE CLASTS. 34
2.23. FINE GRAINED RIM OF PSEUDOTACHYLYTE VEIN. 35
2.24. DIFFUSE MARGIN OF A PSEUDOTACHYLYTE 36
2.25. BRITTLE SHEARING OF STILPNOMELANE 37
2.26. CALCITE AMYGDULES WITHIN A PSEUDOTACHYLYTE VEIN 38
2.27. COLLAPSED CALCITE-FILLED AMYGDULE. 38
2.28. BRECCIATION AND CATACLASIS IN MF CORE 40
2.29. FOLIATED CATACLASITE DERIVED FROM THE FOOTWALL GREYSCHIST. 41
2.30. CLAST RICH LAYER IN THE FOLIATED CATACLASITE. 41
2.31. TERNARY PLOTS OF NEWLY GROWN CHLORITE AND MUSCOVITE 42
2.32. MATRIX-RICH DOMAIN IN THE GREYSCHIST DERIVED FOLIATED CATACLASITE 43
2.33. FE-RICH DISSOLUTION SEAMS. 44
2.34. HANGING WALL-DERIVED FOLIATED CATACLASITE. 44

2.35. OVERGROWTHS OF CHLORITE UPON A QUARTZ CLAST. 45
2.36. SERRATED EDGES ON TWO ALBITE GRAINS INDICATE DISSOLUTION HAS OCCURRED. 46
2.37. DISSOLUTION SEAMS OF MAGNETITE 46
2.38. CATACLASITE AND ULTRACATACLASITE PHOTOMICROGRAPHS 47

3.1. CROSS SECTION OF THE MOONLIGHT FAULT ZONE IN STONY CREEK 49
3.2. SUB-PARALLEL NATURE OF WALL ROCK FOLIATION ADJACENT TO THE MOONLIGHT FAULT. 50
3.3. SEDIMENTARY ROCKS IN THE FOOTWALL OF THE MOONLIGHT FAULT. 51
3.4. BOULDER OF QUARTZ SANDSTONE WITH QUARTZ PEBBLE BEDS. 52
3.5. REPRESENTATIVE PHOTO OF THE FOOTWALL GREYSCHIST WITH KINK BANDING. 53
3.6. DISCRETE SHEAR SURFACES WITHIN THE SEDIMENTARY PACKAGE 54
3.7. STRUCTURAL FEATURES IN THE STONY CREEK HANGING WALL.. 55
3.8. PSEUDOTACHYLYTE FAULT AND INJECTION VEINS IN HANGING WALL GREENSCHIST FLOAT. 56
3.9. SLICKENSIDED BASE OF SEDIMENTARY PACKAGE 57
3.10. 1 M WIDE BRECCIA CROSSCUTTING FOOTWALL GREYSCHIST 58
3.11. PSEUDOTACHYLYTE VEIN MARGIN WRAPPING AROUND AN OPAQUE GRAIN 59
3.12. VERY FINE CHLORITE GRAINS WITHIN THE MATRIX OF THE BLACK VEIN 60
3.13. ULTRACATACLASITE CONTAINING COMMINUTED QUARTZ AND ALBITE CLASTS. 61
3.14. SHEAR OBLIQUE TO THE FOLIATION IN BRECCIA 62

4.1. CROSS SECTION OF THE MOONLIGHT FAULT ZONE IN MOONLIGHT CREEK. 63
4.2 FOLIATION IN THE HANGING WALL QUARTZOFELDSPATHIC GNEISSES AND GREYSCHISTS. 64
4.3. OUTCROP PHOTO OF QUARTZ SANDSTONE WITH PEBBLE BEDS 65
4.4. FOLIATION AND KINK BAND AXIAL PLANES IN THE FOOTWALL GREYSCHIST. 66
4.5. BLACK AND GREEN GOUGE IN THE CORE OF THE MOONLIGHT FAULT. 67
4.6. FOLIATION PARALLEL PSEUDOTACHYLYTE VEIN SHOWING MULTIPLE MELT POOLS. 68
4.7. CATACLASTIC FEATURES IN THE HANGING WALL GREYSCHIST 69
4.8. ZONE OF BLACK SHEARS CROSSCUTTING THE QUARTZOFELDSPATHIC GNEISS FOLIATION. 70
4.9. THIN BLACK LAYER AT THE TOP OF THE SEDIMENTARY PACKAGE 71
4.10. 15 M WIDE DEFORMATION ZONE IN THE GREYSCHIST 72
4.11. INCOHESIVE BRECCIA 750 M FROM THE TRACE OF THE MOONLIGHT FAULT. 73
4.12. SCANNED THIN SECTION DISPLAYING DUAL PSEUDOTACHYLYTE VEINS. 74
4.13. COLOUR VARIATION WITHIN THE PSEUDOTACHYLYTE. 75
4.14. LATHS IN THE PSEUDOTACHYLYTE MATRIX 75
4.15. NEWLY GROWN CHLORITE IN THE STRAIN SHADOW OF A QUARTZ GRAIN 76
4.16. ULTRACATACLASITE IN THE HANGING WALL WITH PHYLLOSILICATE-RICH LAYERS 77
4.17. STYLOLITE UNDULATING THROUGH THE SEDIMENTARY PACKAGE. 77
4.18. DEFORMATION ASSOCIATED WITH STYLOLITE DEVELOPMENT 78
4.19. FAULT CORE GOUGE WITH CLASTS SURROUNDED BY FINE PHYLLOSILICATES. 79

5.1. CROSS SECTION OF THE MOONLIGHT FAULT ZONE IN TWELVE MILE CREEK 81
5.2. BRECCIATED GREYSCHIST AND INTACT GREYSCHIST IN TWELVE MILE CREEK 82
5.3. SEDIMENTARY PACKAGE MATRIX-SUPPORTED CONGLOMERATE 83
5.4. TWO SCHIST CLASTS WITH RIMS OF CALCITE WITHIN THE SEDIMENTARY PACKAGE 84
5.5. FOLIATION IN THE FOOTWALL SEMI-SCHISTS RELATIVE TO THE MOONLIGHT FAULT 85
5.6. PHOTO SHOWING OUTCROP OF THE BULK LAYERING IN THE BRECCIATED SCHIST 86
5.7. SCANNED THIN SECTION OF THE BRECCIATED SCHIST 87
5.8. MOONLIGHT FAULT PLANE SHOWING THE ULTRACATACLASITE 88
5.9. GREY FAULT GOUGE IN THE FOOTWALL OF THE MOONLIGHT FAULT 89
5.10. SHEAR ZONE WITHIN THE BRECCIATED SCHIST 89

5.11. LAYERING WITHIN THE FAULT-DEFINING ULTRACATACLASITE 90
5.12. COMPLEXLY DEFORMED VEINS IN THE ULTRACATACLASITE. 91

6.1. EXPECTED ATTITUDES OF NEWLY FORMED FAULTS. 107
6.2. STRESS COMPONENTS AFFECTING THE STABILITY OF A COHESIONLESS FAULT PLANE 108
6.3. PLOT OF THE DIFFERENTIAL STRESS REQUIRED FOR RESHEAR ON NORMAL FAULTS 110
6.4. PLOT OF THE DIFFERENTIAL STRESS REQUIRED FOR RESHEAR ON NORMAL FAULTS 111

1. Introduction

Extensional sedimentary basins that undergo shortening experience uplift of sediments and reverse reactivation of pre-existing faults in a process termed basin inversion (eg. Cooper et al., 1989; De Graciansky et al., 1989; Buchanan and McClay, 1992; Bonini et al., 2012). Where the tectonic stresses within the earth are resolved into three orientations (principal compressive stresses, $\sigma_1 < \sigma_2 < \sigma_3$) Anderson (1905), the maximum compressive stress (σ_1) within an extensional regime is vertical while in a compressional regime, ie. basin inversion, σ_1 is horizontal. Basin bounding faults formed during extension dip at c. 60˚ so upon reversal to a compressional regime they tend to lie at high angles to the maximum compressive stress and thus are in an unoptimal orientation for reactivation (eg. Collettini and Sibson, 2001; Sibson, 2009).

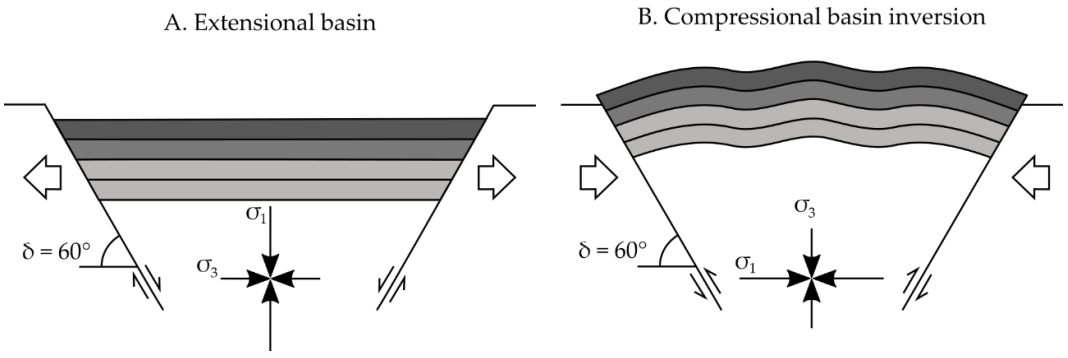

Figure 1.1. Ideal coaxial extension and inversion of a sedimentary basin bounded by first formed faults which dip at 60˚ (After Sibson, 2009).

High angle reverse faults that form during basin inversion have been studied predominately due to their control on hydrocarbon maturation and formation of structural traps (eg. Macgregor, 1995; Turner and Williams, 2004) but also the role of existing high-angle faults as potential seismogenic sources (Sibson, 2009) and sites of ore deposit generation (Sibson et al., 1988). Research on the mechanics of high angle reverse faults during inversion consists of theoretical models on fluid overpressure (eg. Sibson, 1985, 1990a) as well as 'weak' faults modelled in sandbox experiments (eg. Panien et al., 2005; Marques and Nogueira, 2008). However, there

have been very few field-based studies that document the structure and fault-rock assemblages of reactivated normal faults. This represents a gap in our understanding of the mechanics of reactivated normal faults, because fault zone structure and the mechanical properties of fault rocks can influence reactivation (eg. Bonini et al., 2012). This thesis aims to provide the first detailed account of the structure and fault rock sequences of a major, basin-bounding normal fault that was reactivated as a high-angle reverse fault.

The MFZ in west Otago, is a regionally significant structure that was active in the early Oligocene as a basin-bounding normal fault in an extensional tectonic regime, controlling local deposition of up to 4 km of marine and non-marine sediments (Turnbull et al., 1975; Norris et al., 1978; Norris and Carter, 1982). It is then believed to have undergone reactivation and reverse movements during the Miocene in relation to a change in the plate motion vector and the inception of the Alpine Fault plate boundary (Turnbull et al., 1975; Norris et al., 1990b). During this last phase the Moonlight Fault dipped steeply relative to the maximum compressive stress ie. unoptimally oriented during basin inversion. The along strike surface exposures of the Moonlight Fault will be examined by a combination of detailed field mapping, optical microscopy, X-ray diffraction (XRD), Scanning Electron Microscopy (SEM) and quantitative Energy Dispersive Spectroscopy (EDS) to provide insights to how high angle reverse movements have been accommodated during basin inversion.

1.1 Geological Setting and previous work

1.1.1 Regional Geology

The basement rocks of the South Island, New Zealand, can be divided into the Western and Eastern Provinces. The Western Province is made up metamorphosed sediments, intruded by Paleozoic granitoids, separated from accretionary, island arc-related sediments of the Eastern Province by the largely plutonic Median Tectonic Zone or Median Batholith (Bishop et al., 1985; Bradshaw, 1989; Frost and Coombs, 1989). West Otago is underlain by the Haast Schist, a metamorphic belt

made up of the Caples and Torlesse Terranes of the Eastern Province (Figure 1.2). The Haast Schist can be further divided into the Alpine Schist, which lies along the Southern Alps, and the Otago Schist, which is found from north-west Otago to East Otago and will be the focus of this study. Metamorphic facies vary across the Otago Schist, ranging from prehnite - pumpellyite facies along the flanks of the medial antiform to upper greenschist facies in the centre of the medial antiform (Mortimer, 2000). Textural zones (TZ) in the Otago Schist (Bishop, 1972; Norris and Bishop, 1990a), based on white mica width and foliation development, are also mirrored around this medial axis with the lower textural grades (TZI) on the flanks and the higher textural grades (TZIV) located in the centre (Turnbull et al., 2001).

Structures formed during five phases of deformation have been recognised in West Otago by Craw (1985). The first and second deformation phases (D_1; D_2) occurred during mid-Jurassic to mid-Cretaceous greenschist facies metamorphism (Mortimer, 1993a), resulting in isoclinal ductile folding and the formation of macroscopic nappes including the large, isoclinal Waipara Nappe and the large, tight, northwards closing Tyndall Nappe. D_3 was post-metamorphic and characterised by the formation of the open to tight Niger Nappe and east-west over thrusting of macroscopic nappes (Figure 1.3). D_4 was associated with post-Oligocene reverse movement within the Moonlight Fault Zone that formed north trending chevron folds and the broad N to NE trending Earnslaw Synform and Shotover Antiform. D_5 was characterised by mesoscopic conjugate sets of crenulations and intrusions of lamprophyre dikes or associated carbonate veins filling axial fold surfaces in the Miocene (Adams, 1981), some of which crosscut D_4 features (Craw, 1985). Craw (1985) also proposes that there may be an early 'missing' phase.

1.1.2 Geological History of basement terranes

In the South Island the Torlesse Supergroup is divided into two terranes, the Permian to Late Triassic Rakaia terrane and the Late Jurassic to Early Cretaceous Pahau terrane. It is widely accepted that these terranes were formed adjacent to the active Gondwana margin forming largely as distal turbidite deposits of granitoid-derived sediment with minor shallow marine sediments and volcanics, however the source of these sediments is less clear. In an attempt to address this problem

sandstone and conglomerate petrography, sedimentary geochemistry, detrital mineral geochronology and isotope geochemical studies have been used (eg. Andrews et al., 1976; MacKinnon, 1983; Roser and Korsch, 1999; Wandres et al., 2004a, b). Various sediment sources have been proposed, including Marie Byrd Land in Antarctica (Korsch and Wellman, 1988; Wandres et al., 2004b), a provenance east of present-day New Zealand (Andrews et al., 1976) and the New England Fold Belt in eastern Australia (Adams and Kelley, 1998; Pickard et al., 2000). The Pahau terrane is believed to be locally derived, with sediment input from both the Median Tectonic Zone (Mortimer, 1994; Wandres et al., 2004a) and the reworked Rakaia terrane (MacKinnon, 1983; Roser and Korsch, 1999; Wandres et al., 2004a).

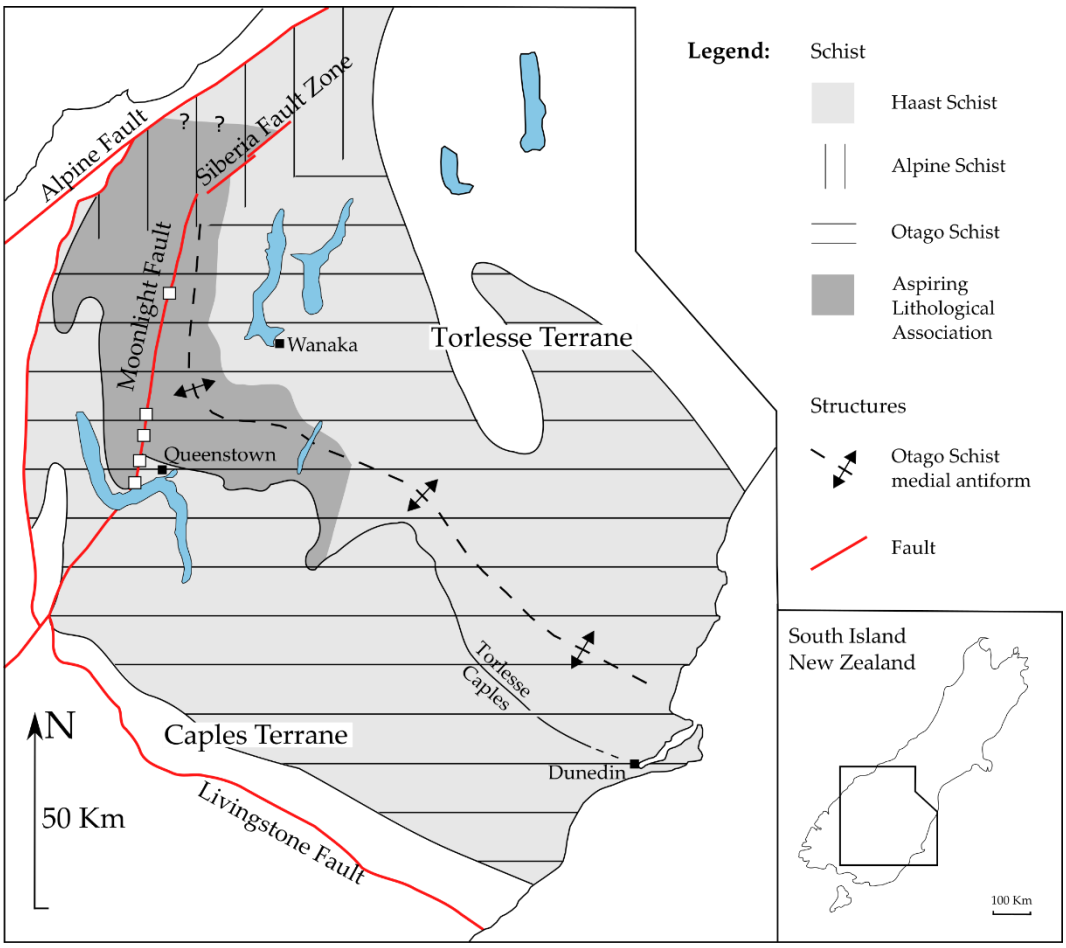

Figure 1.2. Map of the Otago Region showing the metamorphic overprint of the Haast Schist from the collision of the Caples and Torlesse terranes (+Aspiring Lithological Association). The Haast Schist is further divided into the Alpine and Otago Schist, the high grade core of the latter lies around the medial antiform (After Mortimer and Roser, 1992; Mortimer, 2000; White, 2002). White boxes along the Moonlight Fault trace are the study areas enlarged in Figure 1.6.

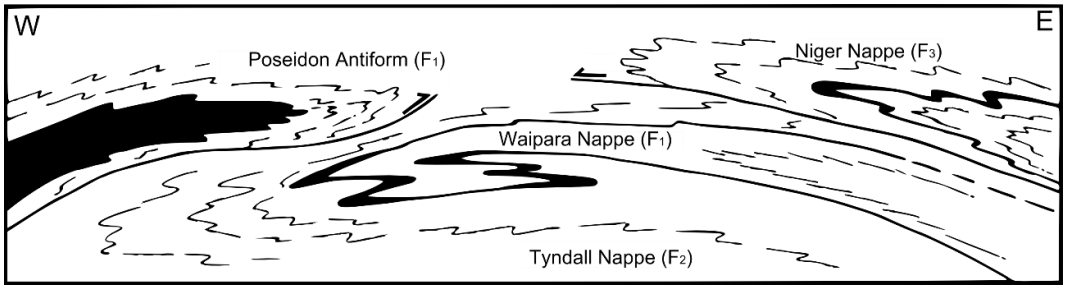

Figure 1.3. Sketch cross section of the Otago Schist from the Humboldt Mountains (West) to Lake Wanaka (East) showing over thrusting of D_1, D_2 and D_3 structures. Greenschist is black (After Craw (1985)).

The Caples terrane consists of largely offshore volcaniclastic turbidites that were deposited into a trench-complex in the Late Permian to Early Triassic and then underwent low grade metamorphism and deformation in the Late Triassic to Early Jurassic (Bishop et al., 1976; MacKinnon, 1983; Adams et al., 2009a). The geochemistry of these metasediments indicate a largely andesitic-dacitic source, likely a volcanic arc system, with minor sediment input from plutonic sources (Bishop et al., 1976; Turnbull, 1980). Adams et al. (2009a) suggest that the gradual diminution and disappearance of detrital zircon from Caples terrane sediments in the Late Triassic indicate increasing isolation from a continental source, believed to be the New England Fold Belt of eastern Australia.

The Torlesse and Caples terranes collided in the Jurassic – Cretaceous Rangitata Orogeny as they were incorporated into the accretionary prism of a volcanic arc system on the edge of Gondwana, and underwent metamorphism to form the Otago Schist. Geobarometry on the highest grade Otago Schist assemblages (garnet-biotite-albite zone greenschist) indicates that they underwent metamorphism at P 8 – 10 kbar at T 350 – 400°C (Mortimer, 2000).

Various authors have attempted to date the metamorphism of the Otago Schist using K-Ar, $^{87}Sr/^{86}Sr$ and $^{4°}Ar/^{39}Ar$ methods (Adams and Gabites, 1985; Adams and Robinson, 1993; Adams and Graham, 1997; Little et al., 1999; Mortimer, 2000; Forster and Lister, 2003; Gray and Foster, 2004). It is generally accepted that exhumation of the Haast Schist was complete by c. 105 Ma, as sediments of this age are found atop the schist (Adams and Gabites, 1985; Mortimer, 1993a), although the cooling rate and exhumation history are less clear. Adams & Graham (1997) suggested either one period of metamorphism at c. 200 Ma (Early Jurassic) followed

by slow uplift and cooling, or, metamorphism at c. 200 Ma and again (Hydrothermal metamorphism) at 115 Ma (Mid. Cretaceous) followed by rapid uplift. Little et al. (1999) proposed that peak metamorphism occurred at 170 – 180 Ma and further metamorphism occurred as reheating around 120 Ma and 75 – 84 Ma (Late Cretaceous). Gray & Foster (2004) suggest that peak metamorphism occurred between c. 160 – 140 Ma and 120 Ma followed by gradual or no cooling until c. 110 Ma where, through some form of extensional exhumation, the high grade core was uncovered between 109 – 100 Ma. Mortimer (1993a) proposed that this Late Cretaceous extensional tectonic regime was achieved through extensional faulting while Forster & Lister (2003) propose that this was accommodated by large-scale ductile shear zones linking brittle normal faults, some of which are reported in the Dunstan Range of Central Otago.

1.1.3 The Aspiring Lithological Association

For any study in the region north of Lake Wakatipu, a note must be made on the debate of the status of the Aspiring Lithological Association (ALA), first proposed by Craw (1984). Craw proposed the ALA as distinct to the adjacent Caples and Torlesse Terranes based on the observation of the ALA being dominated by pelitic and basic metavolcanic schist defining an oceanic assemblage, as opposed to the coarse clastic flysch sequences of the neighbouring terranes. Norris & Craw (1987) reviewed its character and structural relationships to the adjacent terranes, subsequently elevating the ALA to terrane status. Mortimer & Roser (1992) suggested that the ALA was a part of the Torlesse (Rakaia) Terrane on the basis of bulk rock geochemistry. They also note that the Rakaia-ALA boundary of Craw (1984) coincides with an increase of thickness of segregation lamellae in psammitic schist, giving the impression of being more micaceous than thinner segregated schist. On the basis of isotope geochemistry Adams & Graham (1997) and Adams et al. (2009b) argued that the closest correlative of the ALA was not the Rakaia Terrane but the Waipapa Terrane of the North Island. This conclusion was reinforced by the dating of detrital zircons from the ALA by Jugum et al. (2013) who found that the zircon ages also point towards a correlation with the Waipapa Terrane. The ALA structurally lies beneath the Caples and Torlesse Terranes (Norris and Craw, 1987; Mortimer, 1993a; Jugum et al., 2013) (Figure 1.4) and if treated as

an extension of the Waipapa Terrane, this terrane would not terminate at the Alpine Fault in Marlborough as previously thought, but would continue to the east of the Alpine Fault in west Otago. For the purpose of this report this region will be referred to as the ALA and will be treated as an area of the Torlesse Terrane. Clearly more work is needed to confirm if the ALA is indeed a part of the Waipapa Terrane.

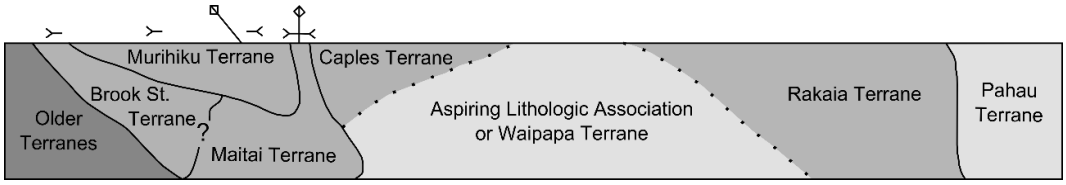

Figure 1.4. Schematic cross-section of New Zealand's current tectono-stratigraphic terranes prior to movement of the Alpine Fault (adapted from Jugum et al. (2013)).

1.1.4 The Moonlight Fault Zone

The Moonlight Fault Zone was first described at Bobs Cove on the shores of Lake Wakatipu by Hacket (1864) where it is revealed by a discontinuous thin sliver of Oligocene marine sediments (Figure 1.6). Many subsequent authors studied these sediments (eg. Park, 1909; Hutton, 1939; Grindley, 1963) while others described similar, isolated outcrops of the Oligocene sediments south of Lake Wakatipu (McKay, 1881; Turnbull, 1969) and to the north (Barry, 1966; Turnbull, 1969). Hutton (1939) collectively termed the sediments found along the MFZ the 'Bobs Cove Beds'. Turnbull et al. (1975) described all of the known infaulted sedimentary packages north of the Oreti River and proposed a tectonic history of the MFZ which lies within a wider zone of tectonic instability, the Moonlight Tectonic Zone (Norris et al., 1978).

It has been proposed that the MFZ has undergone at least 3 distinct phases of movement (Turnbull et al., 1975; Norris et al., 1978).

1) A somewhat enigmatic phase (or phases) of pre-Oligocene strike slip movement, which produced a 1 km wide zone of deformation and post-metamorphic kink folding in the schist. The lateral offset of this phase can be constrained to 1 -2 km as it has offset the contact between the Dun Mountain Ophiolite and Caples Terrane south of Lake Wakatipu (Norris et al., 1978). This phase may also account for large differences in foliation attitude and metamorphic grade that occurs across the fault.

2) An early Oligocene phase of extension that correlates with regional extension and subsidence. Regional extension during this time occurred across much of the southern South Island to form a series of rapidly-subsiding, fault-controlled basins that were filled with sediments up to a few kilometres thick upon the schist basement (Turnbull et al., 1975; Norris et al., 1978). Norris et al. (1978) suggested that the MFZ initiated during the early Oligocene as one of the basin bounding normal faults down-throwing basement schist to the west allowing for the deposition of the Bobs Cove Beds. The sediments which form the Bobs Cove Beds were derived from the newly upthrown footwall of the Moonlight Fault. They define a depositional sequence from mass-emplaced breccias to bioturbated shallow marine sediments to mass-flow slope sediments (Turnbull et al., 1975). Incorporating observations from Fitzharris (1965) and Wood (1966), Norris et al. (1978) also suggested that the MFZ continued south of the Oreti River, through Blackmount in the west of the Takitimu Mountains to the eastern edge of Lake Hauroko in western Southland.

3) A post-Miocene phase of high angle reverse movement as Otago underwent broadly north west - south east compression as a result of oblique convergence of the Australian – Pacific plate boundary (Norris et al., 1990b). This reactivation of the MFZ produced deep infaulting of the Bobs Cove Beds and deformation east of the fault trace including kink folds and macroscopic folds with sub-vertical axial planes and shallowly plunging fold axes parallel to the Moonlight Fault (Turnbull et al., 1975; Norris et al., 1978; Craw, 1985). This movement phase is thought to be largely responsible for uplift of the Mt Aspiring massif to the west of the fault (Craw, 1985). For this phase Barry (1966) inferred that the principal stress direction in the Shotover region (σ_1) at the time of reverse faulting (D_4) plunged shallowly ($<10^o$) to the SE based upon a study of conjugate kink bands adjacent to the Moonlight Fault (Figure 1.5). Norris et al. (1978) derived stress orientations from nodal planes resultant from a study of microseismicity in the South Island by Scholtz et al. (1973) which indicates that the current stress field closest to the MFZ is similar to the paleostress field (Figure 1.5).

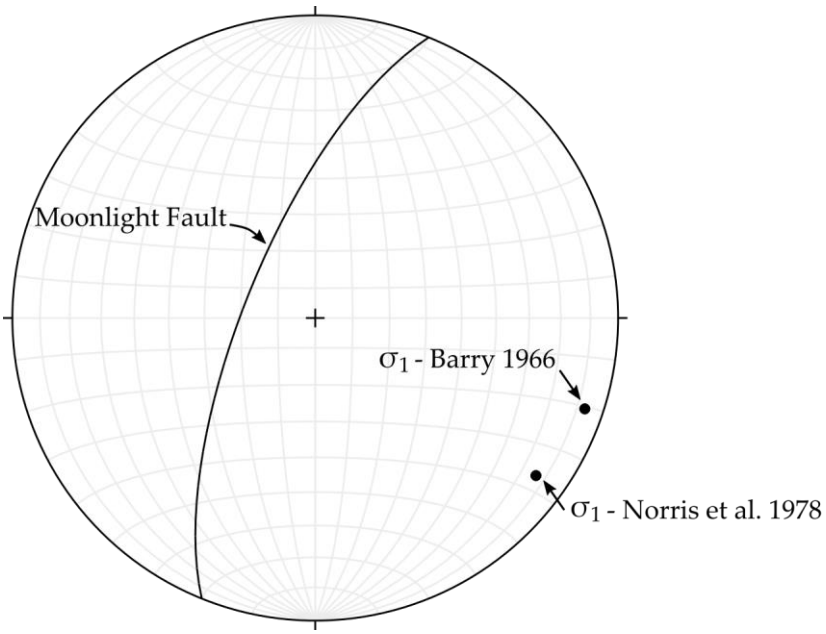

Figure 1.5. Equal area lower hemisphere projection displaying the average orientation of the Moonlight Fault north of Lake Wakatipu (this study) in relation to the maximum compressive stress orientation at the time of faulting, derived by Barry (1966), and the current orientation derived by Norris et al. (1978).

The trace of the Moonlight Fault is relatively well constrained from Lake Wakatipu to the Matukituki Valley however north of the field area, from the head of the East Matukituki Valley, it becomes less clear. Craw (1985) traced the Moonlight Fault north of the East Matukituki Valley to the Burke River and noted that through the Wilkin Valley it changes orientation and character, changing from a north-striking, west-dipping fault through the Shotover-Matukituki area to a northeast striking vertical fault. A subsequent study by White (2002) interpreted that the fault in the Wilkin Valley was a separate structure, the Siberia Fault Zone, and suggested that the Moonlight Fault transitions northward into the Castalia Antiform. A fault has been observed trending northwards from the north side of Mt Castor in the Drake Valley to the Turnbull River, offsetting large NNE trending regional scale folds such as the Haast Antiform and Thomas Synform (Figure 1.6). This is inferred by Rattenbury et al. (2010) to be the northward extension of the Moonlight Fault, although further study is needed to confirm this.

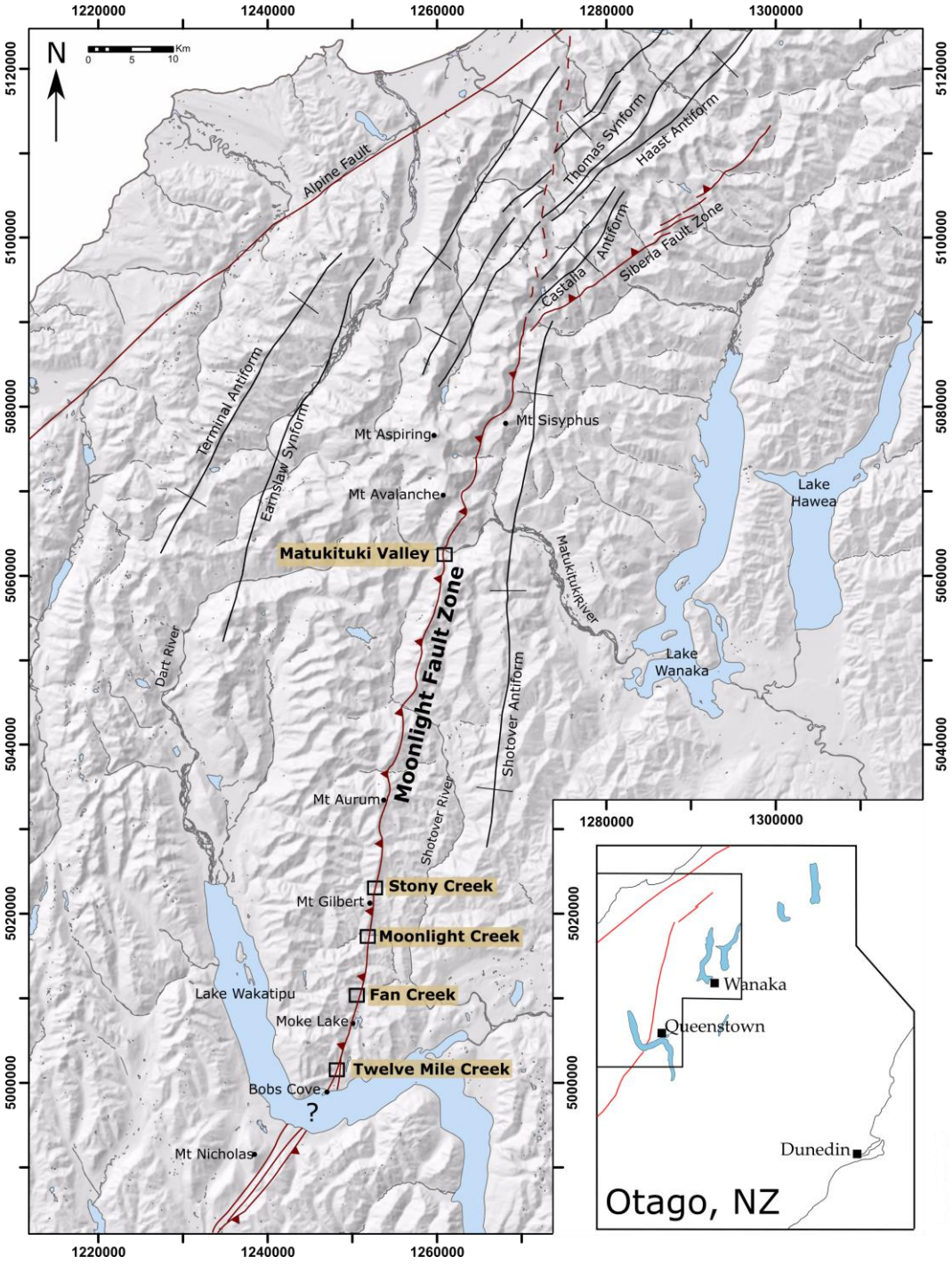

Figure 1.6. Trace of the Moonlight Fault from south of Lake Wakatipu to the Alpine Fault. Inferred Moonlight Fault of Rattenbury et al. (2010) appears as dashed red line, offsetting regional fold structures. Open black boxes show the location of outcrops examined in this study.

1.2 The Moonlight Fault in Fan Creek

A detailed study of the structure and fault rocks of the Moonlight Fault Zone in Fan Creek was carried out by Menzies (2014) for a BSc(Hons) dissertation at the University of Otago. The observations of Menzies (2014) are summarised here and later incorporated into the discussion on the variability of along strike deformation features within the Moonlight Fault Zone. Fan Creek lies 10 km northwest of Queenstown and 2 km north of Moke Lake (Figure 1.6). Exposures in Fan Creek revealed that movements along the Moonlight Fault juxtaposed TZIV (Torlesse terrane) phyllites in the hanging wall against sediments of the Bobs Cove Beds or TZIIB (Caples terrane) phyllites and schist in the footwall. A number of subsidiary fault were also documented.

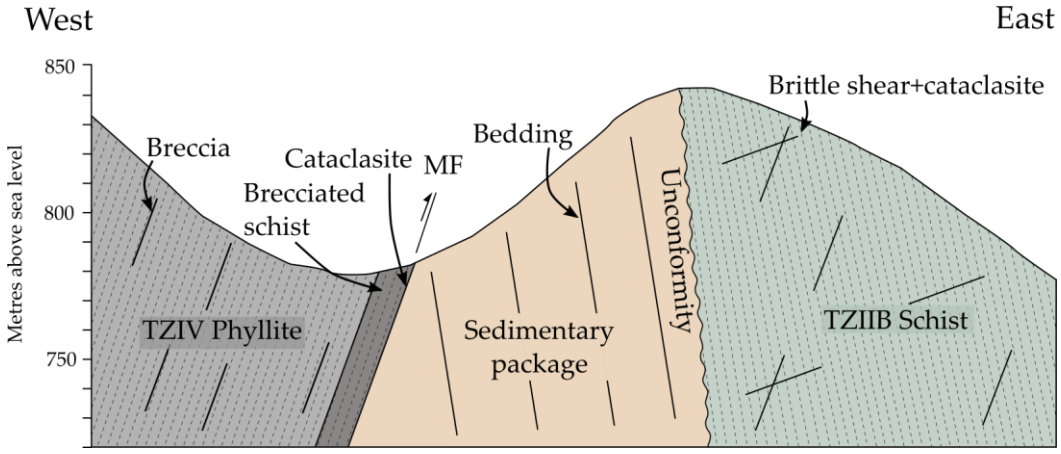

Figure 1.7. Cross section of the Moonlight Fault Zone on the north bank of Fan Creek, displaying the structure and fault rock assemblages. Adapted from Menzies (2014).

1.2.1 Hanging wall

The hanging wall in Fan Creek consists of black TZIV phyllite with a spaced foliation that strikes north-south and dips steeply west (mean: 173/65W) which rotates to strike northeast-southwest within 20 from the Moonlight Fault. This phyllite is host to foliation parallel faults, some of which contain fault breccias up to 10 cm thick. These breccias contain up to 2 mm wide clasts of the host rock supported by a fine grained matrix (<0.1 mm) of quartz, albite, epidote, muscovite/phengite and titanite which is cemented with calcite. Dissolution seams, made evident by concentrations of insoluble titanite along the edges of clasts, lie sub-parallel to the breccia boundary. Drag of some seams indicate deformation in a reverse sense. It

also contains clasts of reworked matrix, indicating multiple slip events may have occurred.

Also present in the hanging wall are kink folds and shear bands, both of which increase in frequency within the damage zone of the Moonlight Fault while immediately adjacent to the Moonlight Fault the hanging wall black phyllite becomes brecciated. Within a few metres of the main fault trace the brecciated phyllite is cut by up to 30 cm thick quartz veins. 8 veins were observed, emanating from the fault plane and tapering upwards into the hanging wall.

1.2.2 Fault core

In areas where hanging wall and footwall schists are in contact, the fault core consists of an up to 30 cm wide red gouge. This contains randomly oriented angular to sub-rounded clasts of quartz and albite with minor titanite and epidote. The matrix of the gouge consisted of kaolinite and hematite.

Instead, where the hanging wall schists are in contact with footwall sediments, the fault core contains a black foliated cataclasite up to 10 cm thick. This contains sub-rounded quartz and albite grains that become progressively altered to fine grained phyllosilicates (chlorite, muscovite/phengite) towards the fault trace. The phyllosilicate grains become aligned sub-parallel to the fault plane to form an interconnected network defining the foliation. The modal abundance of phyllosilicates increases towards the main fault plane, suggesting that some of the phyllosilicate phases are authigenic. This is supported by microstructural observations that the phyllosilicates are fine-grained fibrous overgrowths upon clasts of quartz and feldspar and the space filling nature of these new phases.

1.2.3 Footwall

Sedimentary Package

The sedimentary package lies in the footwall immediately north of Fan Creek with a maximum thickness of approximately 75 m. The package includes a basal conglomerate and overlying yellow sandstone with quartz beds and thin mud beds. The bedding here is locally overturned, dipping steeply south-east (mean

054/83SE). Deformation within the sedimentary package consists of faults that largely lie sub-parallel to bedding with steeply plunging slickenlines.

Footwall schists

The footwall is made up of three types of schist. The first, a c. 10 m thick weakly foliated green phyllite lies immediately adjacent to the Moonlight Fault at the schist-schist contact. It is faulted on its eastern contact against a brecciated schist which contains angular fragments of schist. These two schist units contain a strike parallel to the Moonlight Fault (mean 027/72W). The foliation in this brecciated schist steepens and then overturns in the adjacent schist, a light-green TZIIB schist, to a steep south-eastern dip (mean 033/78E). This eastward dipping foliation is a local feature however, with the regional foliation dipping to the west (Barber and Craw, 2002). This unit is host to small faults bearing green cataclasites of variable orientations.

2. Matukituki Valley

2.1 Overview

Outcrops of the Moonlight Fault Zone in the West Matukituki valley occur c. 40 km northwest of Wanaka, 1 km southwest of the Raspberry Flat carpark. Movements along the Moonlight Fault in the Matukituki valley have juxtaposed well foliated TZIV greenschists in the hanging wall against chevron folded TZIV greyschists in the footwall (Figure 2.1). The footwall greyschists could be studied immediately adjacent to the Moonlight Fault trace while the hanging wall greenschists outcrop extensively in water-worn outcrops along Downs Creek, 400 - 500 m to the west of the Moonlight Fault, as well as sporadically in outcrops closer to the main fault trace (Figure 2.2). Below, the host rocks will be described first, followed by the structure of the fault zone and then fault-related rocks and microstructures.

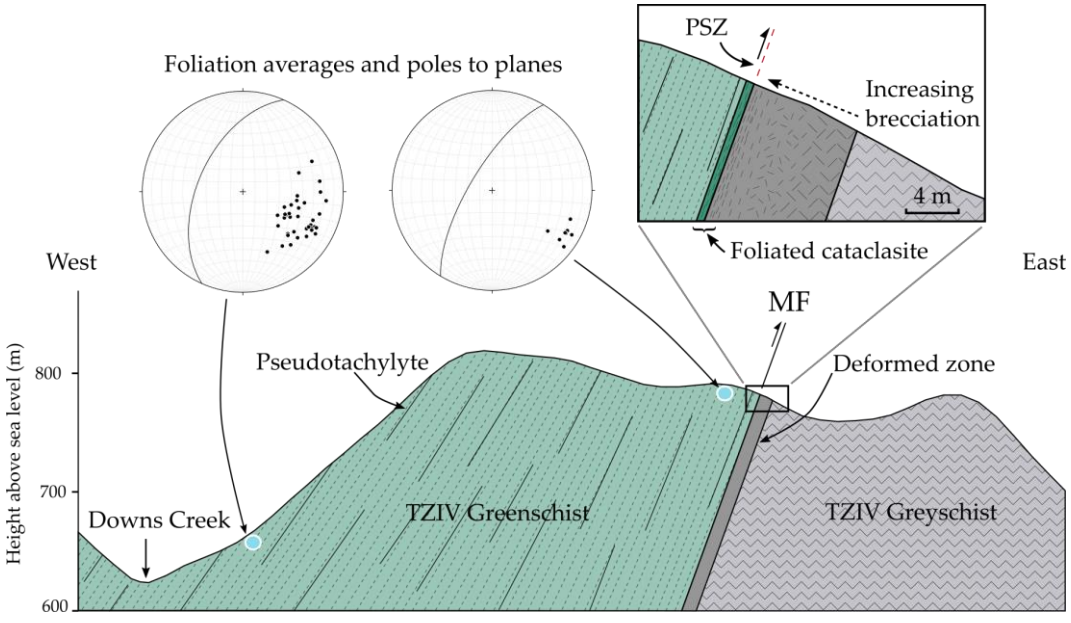

Figure 2.1. Cross section of the Moonlight Fault Zone in the Matukituki Valley. *Inset:* details of the main fault core including brecciation towards the fault core which hosts foliated cataclasites. Equal area lower hemisphere projections display the rotation of the hanging wall foliation dip into alignment with the Moonlight Fault.

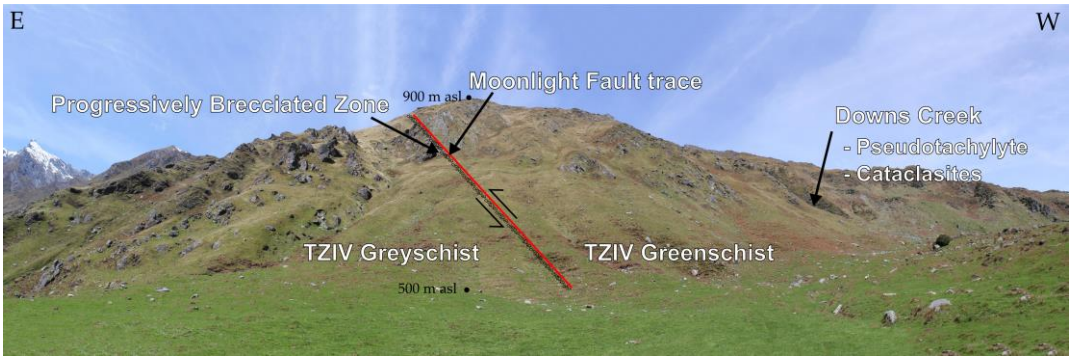

Figure 2.2. Overview of the Moonlight Fault Zone in the West Matukituki Valley. Fault rocks within the hanging wall greenschist include pseudotachylytes and cataclasites while in the footwall a brecciated zone lies adjacent to the fault trace. Note: This overview is looking south while the previous cross-section looks north.

2.2 Host Rocks

2.2.1 Hanging wall greenschists

Structure

The hanging wall consists of a light grey-green greenschist with lesser bands of light green epidote-rich and dark grey phyllosilicate-rich layers (Figure 2.3). The hanging wall greenschists contain a steeply west dipping foliation (average 025/54W), the dip increasing with proximity to the main trace of the Moonlight Fault (Figure 2.1). The greenschist foliation has a mean lineation of 54/303 (Figure 2.3). The greenschists have been complexly deformed, folding lithological variations and quartz veins. Fold axes in the greenschists lie in the plane of the foliation and consistently plunge in the same steep northwest direction (47/309) as the mean lineation (Figure 2.3).

Microstructural

The greenschist predominately consists of chlorite, epidote, albite and titanite with minor stilpnomelane, actinolite, calcite, quartz, biotite, apatite, and disseminated chalcopyrite. Elongate crystals of albite, tabular chlorite and stilpnomelane, together with bulk compositional layering, define the foliation (Figure 2.4). Stilpnomelane grains are commonly 10 – 50 µm in width and largely appear in layered bands. At times chlorite (10 – 50 µm in width) displays brown – purple anomalous interference colours indicative of the Mg-rich end member clinochlore. Epidote shows associations with all other minerals and forms as

granular clusters or individual crystals which appear as subhedral <10 μm crystals within larger albite crystals or larger (100 - 200 μm) more disaggregated anhedral crystals. Albite grains are commonly elongate (length to width ratio 3:1) with poikiloblasts of epidote that can show a helictic structure preserving an earlier tectonic foliation. Actinolite and occasionally biotite occurs intermittently as intergrowths with chlorite. Calcite occurs in veins parallel to the foliation, commonly with quartz. Titanite occurs as very high relief elongate grains of <50 μm in length.

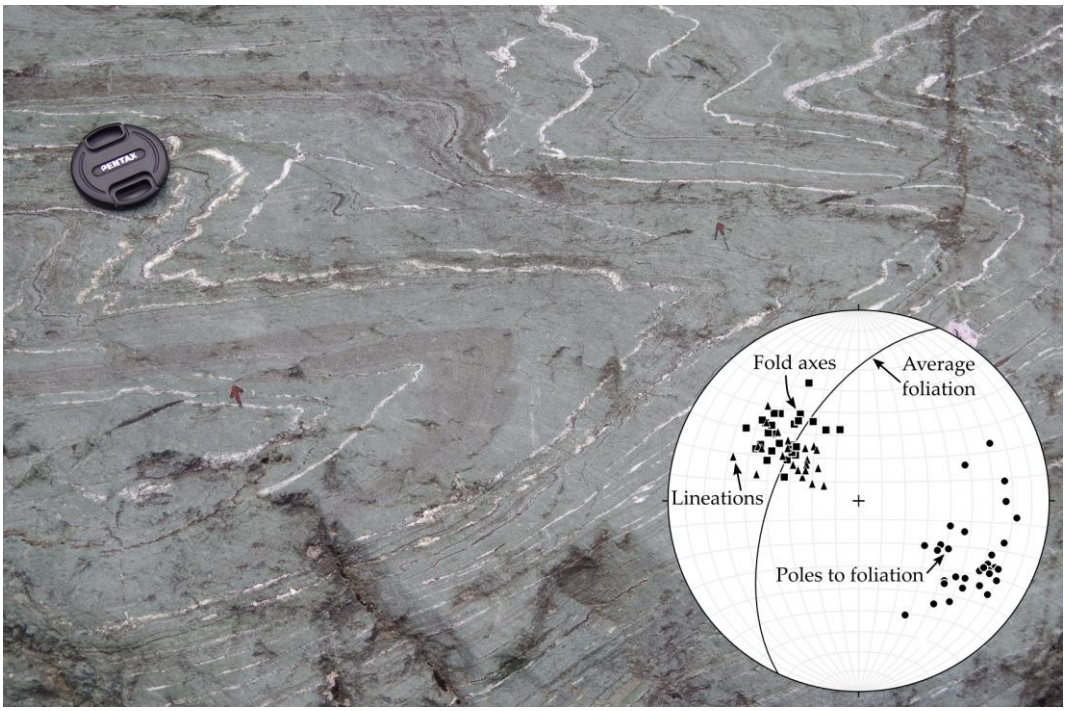

Figure 2.3. Representative photo of the folded greenschists in Downs Creek. Dark bands are more phyllosilicate (stilpnomelane) rich. Equal area lower hemisphere projection showing the foliation, lineation and fold axis data in Downs Creek. Note that a thin, dark black pseudotachylyte vein runs from lower-left to upper-right (marked by black arrows drawn on outcrop).

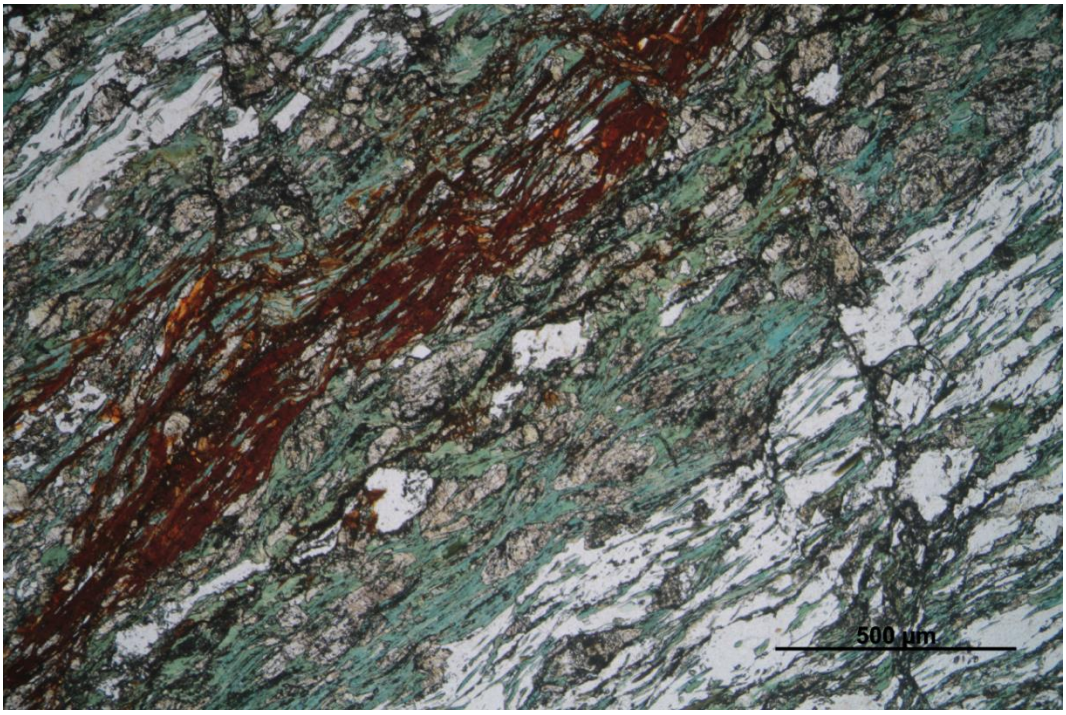

Figure 2.4. Internal foliation of greenschist defined by chlorite (green), stilpnomelane (brown) and albite (white). High relief anhedral grains are epidote.

2.2.2 Footwall greyschists

Structure

The footwall consists of greyschist, made up of >1 mm thick segregations of dark grey to pale green phyllosilicate rich layers and white, quartz rich layers. It contains a spaced foliation and host to tight (interlimb angle ave. 65^{o}) chevron folds with an average wavelength and amplitude of 6 cm and 2.5 cm, respectively. The greyschist fold axes have a shallower, southerly trend (34/174) and lie subparallel to the Moonlight Fault trace (Figure 2.5).

Microstructural

The greyschist is predominately made up of chlorite, quartz, muscovite, albite and calcite with minor epidote, titanite, clinozoisite and rutile. The foliation is defined by the alignment of muscovite crystals (up to 50 µm in width) and segregations of polycrystalline quartz, muscovite and twinned calcite from chlorite-rich layers (Figure 2.6). Chlorite is found as a matrix of colourless to very faintly green pleochroic, at times elongate crystals with anomalous grey interference colours (Figure 2.6). Clinozoisite, defined by its inky blue interference colour, is frequently

found as rims around elongate subhedral epidote grains (up to 300 μm in length and 100 μm in width) as well as individual elongate euhedral grains (up to 200 μm in length and 60 μm in width).

2.3 Fault zone structure and deformation

A direct measurement of the orientation of the Moonlight Fault was not obtained, but structure contour analysis of the mapped fault trace revealed an average orientation of 012/70W, consistent with measurements of the fault plane made in other creek sections along strike.

Three main types of fault rock were identified in the MFZ in the Matukituki Valley:

1) Pseudotachylyte that occurs extensively in the hanging wall greenschists (see Section 2.3.1).
2) Cataclasites that occur in brittle fault networks in the hanging wall (see Section 2.3.2).
3) Fault breccias and foliated cataclasites that occur close to the main trace of the MFZ and define a strain transition in footwall greyschists (see Section 2.3.3).

The field characteristics and structural settings of each of these fault rocks are described below. Fault rock classification will follow the scheme of Woodcock and Mort (2008).

2.3.1 Hanging wall pseudotachylyte

In-situ pseudotachylyte was identified in the MFZ immediately adjacent to the trace of the Moonlight Fault and in water-worn outcrops in Downs Creek 400 - 500 m to the west of the main trace of the Moonlight Fault (Figure 2.1). The pseudotachylytes were described in detail from the Downs Creek outcrops. Sibson (1975) separated pseudotachylyte into *fault veins*, which are formed on frictional melt generation surfaces, and *injection veins*, which typically branch from fault veins at high angles (>60°).

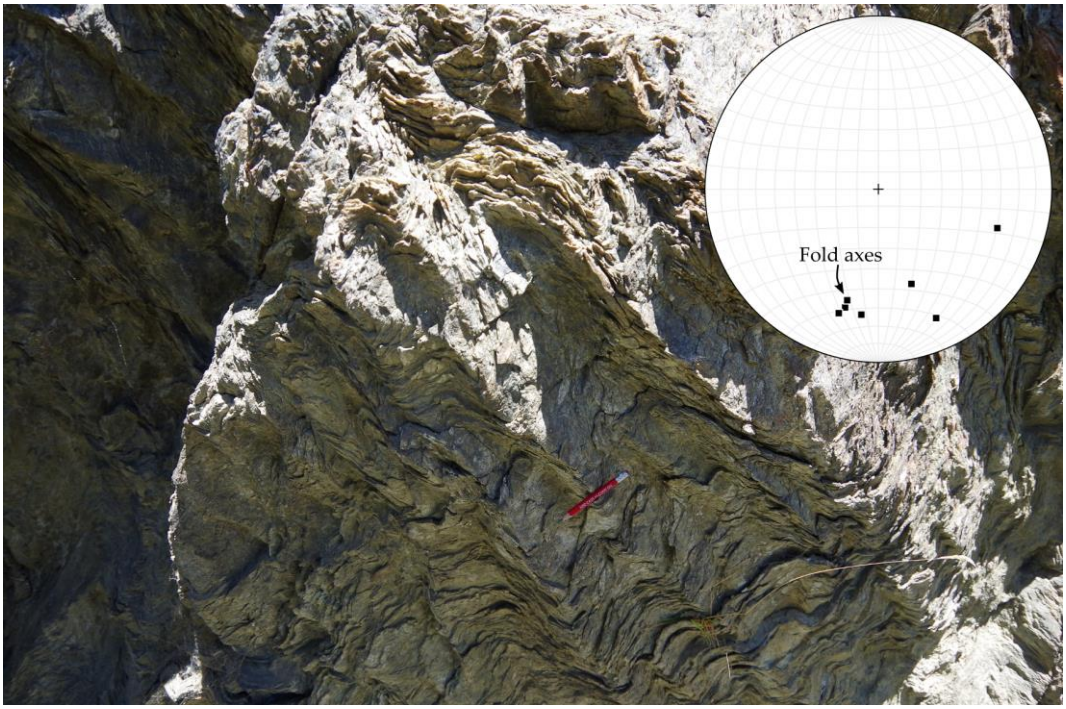

Figure 2.5. Chevron folded footwall greyschist. Equal area lower hemisphere projection shows the orientation of the chevron fold axes.

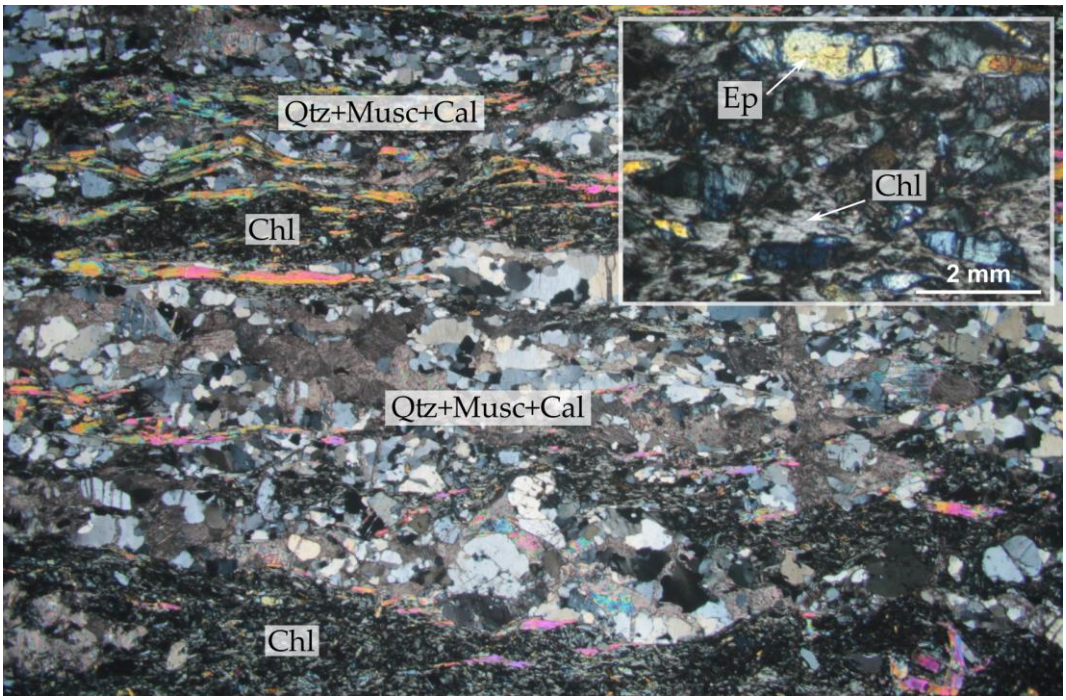

Figure 2.6. Segregations in the greyschist defined by quartz-muscovite-calcite and chlorite layers. *Inset*: Anomalous grey chlorite makes up matrix of the chlorite-rich segregations. Epidote grain shows clinozoisite rims (blue).

Pseudotachylyte fault veins in Downs Creek

Single fault veins can be traced for no more than 15 m, although in some cases this is due to the limited lateral continuity of the outcrops. Pseudotachylyte fault veins appear in two forms;

1) Sharp, planar features that on average lie sub-parallel to the steeply west dipping greenschist foliation, although in detail often crosscut the foliation at low angles (Figure 2.7 & Figure 2.8). These veins appear as aphanitic, dark grey/black veins that range in thickness from c. 200 μm to 7 mm, although most are <2 mm wide (Figure 2.8). Fault vein thickness varies significantly along strike, and in some cases fault veins taper to zero thickness. Normally there is only one vein present, although in some cases up to three parallel veins are linked by melt pools and injection veins. The foliation parallel veins are abundant in the hanging wall greenschists; along a 2.6 m transect over a particularly well exposed section of outcrop, eight discrete foliation-parallel pseudotachylytes were found with an average spacing of 23 cm.

2) Much more irregular anastomosing veins and pseudotachylyte-filled fracture networks that cut the greenschist foliation at high angles (Figure 2.7 & Figure 2.9). The veins and fracture networks occur in up to 30 cm wide zones that often link foliation parallel pseudotachylyte veins to form complex stepover regions (Figure 2.9).

One pseudotachylyte vein had well-defined slickenlines developed on the surface between the fault vein and enclosing greenschist host rock. Although it is difficult to tell whether the slickenlines are genetically related to the formation of the pseudotachylyte fault veins, or whether they were formed during later shearing concentrated along the margin of the fault vein, they indicate almost pure dip slip movement. Evidence from microstructural analysis (presented in Section 2.4.1) suggests that the pseudotachylyte veins had a reverse sense of movement. Displacement on foliation parallel fault veins was difficult to determine due to their foliation-parallel habit (and, therefore, lack suitable offset markers). However, general observations of markers on either side of fault veins indicates that displacements do not likely exceed a few tens of centimetres. The pseudotachylytes

that cross cut the foliation at high angles also appear to have accommodated displacements of at most a few metres.

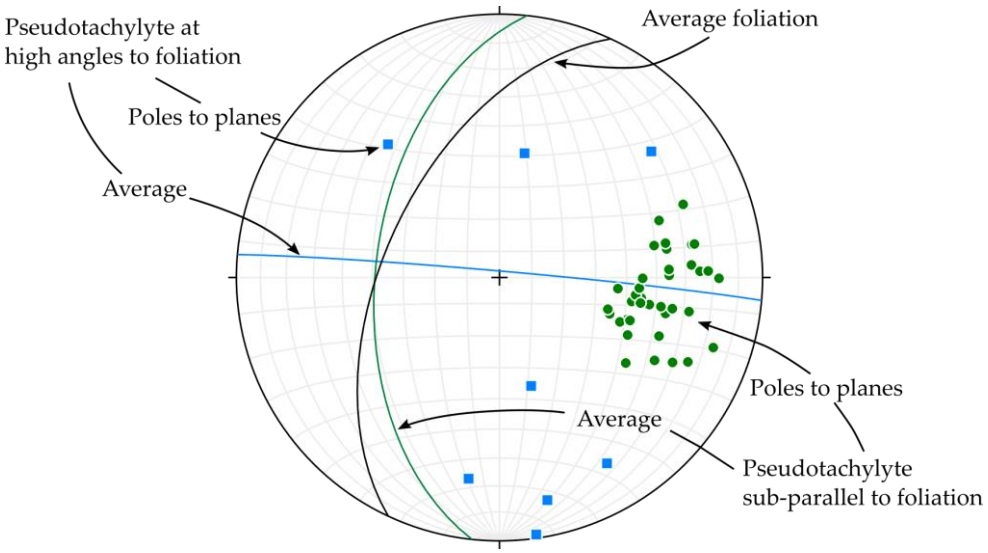

Figure 2.7. Equal area lower hemisphere projection showing the orientation of pseudotachylyte fault veins in relation to the foliation in the hanging wall greenschists.

Figure 2.8. Pseudotachylyte fault vein that lies sub-parallel to the steeply west-dipping greenschist foliation. The vein shows variable thickness along its length.

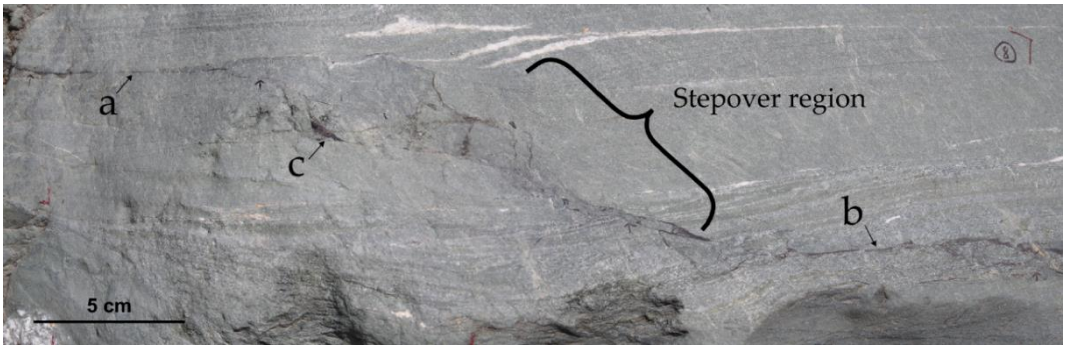

Figure 2.9. Pseudotachylyte fault veins showing an orientation sub-parallel to foliation (labelled a, b) are linked across a complex stepover region where the geometry becomes more complex and thick melt pools (labelled c) occur.

Pseudotachylyte Injection Veins

Injection veins are found infrequently along the fault veins, branching off into the host rocks at high angles (>60˚) (Figure 2.10). They range from 250 µm – 4 cm in length and 300 µm - 1 mm in width at the point where they branch off from the pseudotachylyte fault veins. They appear to be extensional with no visible offset along their length.

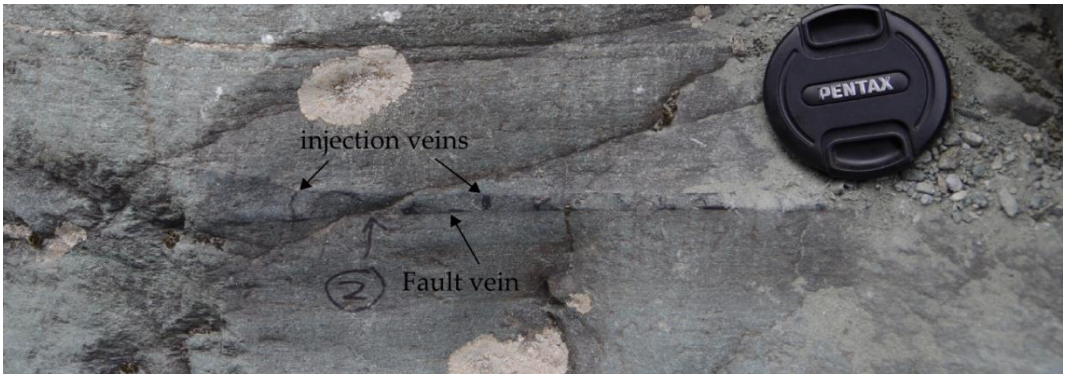

Figure 2.10. Pseudotachylyte injection veins emanating from a fault vein into the surrounding foliated greenschists.

Mixed pseudotachylyte – brittle fault

One pseudotachylyte vein was found to occur as a continuation of a cataclastic fault network that cross cuts the greenschist foliation at high angles (140/34W). Drag of the greenschist foliation and offset of quartz pods indicate top-to-the-east (thrust) movement on the cataclasite (Figure 2.11). Within the area of offset quartz pods the deformation zone is up to 15 cm wide and does not contain pseudotachylyte. Where pseudotachylyte is present the zone of cataclastic

deformation is much thinner (2 - 4 cm). The pseudotachylyte vein is zoned and its colour differs from other veins described above by containing an altered light brown interior with a darker brown rim (Figure 2.11).

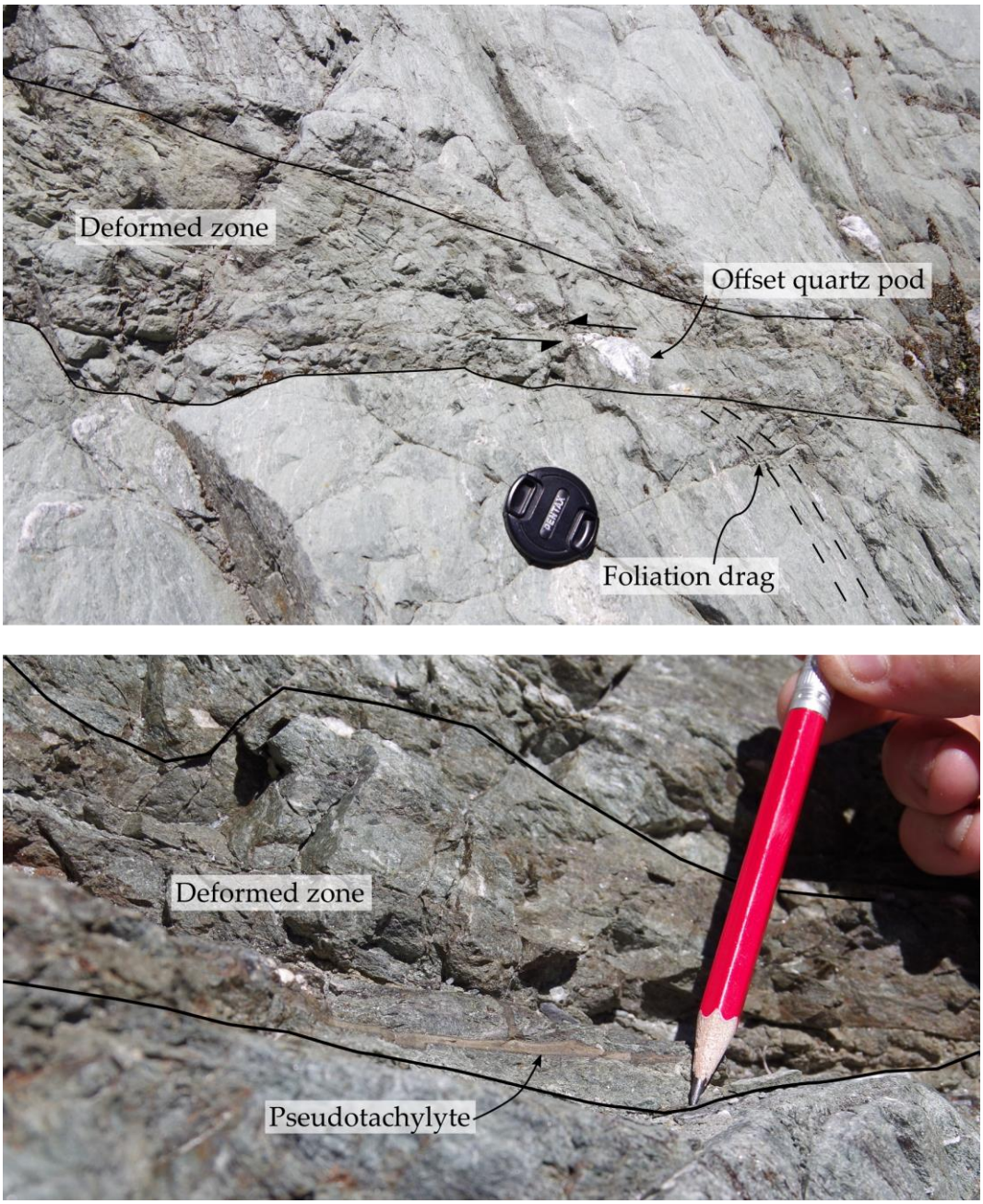

Figure 2.11. *Top:* Small brittle fault showing 5 cm offset on a quartz pod which indicates top to the east movement, ie. thrust. *Bottom:* Thin deformed zone (<6 cm) where altered pseudotachylyte is present.

2.3.2 Small cataclasite bearing faults in the hanging wall

Networks of small cataclasite-bearing faults are found in the hanging wall greenschists extensively throughout Downs Creek (i.e. 400 – 500 m from the main fault trace). These cataclasites occur in concentrated zones of brittle fracturing separated by wide zones of more intact greenschist. These discrete 'fracture corridors' can be up to several metres wide. The small-scale cataclasites form as singular fractures with up to 10 cm of green, at times, foliated cataclasite and are observed in many places to crosscut and rework pseudotachylyte veins. They accommodate up to 10's of centimetres of movement, at times with offset markers indicating top-to-the-east movement (Figure 2.12), which is reinforced by showing shallow to steeply westerly plunging slicken lines (Figure 2.13). Overall, therefore, these cataclastic zones represent relatively young, east-verging thrust/reverse faults.

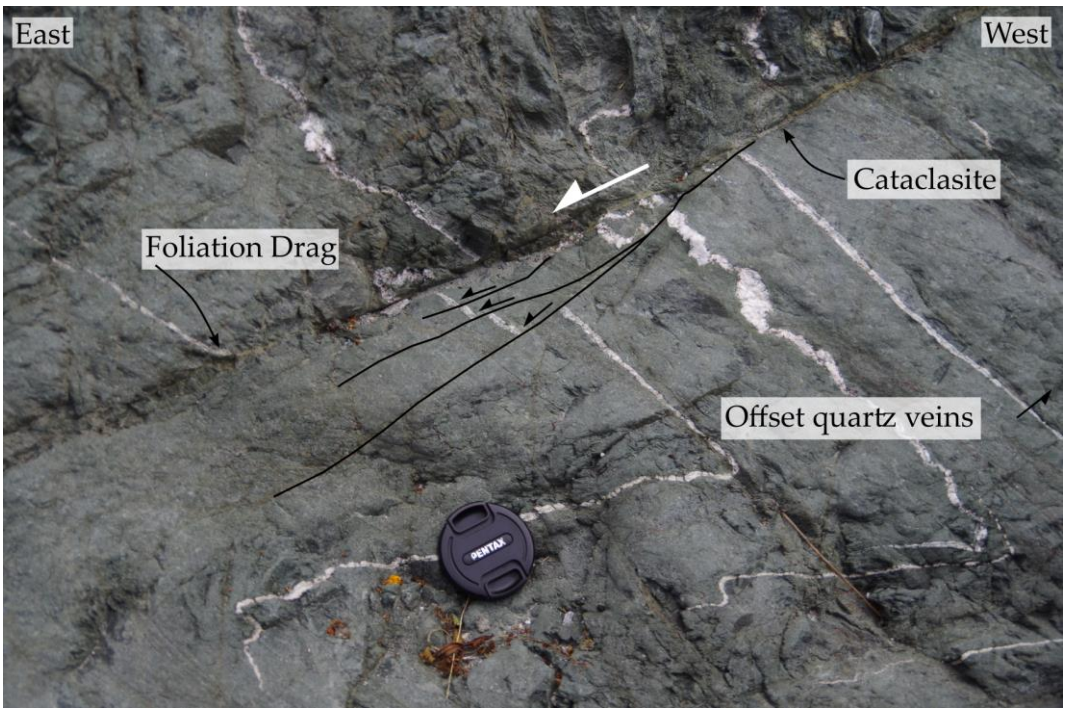

Figure 2.12. Small scale cataclasite bearing fault in Downs Creek offsetting quartz veins in the greenschist. Foliation drag and subsidiary fractures indicate top-east movements.

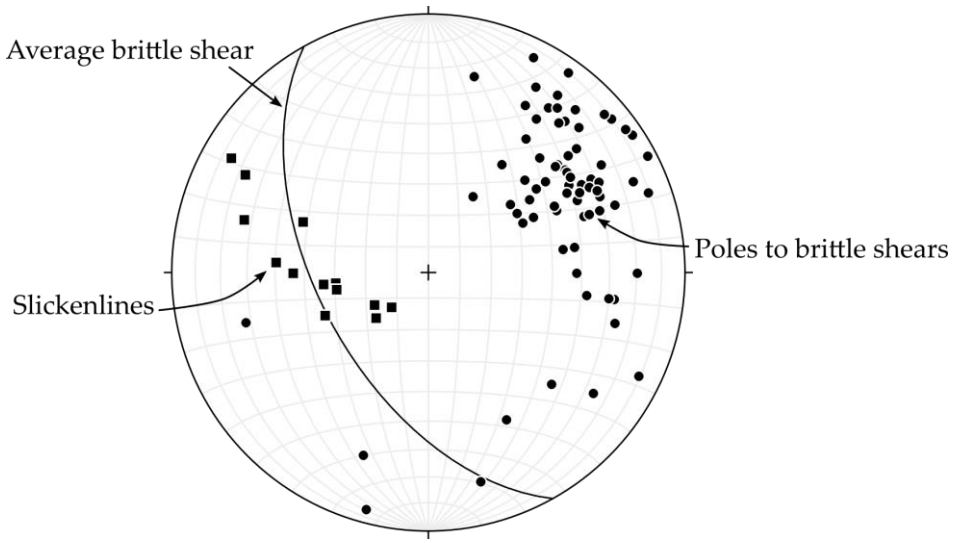

Figure 2.13. Equal area lower hemisphere projection showing the small cataclasite-bearing faults in the hanging wall greenschist. On average the faults dip moderately W-SW with moderately- to steeply-west plunging slickenlines.

2.3.3 Breccias and foliated cataclasites in the footwall and fault core

The central fault core is exposed in a narrow gully separating hanging wall greenschists from the footwall greyschists. Fault-related rocks in the footwall greyschists were observed at distances of up to 15 m from the fault core (Figure 2.1). The 15 m-wide deformed zone in the footwall displays fabrics indicative of increasing strain towards the main trace of the MFZ, progressing from intact greyschist to brecciated greyschist to foliated breccia and cataclasite (Figure 2.1 & Figure 2.14). This transition as observed in the field is described below, and supporting microstructural observation are provided in Section 2.4.3.

10-15 metres from the fault core

At 15 m distance from the fault core, the chevron-folded greyschist is intact with no signs of brittle fault-related deformation (Figure 2.14a). At a distance of c. 10 m from the fault core the greyschist host rock shows signs of brecciation (Figure 2.14b). Fold hinges and limbs are recognisable although the fold limbs are often cut and dissected by discrete black shears (Figure 2.14b). The breccia contains >75 % clast to matrix volume, and the clasts are clearly derived from the local greyschist host rock without having experienced much rotation or translation. It can be classified as a crackle breccia (Woodcock and Mort, 2008).

8 metres from the fault core

At a distance of 8 m from the fault core the greyschist fold hinges become increasingly highly deformed. This breccia contains >60 % clasts, with some clasts unable to be easily fit back together, having experienced significantly more fracture and rotation and thus, can be classified as a mosaic breccia.

4 metres from the fault core

At a distance of c. 4 m from the fault core a chaotic breccia is present as it has been increasingly sheared and is entirely absent of any remnant greyschist features (Figure 2.14c). It contains up to 2 cm sub rounded clasts set in a very fine grained black matrix. In outcrop the fabric appears completely random, but on a cut face the matrix contains thin seams which define a weak foliation sub-parallel to the Moonlight Fault.

1-2 metres from the fault core

At a distance of 1 – 2 m from the fault core a well foliated breccia is observed (Figure 2.14d). The foliation is defined by the preferred alignment of the long axes of quartz and albite clasts. Cut faces show a greater proportion of matrix than the breccias at greater distances from the fault core. The matrix contains dark seams up to 5 mm in width that define a foliation sub-parallel to the Moonlight Fault.

Foliated cataclasite in the fault core

Foliated cataclasites are found in the gully marking the central fault core, with a total thickness of up to 2 metres. Two types of foliated cataclasites are present: 1) On the east side of the gully, a dark grey to black foliated cataclasite interpreted to be derived from the footwall greyschists (Figure 2.14e). It contains dark black seams up to 3 cm wide that define a foliation sub-parallel to the trace of the Moonlight Fault. 2) On the west side of the gully, a dark green foliated cataclasite interpreted to be derived from the hanging wall greenschist. At a finer scale, the green foliated cataclasites contain dark green or black seams that anastomose around lighter quartz- and albite-rich regions containing clasts aligned parallel to the foliation.

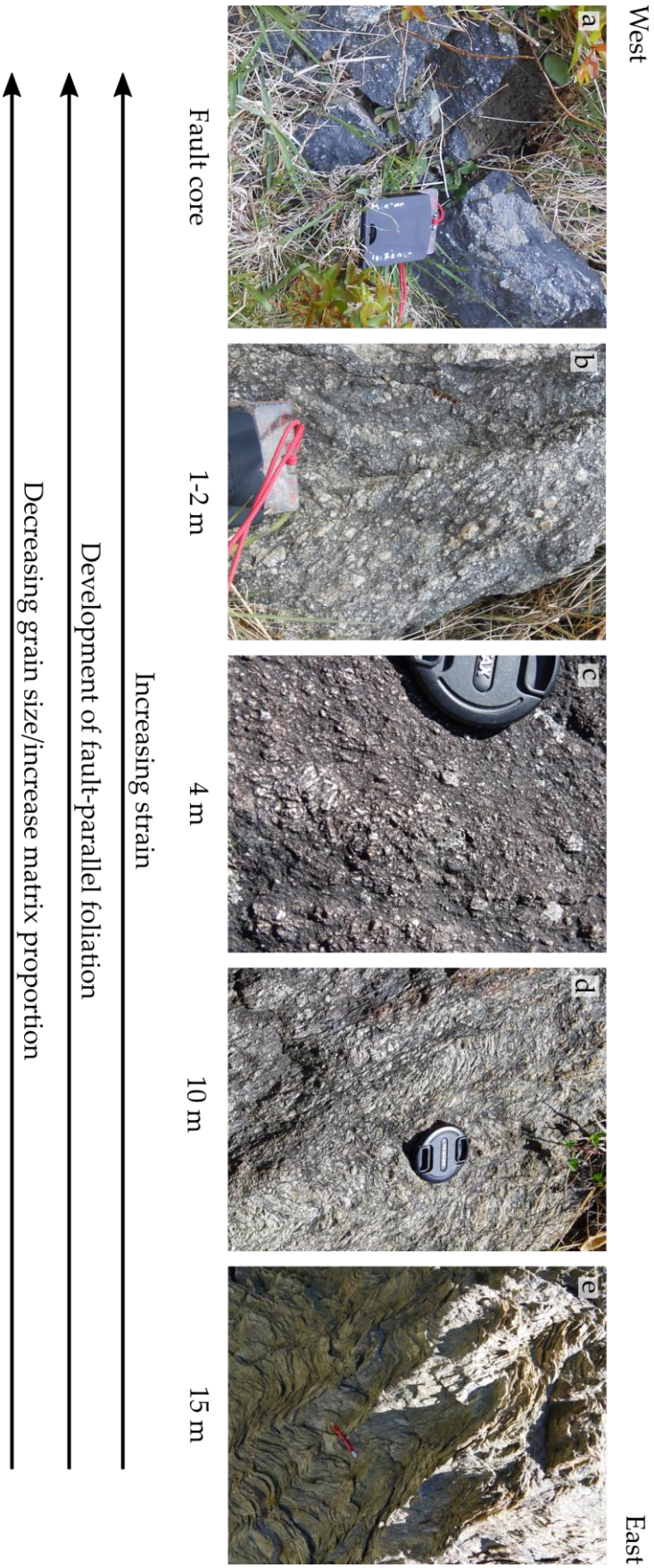

Figure 2.14 Transition from intact hanging wall greyschist (e) into the central fault core (a) of the Moonlight Fault over a distance of c. 15 m.

2.4 Fault rock microstructures

2.4.1 Pseudotachylytes

Pseudotachylyte veins observed in the Matukituki Valley generally consist of lithic clasts - fragments of host greenschist that resisted melting - which lie within a matrix of either optically observable grains that crystallised from melt (microlites) and/or a very fine cryptocrystalline matrix whose mineralogy is unresolvable by optical microscopy.

Clasts

Lithic fragments are predominately quartz and albite with lesser amounts of apatite, polycrystalline greenschist fragments and reworked ultracataclasite. The quartz and albite grains are highly variable in size, reaching up to 200 μm although more commonly 10 - 100 μm. Albite clasts are often fractured or completely disaggregated, containing melt embayments and alteration rims of potassium feldspar (microcline) (Figure 2.15). The larger fractures are infilled by the cryptocrystalline pseudotachylyte matrix. Quartz clasts appear in polycrystalline and monocrystalline forms, the former contains melt embayments which preferentially intrude along grain boundaries. The monocrystalline quartz clasts remain much more intact, appearing as rounded to sub rounded spherical and elongate clasts, some of which display undulose extinction. Apatite occurs as grains typically <10 μm in size, and rarely up to 20 μm. Fragments of the host greenschist were also found in one thin pseudotachylyte vein, distinguished from other clasts by the presence of sub-parallel chlorite and high relief epidote grains (Figure 2.16). These fragments are sub-rounded to sub-angular and range from 40 - 340 μm in length and 20 – 90 μm in width. These elongate clasts lie parallel to the vein walls with the internal foliation of all clasts ranging from sub-parallel to high angles to the vein walls, and thus the host greenschist foliation. Clasts of ultracataclasite, which are interpreted to form in the initial stages of pseudotachylyte generation, were also found as reworked clasts in the pseudotachylyte fault veins. These clasts show extensive melt embayments and partial incorporation into the melt (Figure 2.17).

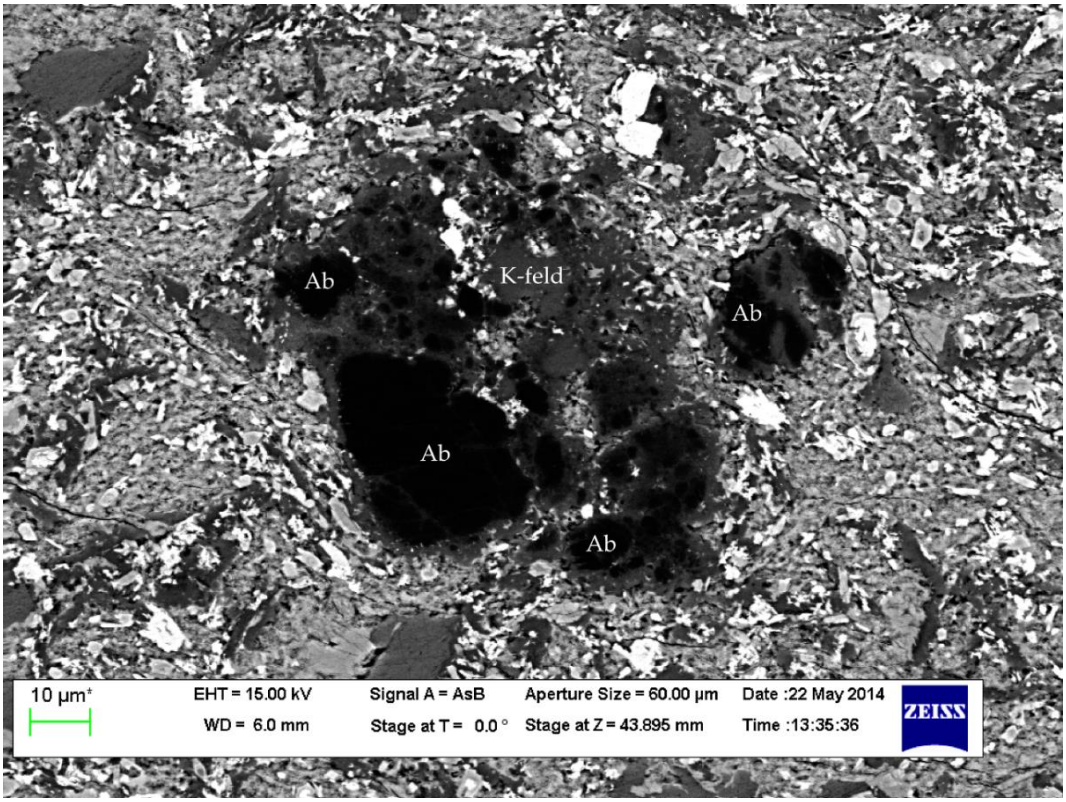

Figure 2.15. Backscatter electron image of an albite grain (Ab) surrounded by alteration rims of potassium feldspar (K-feld) within a mainly crystalline matrix.

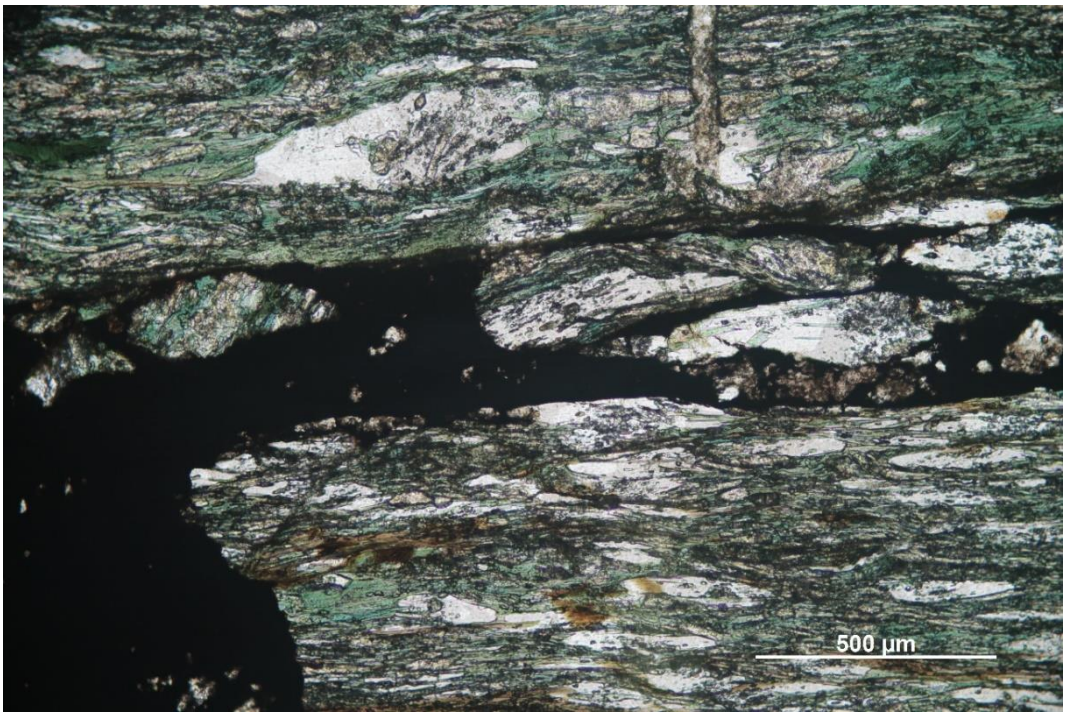

Figure 2.16. Cross-polarised photomicrograph of host greenschist fragments within a pseudotachylyte vein. Note that the foliation in clasts on the left does not align with the host rock, indicating it was caught up and rotated within the pseudotachylyte melt.

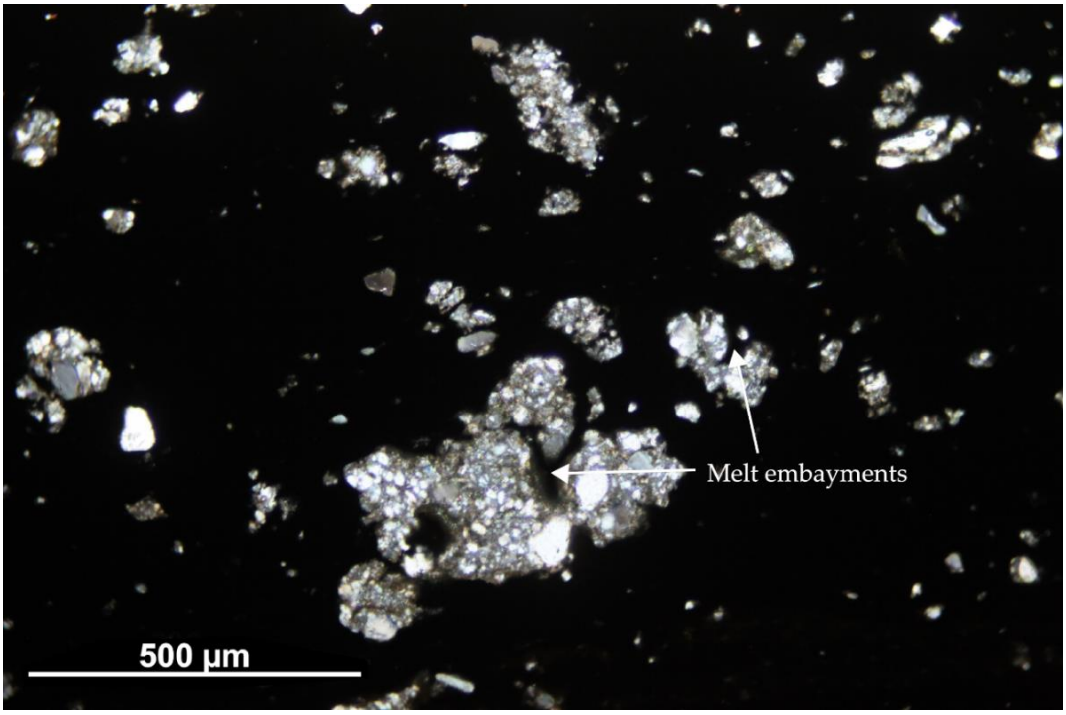

Figure 2.17. Cross polarised photomicrograph of reworked ultracataclasite clasts within a pseudotachylyte. The clasts contain extensive melt embayments.

Microlites

One pseudotachylyte vein contains radial spherulites of Ti-rich amphibole (kaersutite) which sit in a potassium feldspar (microcline) rich matrix (Figure 2.18). The spherulites lie adjacent to the pseudotachylyte margins and within the vein core where their presence/absence defines a series of asymmetrical flow bands whose limbs lie sub-parallel to the vein wall (Figure 2.19). Singular spherulite crystals commonly appear as elongate tabular crystals, although they can have a more dendritic habit. Individual crystal size is variable between and within individual spherulites, but typically 5-15 µm in length and 1-3 µm in width. Spherulites near the pseudotachylyte margin are generally smaller being <5 µm long and 1-2 µm wide. The spherulites commonly form/nucleate at high angles to remnant albite clasts and ilmenite microlites (Figure 2.20). The ilmenite microlites are most commonly granular in form, although they were also observed with dendritic habits of up to 20 µm length.

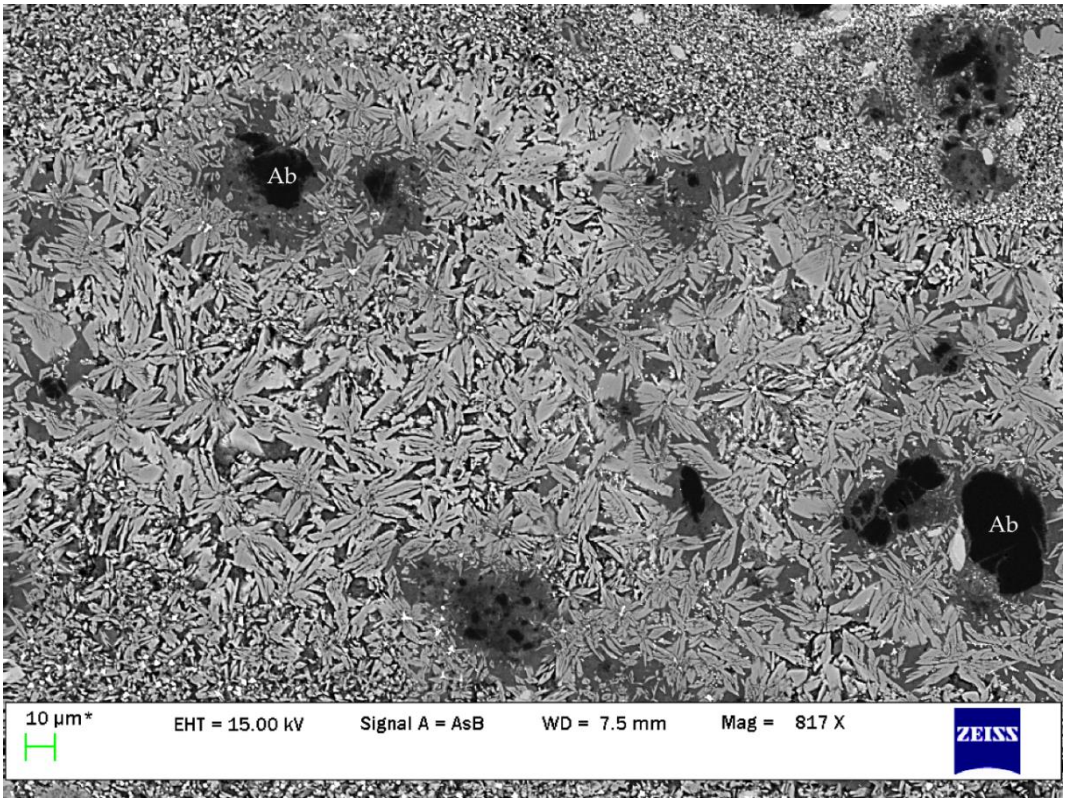

Figure 2.18. Backscatter electron image of radial spherulites of amphibole forming within k-feldspar matrix (dark grey) which appears to be a breakdown product of albite (Ab).

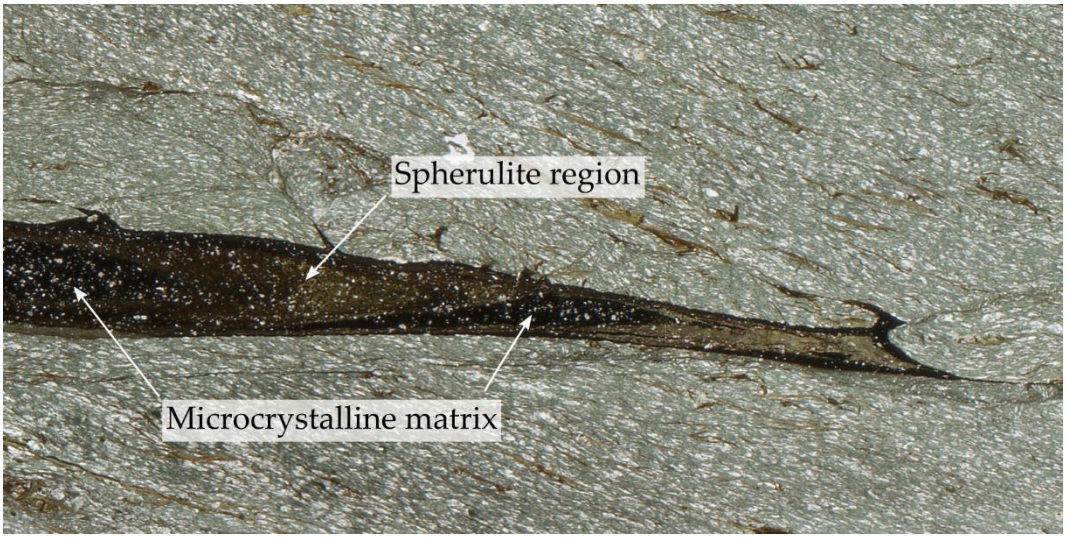

Figure 2.19. Scanned thin section displaying flow banding (colour difference) in a pseudotachylyte vein defined by the presence or absence of amphibole spherulites.

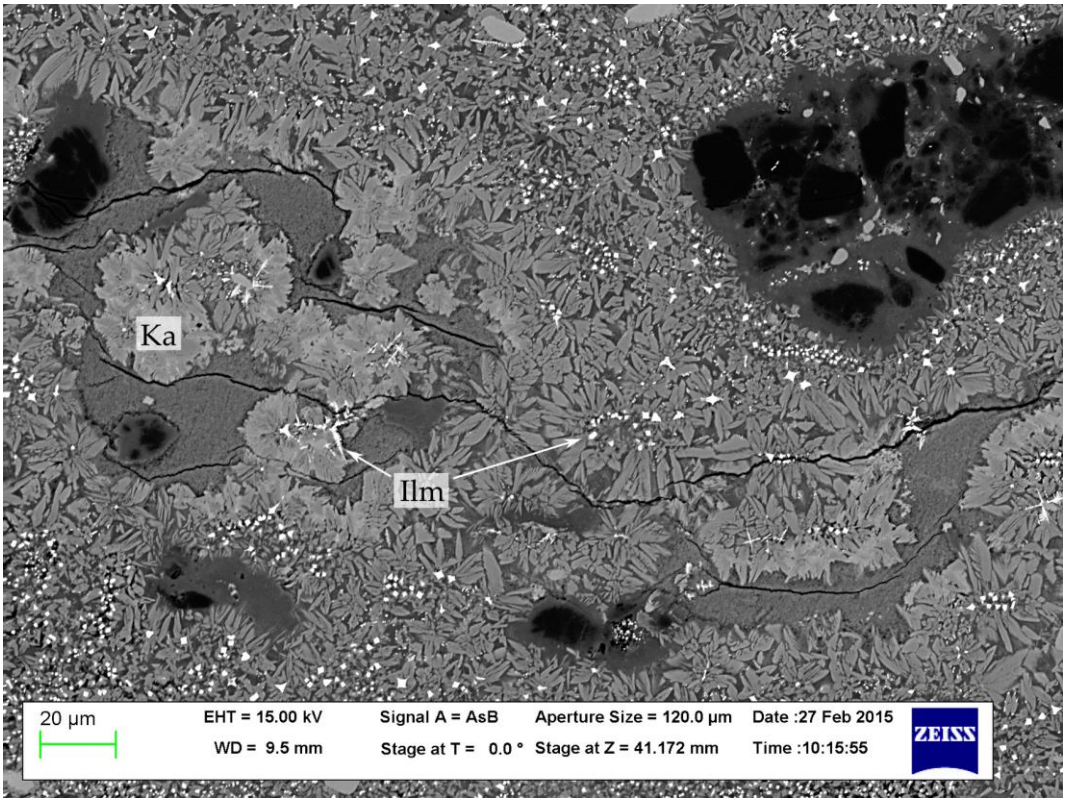

Figure 2.20. Backscatter electron image showing kaersutite spherulites (Ka) forming around ilmenite (Ilm) microlites which have either a granular or dentritic form.

Matrix

The matrices of the pseudotachylytes in Downs Creek were either microcrystalline or cryptocrystalline. Minerals within the microcrystalline matrices include very fine (<2 µm) titanite grains which form in clusters (Figure 2.21) and iron oxide grains which are largely <1 µm equant grains. The iron oxide grains are abundant in some pseudotachylyte veins, to the point where concentrations form seams that wrap around clasts (Figure 2.22). Other microcrystalline grains were too small for identification.

Quantitative chemical analysis by SEM-EDS revealed that cryptocrystalline matrices consisted of either biotite or chlorite. XRD analysis of DC8_1, a sample that was not able to be viewed in thin section, revealed a mineralogy of quartz, titanite, Fe-rich chlorite and a variation of amphibole.

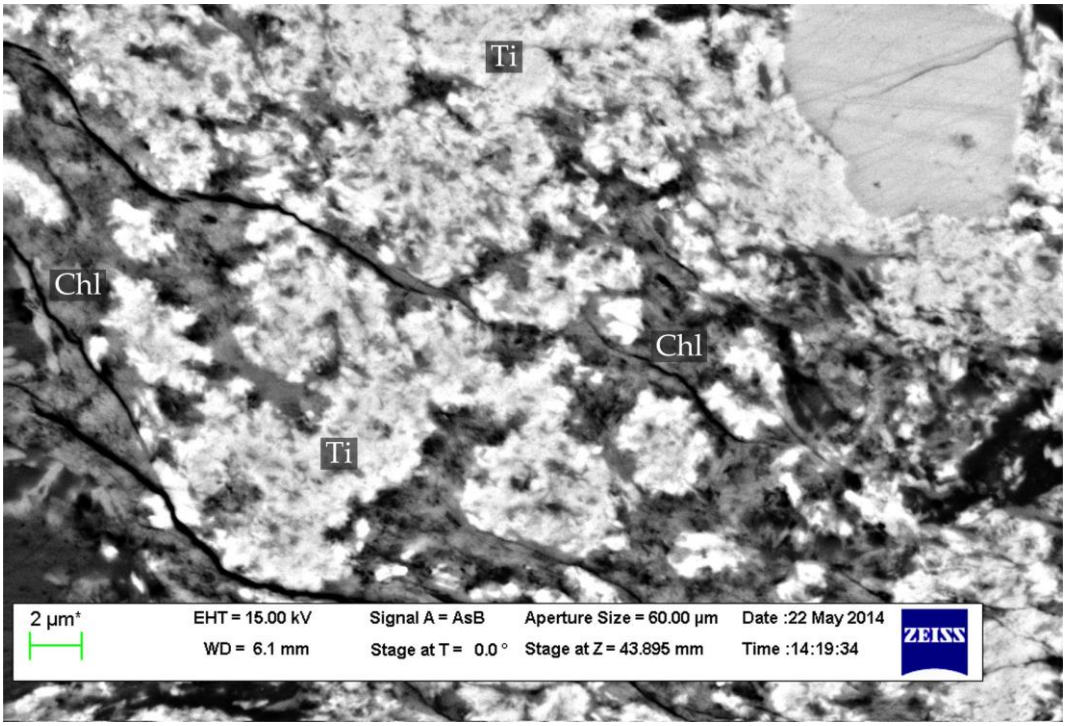

Figure 2.21. Backscatter electron image of titanite grains as clusters within a chlorite matrix of a pseudotachylyte.

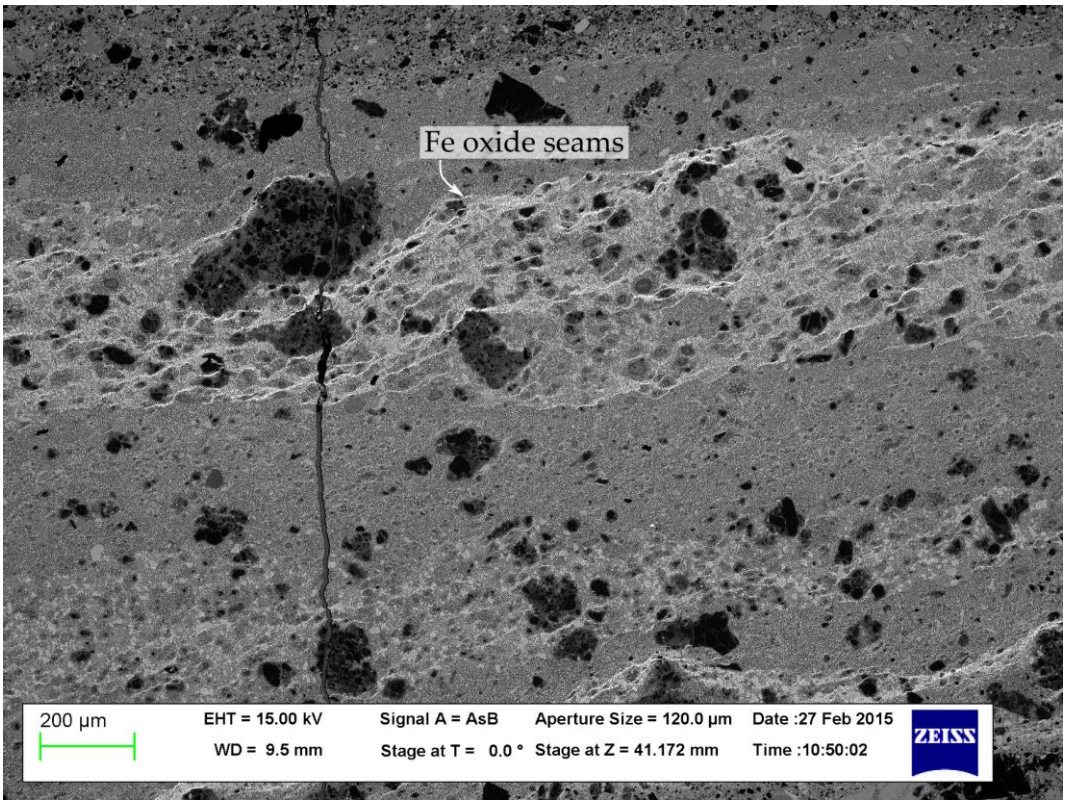

Figure 2.22. Backscatter electron image displaying concentrations of Fe-oxides form seams around fractured and thermally altered quartz and albite clasts.

Pseudotachylyte - host rock contacts

The margins of pseudotachylyte fault veins where they contact the host rocks are either sharp or diffuse. Sharp contacts commonly have very fine grained rims on the pseudotachylyte fault veins (chilled margins), such as the veins that host amygdules and spherulites (Figure 2.23). In one fault vein a more diffuse contact is observed with strands of pseudotachylyte branching into an adjacent ultracataclasite with strands reaching up to 5 mm in length and 0.25 mm in width (Figure 2.24). Ultracataclasites were found along the pseudotachylyte-host rock contact in several samples, reaching up to 2mm in width and commonly pinching out along the length of the fault vein. Clasts within the ultracataclasites consist of sub-rounded quartz, albite, epidote and rare chlorite which lie in a very fine black matrix.

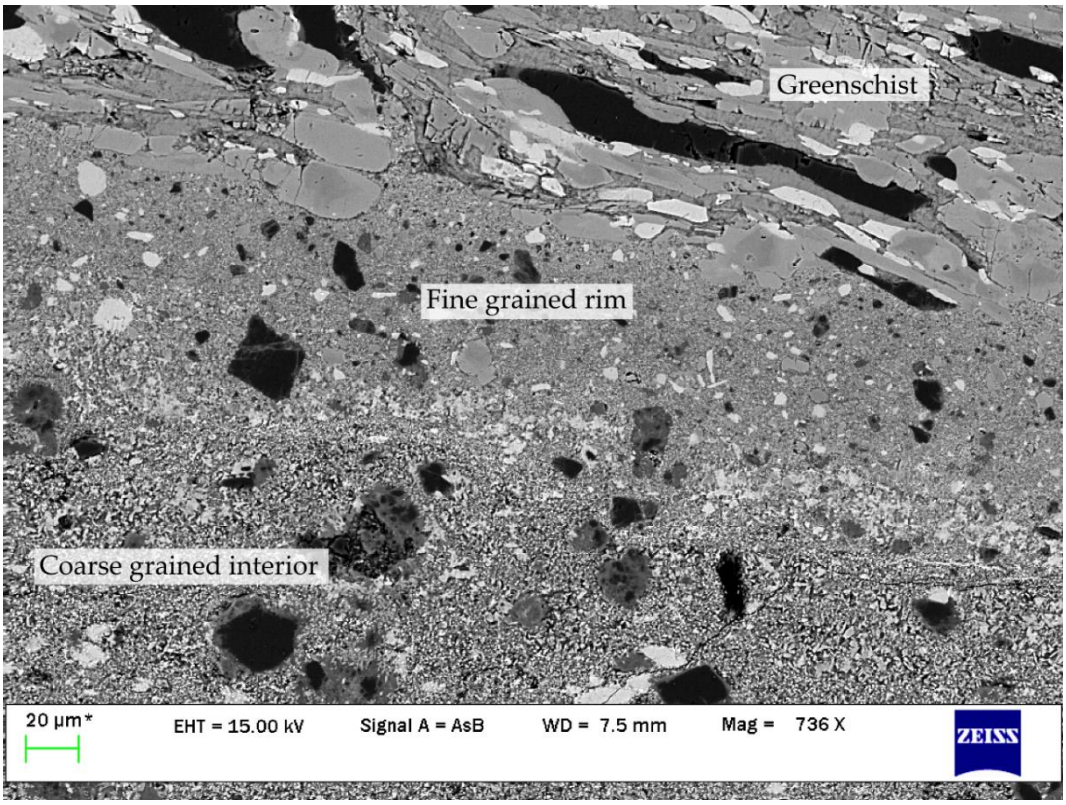

Figure 2.23. Backscatter electron image of a very fine grained rim of pseudotachylyte vein in sharp contact with the host greenschist. Inside of the fine grained rim much larger crystals have grown from the melt.

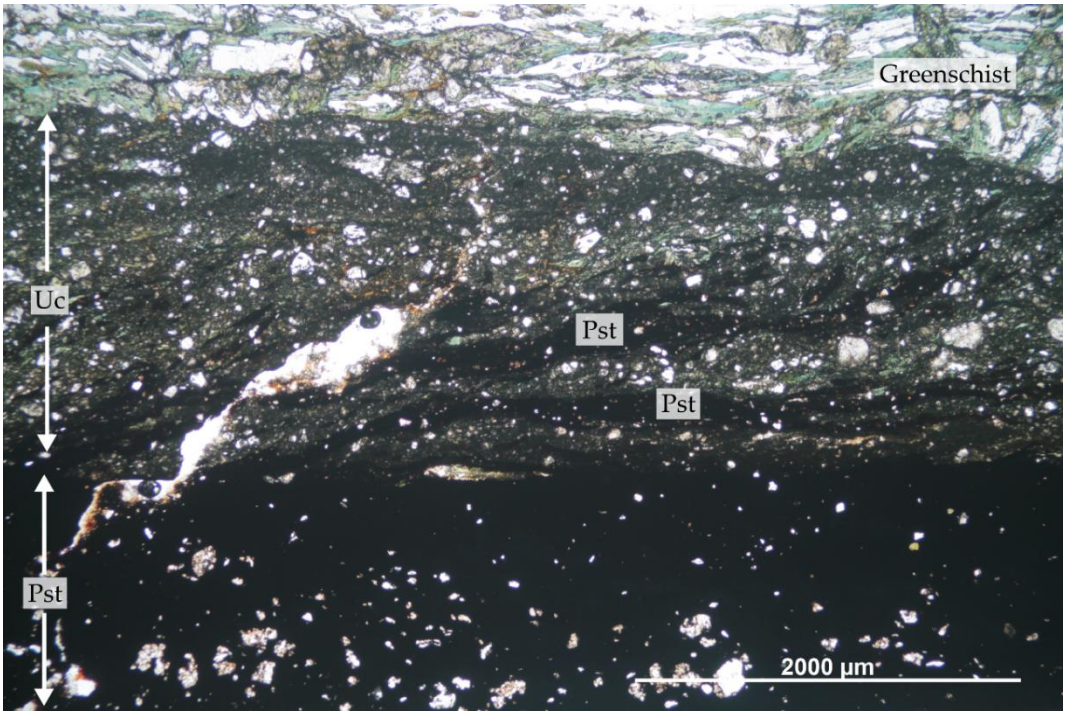

Figure 2.24. Cross-polarised photomicrograph of a diffuse margin of a pseudotachylyte (Pst) fault vein indicated by interfingering with an adjacent ultracatalasite (Uc).

Deformation associated with movement on pseudotachylyte fault veins

The formation of pseudotachylyte fault veins was associated with deformation of the surrounding greenschists. Occasionally, adjacent to fault veins, networks of very thin (<10 µm) veins of pseudotachylyte or ultracataclasite form up to 4 mm wide highly deformed zones within the greenschist. Within such zones deformation is accommodated by fractures and shear bands with small (<100 µm) amounts of separation. Motion on pseudotachylyte-bearing fault veins also created drag of the adjacent greenschist foliation, which is consistent with reverse senses of movement (Figure 2.25).

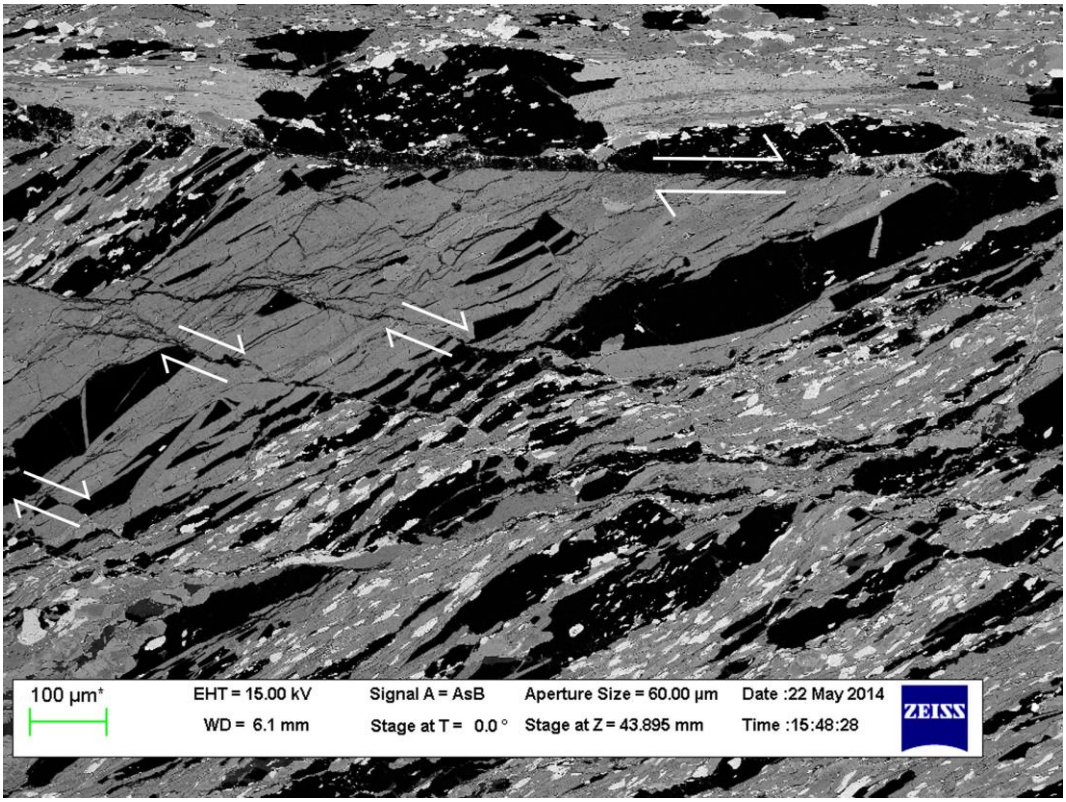

Figure 2.25. Backscatter electron image displaying brittle shearing of stilpnomelane and albite which indicates top to the left movement. In a geographic reference frame this corresponds to a top-to-the-east, reverse sense of movement.

2.4.2 Mixed pseudotachylyte – brittle fault vein

As described in Section 2.3.1, one altered, brown pseudotachylyte vein was found to occur within a small brittle fault that cross cuts the host greenschist foliation at a high angle. The pseudotachylyte within this brittle shear is distinctive compared to more 'typical' black foliation-parallel fault because it is host to ellipsoidal calcite-filled amygdules in the central parts of the vein (Figure 2.26). The amygdules reach up to 500 µm in length and 200 µm in width, although more commonly are 10s of µm in length and 10 – 20 µm in width. The long axes of the amygdules are consistently parallel or sub-parallel to the fault vein margins. Some amygdules have irregular shapes that suggests they collapsed before precipitation of the calcite fill (Figure 2.27). This vein also appears to crosscut an earlier pseudotachylyte vein, as indicated by its fine grained rim that truncates the base of an injection vein.

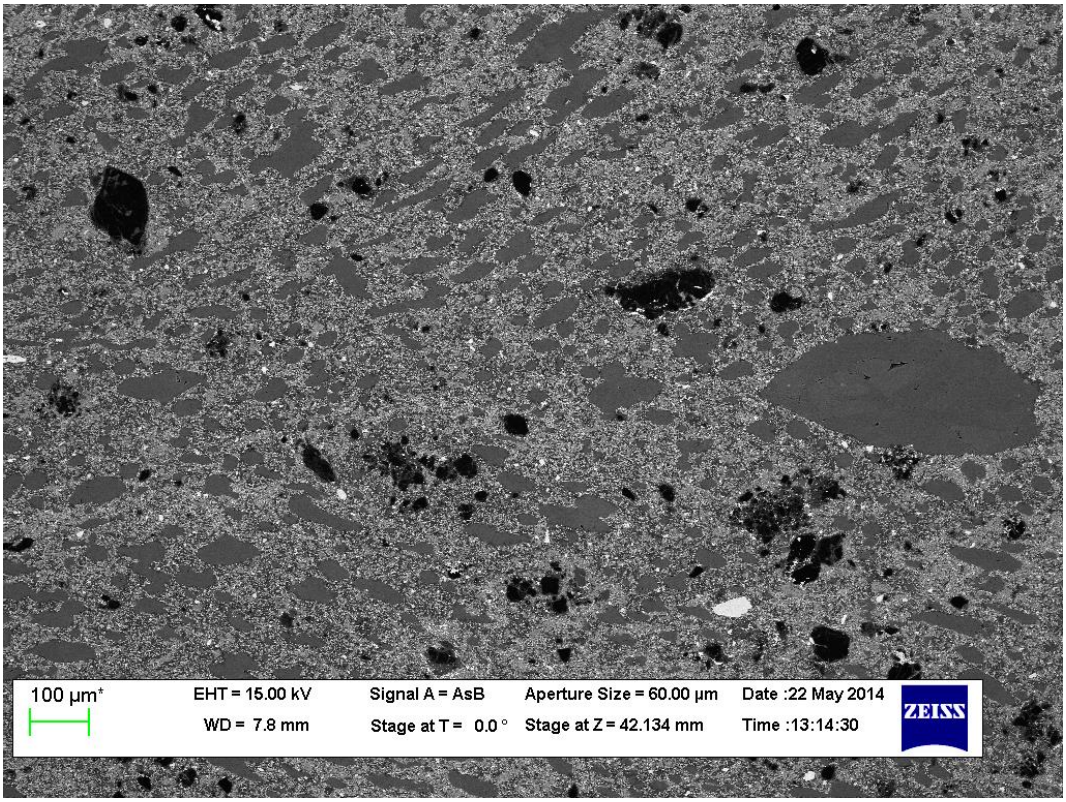

Figure 2.26. Backscatter electron image displaying elongate calcite amygdules within a pseudotachylyte vein. Amygdules are well aligned and reflect flow in the central part of this fault vein.

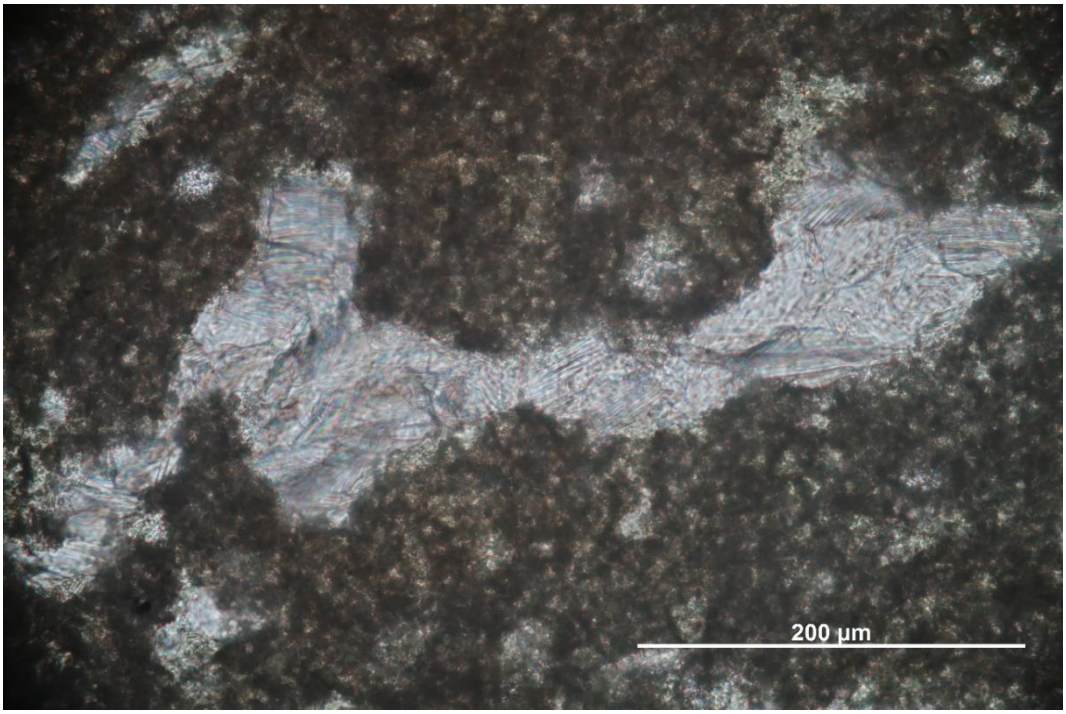

Figure 2.27. Plane-polarised photomicrograph of a collapsed calcite-filled amygdule.

2.4.3 Deformation along the main trace of the Moonlight Fault

As described in Section 2.3.3 deformation along and adjacent to the Moonlight Fault in the Matukituki Valley consists of a c. 10 m wide zone of increasingly brecciated and foliated fault rock in the footwall greyschists and a <1 m wide foliated cataclasite in the hanging wall greenschists (Figure 2.1). The microstructures of these two zones are described separately below.

Footwall greyschists: breccias and foliated cataclasite

With increasing proximity to the main trace of the Moonlight Fault the footwall rocks shows, 1) an increase in the degree of brecciation, 2) a progressive decrease in grain size, 3) an increase in the alignment of phyllosilicate phases and, 4) an increase in total matrix proportion and modal increase in the abundance of phyllosilicates (Figure 2.28).

The foliated cataclasite within the fault core contains quartz, muscovite and chlorite, with minor albite, titanite, and rutile. The foliated cataclasite consists of clast-rich domains and matrix-rich domains, the boundaries of which lie sub-parallel to the Moonlight Fault (Figure 2.29). The clast-rich domains consist largely of quartz, albite and muscovite with the quartz/albite clasts largely polycrystalline and showing cataclastic textures. Muscovite is predominately fine grained and forms an interconnected network around quartz/albite clasts (Figure 2.30). Fragments of the host greyschist are preserved and identified by folded muscovite crystals (up to 40 μm width). This muscovite shows progressive grain size reduction and reorientation into the fault plane towards the ultracataclasite region. Chlorite is present as elongate crystals infilling fractures in quartz/albite clasts.

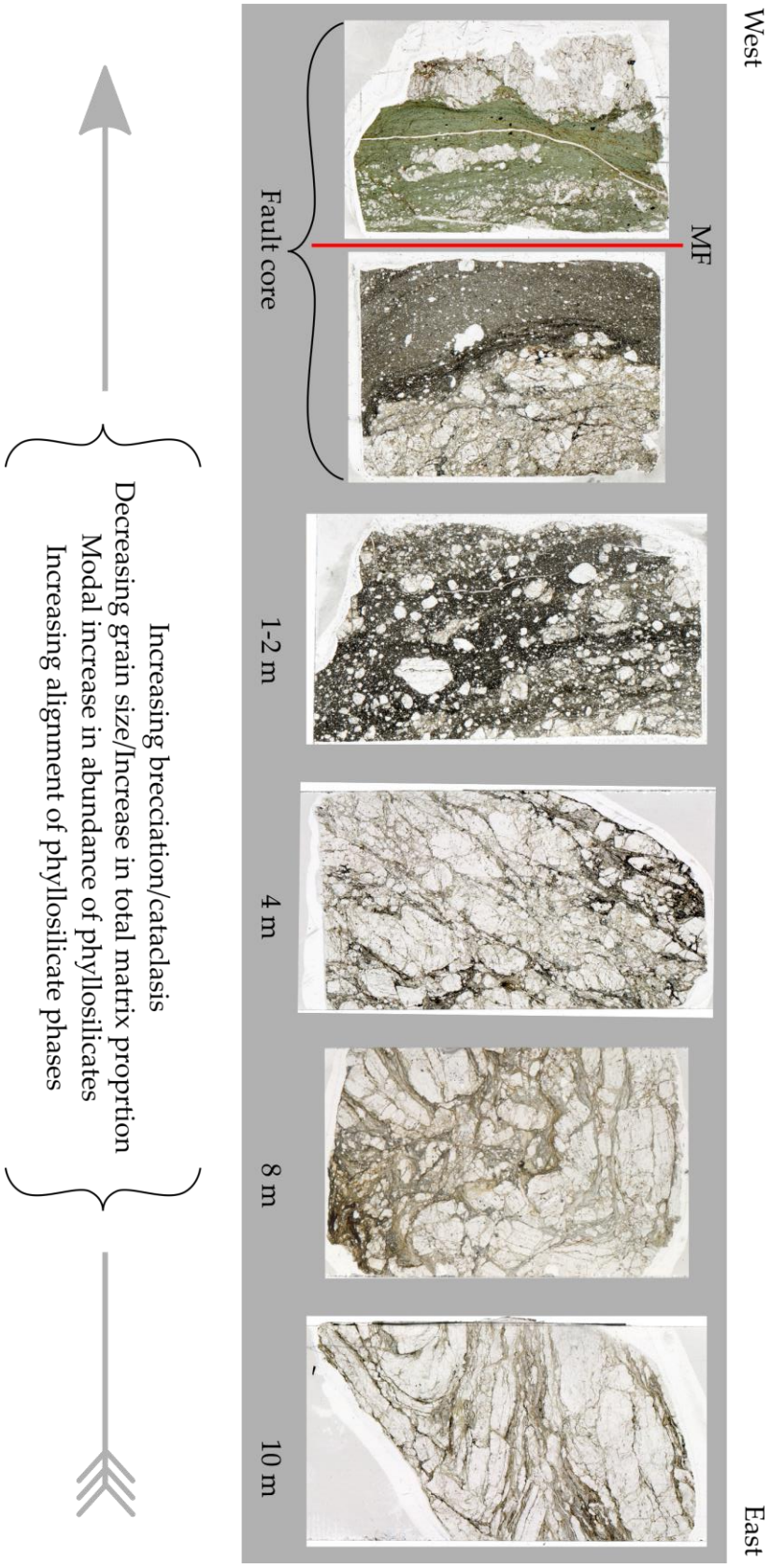

Figure 2.28. Scanned thin sections of the breccias and cataclasites associated with Moonlight Fault (MF) deformation.

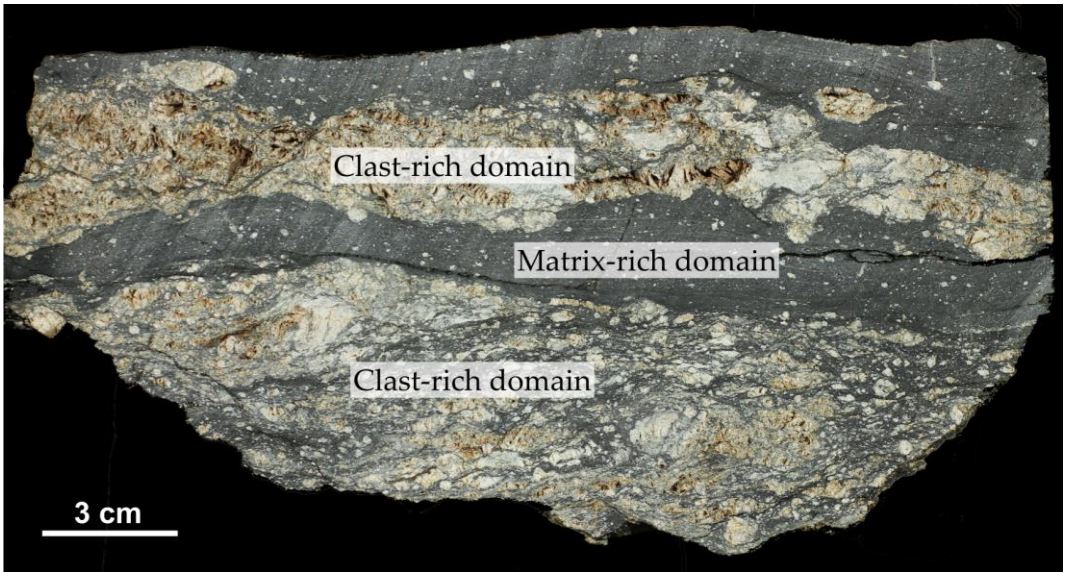

Figure 2.29. Photo of foliated cataclasite derived from the footwall greyschist. This sample was collected at a distance of <1 m from the main fault trace. The sample contains clast-rich and matrix rich segregations. Note that in the clast-rich domains the matrix forms an anastomosing network between clasts.

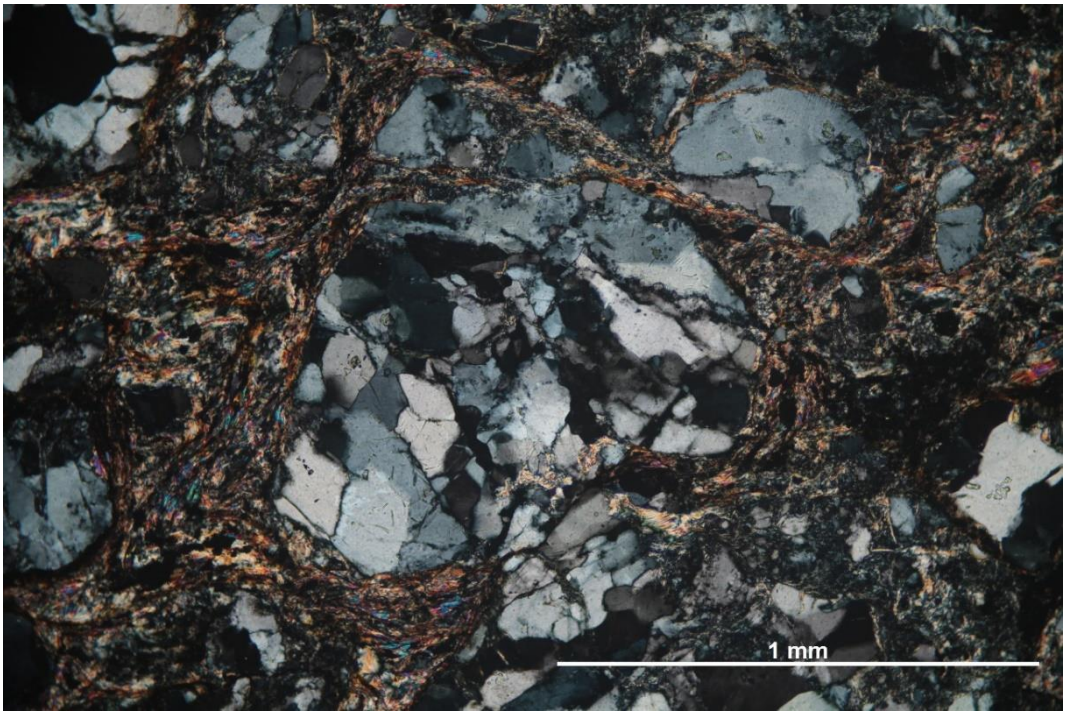

Figure 2.30. Cross-polarised photomicrograph of the clast rich layer in the foliated cataclasite 1 m from the trace of the Moonlight Fault. Phyllosilicates (Muscovite, bright 3rd order birefringence) wrap around a polycrystalline quartz clast forming an interconnected network.

The matrix-rich domain of the greyschist derived foliated cataclasite (DC17_1) is composed predominately of muscovite as identified by quantitative XRD analysis (Table 2.1) (see Appendix C). Quartz and albite clasts (<0.5 mm in size, 38.1 wt. % of total mineralogical component) often contain chlorite overgrowths giving them an elongate appearance. Microprobe analysis on newly grown muscovite and chlorite shows they contain a similar chemical composition to that of the respective host rock minerals (Figure 2.31).

Table 2.1. Quantitative XRD analysis on the bulk and <2 µm fraction of the greyschist derived foliated cataclasite (DC17.1) and greenschist derived foliated cataclasite (DC18.1).

	Mineral weight percent				
	Quartz	*Albite*	*Chlorite*	*Muscovite*	*Titanite*
Bulk					
DC17.1	23.4	14.7	7	54.9	
DC18.1	13.1	9.8	71.7		5.4
<2 µm fraction					
DC17.1	2.8	2.4	11.9	82.8	
DC18.1	1.9	0.7	96.2		1.2

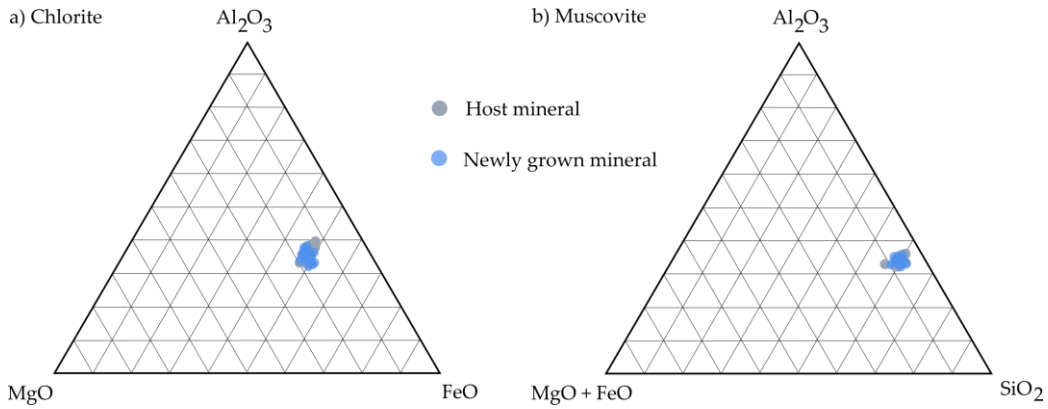

Figure 2.31. Ternary plots to show comparative chemical content of newly grown chlorite (a) and muscovite (b) to remnant chlorite and muscovite in the host rock.

Some clasts of randomly oriented quartz set in a very fine undistinguishable black matrix are present, likely remnant clasts from lower strain breccias (Figure 2.32). Within the matrix-rich domains, anastomosing seams <10 µm in width and up to 200 µm length have preferentially developed sub-parallel to the main fault orientation (steeply west dipping). These seams truncate the top and bottom of quartz and albite clasts such that many clasts are elongate. SEM-EDS analysis indicates that the seams contain concentrations of relatively insoluble titanium

(rutile) and iron oxide (magnetite) indicating that they are dissolution seams (Figure 2.33).

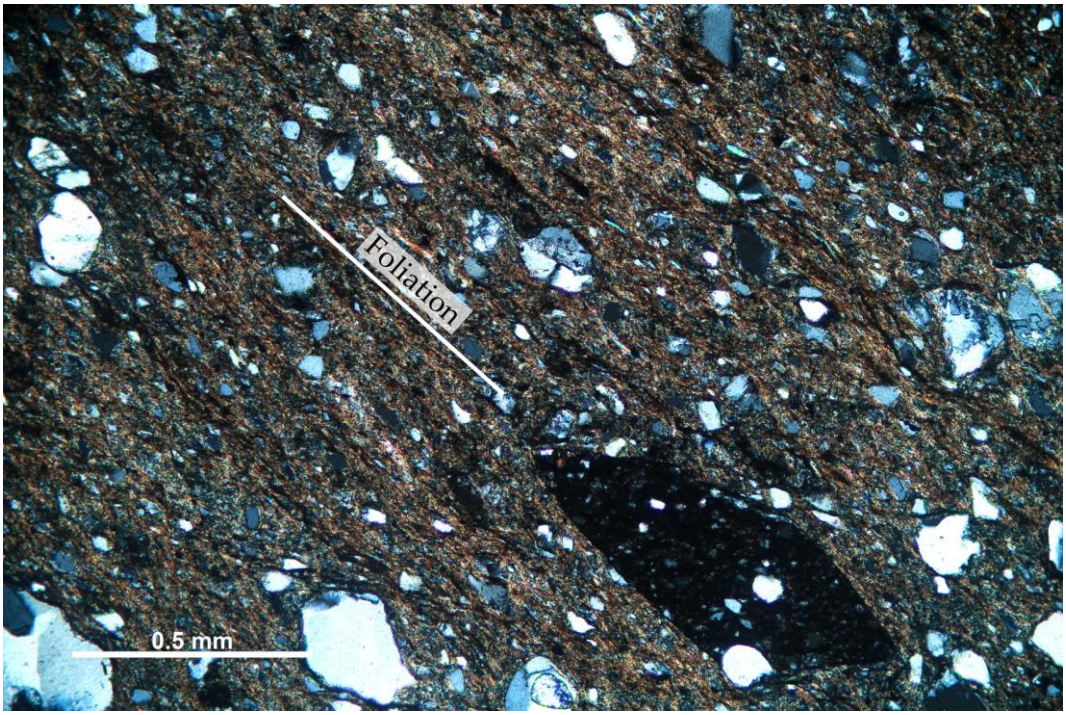

Figure 2.32. Cross-polarised photomicrograph of the matrix-rich domain in the footwall greyschist derived foliated cataclasite. Phyllosilicates form an interconnected network. The large dark clast at the bottom of the image is a clast of incorporated cataclasite.

Hanging wall greenschist: foliated cataclasite

The greenschist-derived foliated cataclasite in the hanging wall (distances <1 m from the fault trace) contains chlorite, albite, quartz, epidote and minor plagioclase, apatite, rutile and titanite. Similarly to the footwall foliated cataclasite it also contains clast-rich and matrix-rich domains. In hand specimen the clast-rich domains form as elongate boudins up to 3 cm wide within a green matrix forming an anastomosing interconnected network (Figure 2.34). Thin section analysis revealed that the clast-rich domains contain predominately albite, polycrystalline quartz with minor chlorite. The chlorite becomes highly deformed adjacent to the matrix-rich domains displaying undulose extinction and kink bands.

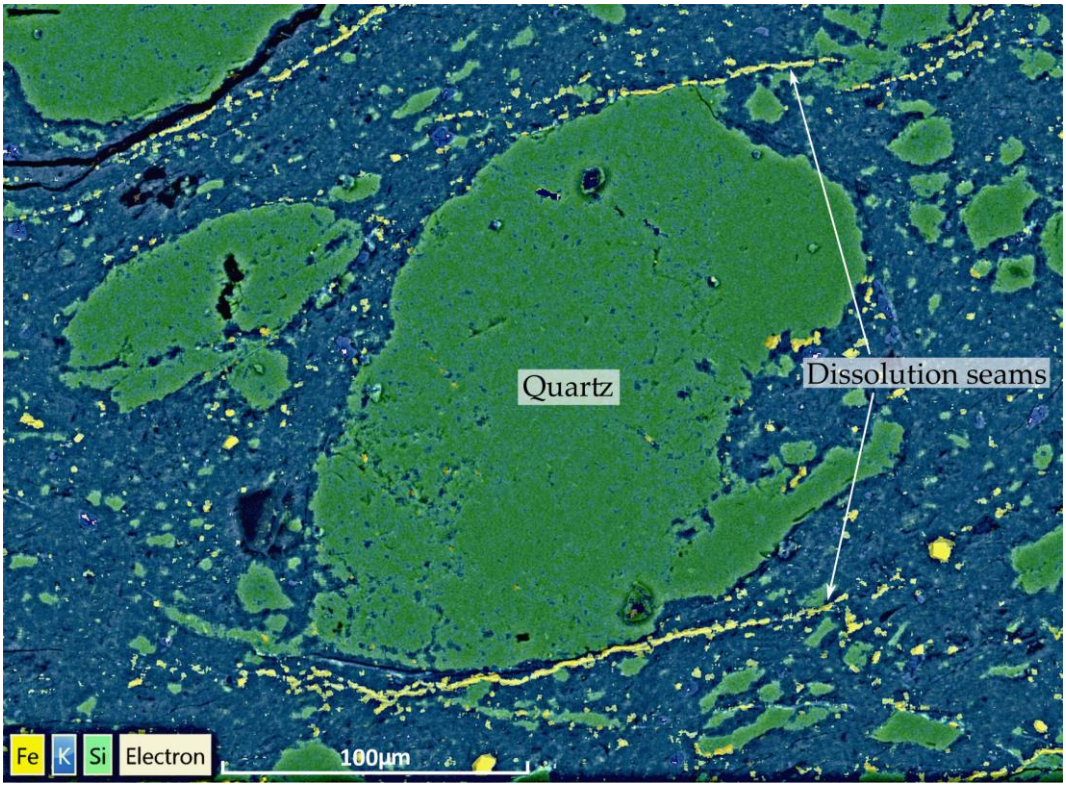

Figure 2.33. SEM-EDS map showing Fe-rich dissolution seams wrapping around a quartz clast in the foliated cataclasite within the fault core. The matrix rich in K is fine-grained muscovite.

Figure 2.34. Photo of hanging wall-derived foliated cataclasite displaying clast-rich and matrix-rich segregations. Clast-rich domains form elongate lenses which align parallel to the foliation.

The matrix-rich domains largely contains chlorite (71.7% bulk fraction, 96.2% <2 µm fraction) with minor epidote, quartz and albite (Table 2.1). The matrix is made entirely of chlorite grains which backscatter electron imagery revealed were up to 5 µm wide. Chlorite also forms in tails around quartz and albite clasts (Figure 2.35).

Epidote forms either very fine grained masses or small (<0.2 mm) elongate crystals which align parallel or sub-parallel to the foliation. Quartz and albite clasts commonly have irregular shapes, infilled with chlorite. Albite clasts are occasionally microboudinaged, fracturing sub-perpendicular to the grains long axes. Albite clasts were also seen protruding into one another with opaque minerals along the boundary indicating that dissolution has taken place (Figure 2.36). Within the matrix foliation-parallel anastomosing black seams of up to 20 μm width and 400 μm length contain concentrations of opaque minerals. These seams are particularly prevalent adjacent to matrix poor regions and are found wrapping around ends of clasts. SEM-EDS analysis revealed these are made up of relatively insoluble iron oxide (magnetite) indicating they are dissolution seams (Figure 2.37).

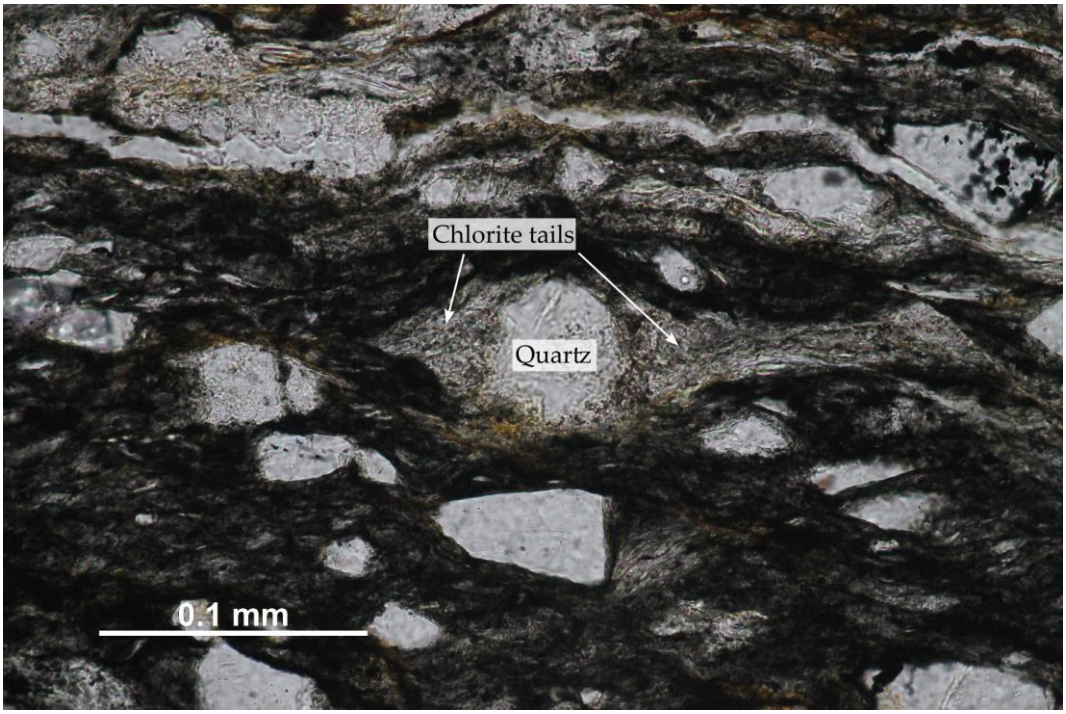

Figure 2.35. Plane-polarised photomicrograph showing overgrowths of chlorite upon a quartz clast. These tails align parallel to the foliation.

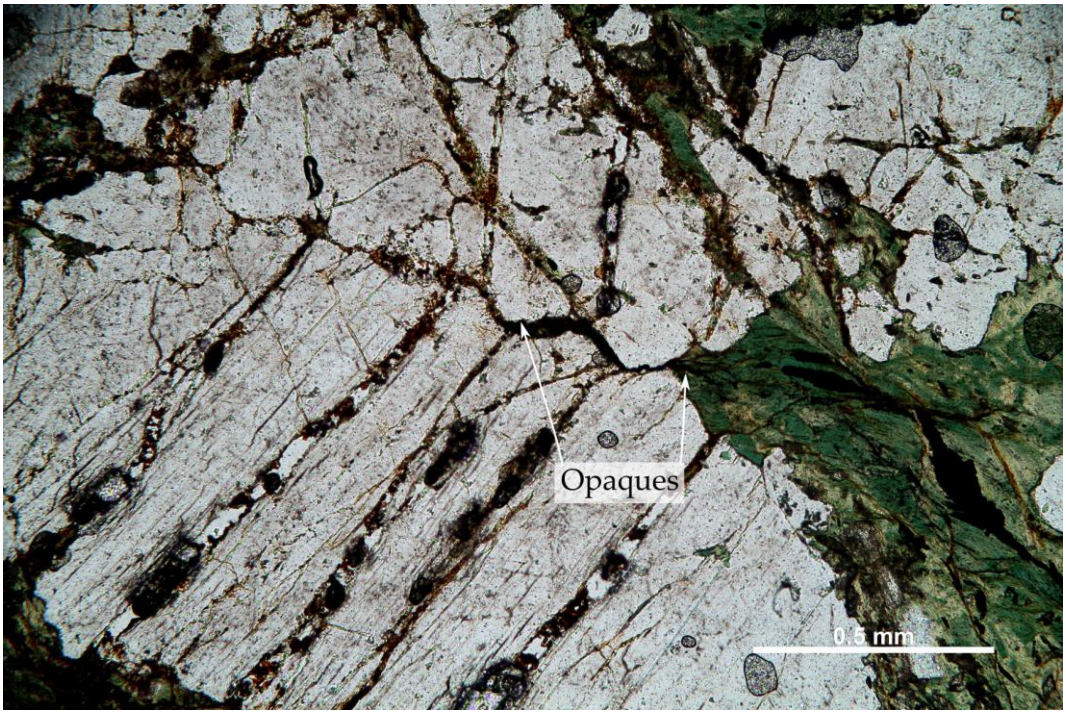

Figure 2.36. Cross-polarised photomicrograph of two albite grains showing serrated edges along their contact which contains concentrations of opaque minerals. These form a seam that passes into the matrix indicating dissolution has occurred.

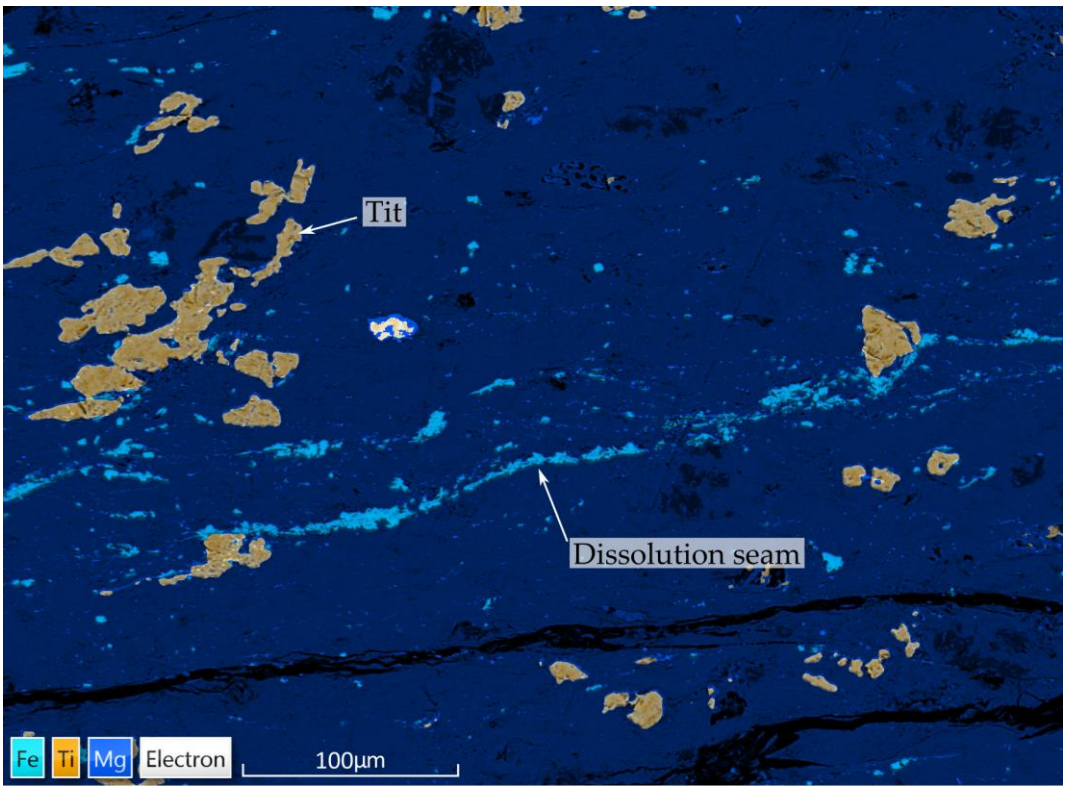

Figure 2.37. SEM-EDS image of dissolution seams of magnetite (iron oxide) forming seams in the foliated cataclasite within the fault core. The seams lie in a chlorite rich matrix (here represented by Mg) and wrap around titanite clasts (Tit).

2.4.4 Small-scale faults

The late-stage brittle fault networks in the hanging wall consist of green cataclasites with ultracataclasites close to slip surfaces. These consist of chlorite, ferro-actinolite, quartz, albite, muscovite, stilpnomelane, epidote, clinozoisite, calcite and titanite. The cataclasites, by definition, contain <30 % large clasts >2 mm with a matrix (<0.1 mm clasts) making up 50-90% of the rock. The matrix contains a wide range of clast sizes and host to sub-rounded to sub-angular clasts of greenschist of largely <10 μm-1 mm, though at times are >1 cm (Figure 2.38). The ultracataclasites are differentiated from the cataclasites a greater matrix proportion (>90%). They also contain a wide range of clast sizes with rounded to sub-rounded clasts varying from <10 μm-1 mm though are typically <0.5 mm. Some of the ultracataclasites were foliated although were too friable for samples to be taken. The matrix of the ultracataclasite has the same mineralogy as the larger clasts though the grain sizes were much finer (<20 μm).

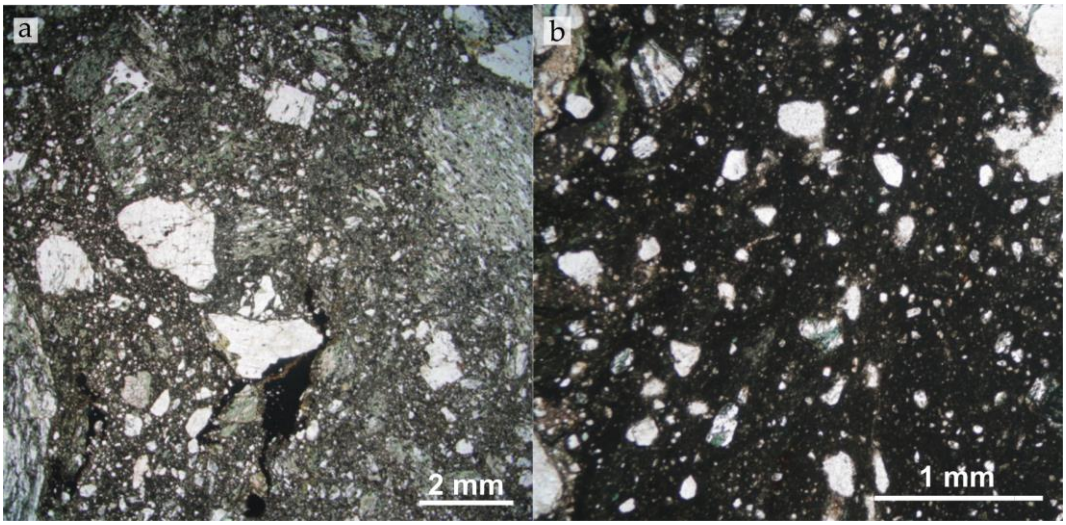

Figure 2.38. a) Cross-polarised photomicrograph of a cataclasite containing large sub-angular to sub-rounded clasts. b) Plane-polarised photomicrograph of an ultracataclasite defined by a much higher proportion of matrix.

3. Stony Creek

3.1 Overview

Stony Creek lies c. 20 km north of Queenstown with outcrops of the Moonlight Fault located c. 5 km upstream of its confluence with the Shotover River. Here, TZIV greenschist in the hanging wall is juxtaposed against a thin (<10 m) sedimentary package in the footwall that lies in faulted contact with TZIV greyschist (Figure 3.1). The Moonlight Fault core is exposed in a narrow gully containing green and black gouges. Observation of the hanging wall was limited due to a few metres immediately west of the fault core due to a steep cliff and gorge forming in relatively competent hanging wall greenschist. In this chapter, firstly the host rocks will be described followed by the structure of the fault zone and the microstructures observed in fault related rocks.

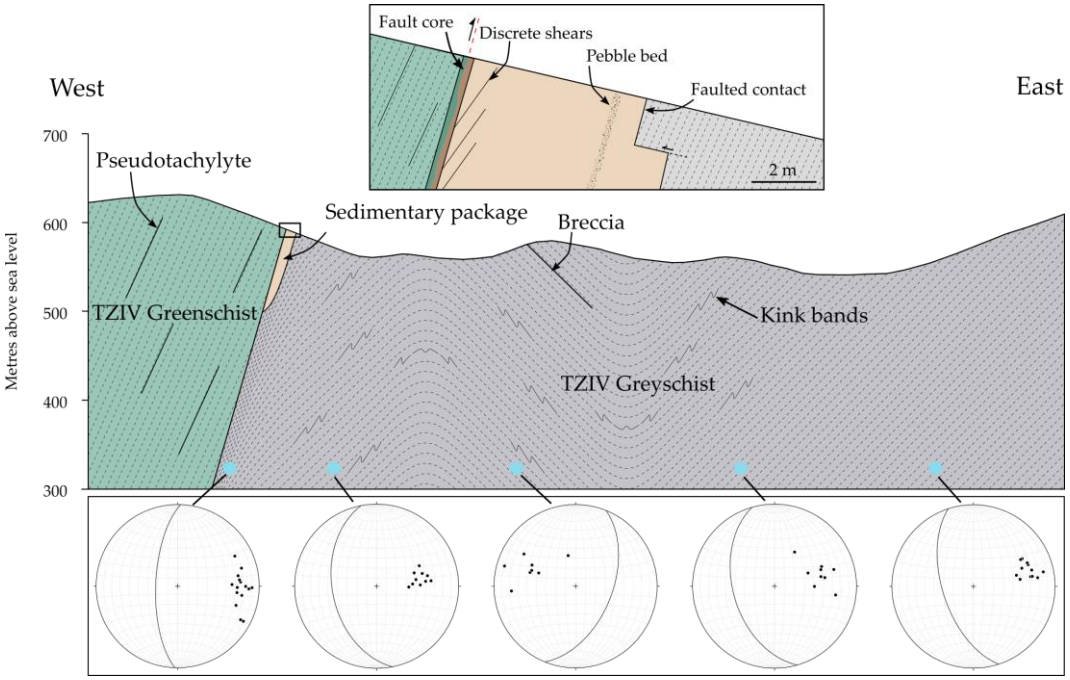

Figure 3.1. Cross section perpendicular to the Moonlight Fault in Stony Creek, illustrating the structure of the fault zone and wall rocks. Equal area lower hemisphere projections showing the orientation of the average foliation and poles to foliation within the fold limbs. Note the parasitic folds within the fold limbs.

3.2 Host Rocks

3.2.1 Hanging wall

Greenschist

The hanging wall greenschist is grey-green with lighter green epidote rich layers and dark grey phyllosilicate rich layers. Magnetite porphyroblasts of up to 3 mm were found in float. The greenschist contains a compositionally spaced foliation that steeply dips to the west (001/67 W) sub-parallel to the dip of the Moonlight Fault (Figure 3.2). The greenschist predominately consists of chlorite, epidote and albite with minor calcite, quartz and titanite. Chlorite appears as elongate crystals (up to 0.2 mm in width) and predominately displays brown – purple anomalous interference colours indicative of an Mg-rich end member. Epidote is abundant, appearing as high relief, disaggregated anhedral crystals (0.3 mm) and small (<0.1 mm) crystals that form granular clusters. Albite grains are commonly elongate, which with chlorite largely define the foliation. Calcite appears in veins and occasionally as isolated crystals displaying characteristic twinning.

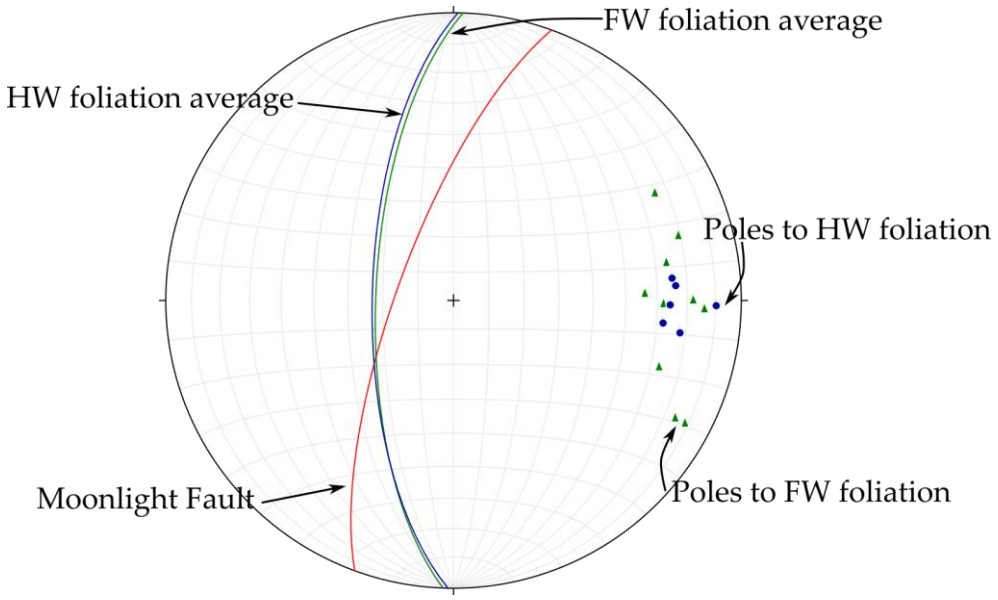

Figure 3.2. Equal area lower hemisphere projection showing the sub-parallel nature of the hanging wall greenschist and footwall greyschist foliation adjacent to the Moonlight Fault.

3.2.2 Footwall

Sedimentary Package

In the footwall immediately adjacent to the fault core is a c. 10 m thick package of sedimentary rocks (Figure 3.3).

Figure 3.3. An up to 10 m thick package of sedimentary rocks in the footwall of the Moonlight Fault.

The base of this sedimentary package is marked by a well-developed series of fault surfaces with dip-slip slickenlines (see Section 3.3.3). A pebble bed was

identified and boulders of the sediments were found in float (Figure 3.4) which show that the sediments are, at least in part, well indurated siliceous sandstones with occasional quartz pebble beds reaching up to 20 cm in thickness. The quartz pebbles are rounded to well-rounded and <1-4 cm in size.

Figure 3.4. Boulder of quartz sandstone with quartz pebble beds.

Thin section analysis of the massive portion of the sediments shows that they predominately consist of quartz, albite and calcite with minor muscovite (<1%) and rare chlorite. Quartz and albite clasts are on average 0.2 mm, sub-rounded clasts that lie within a calcite matrix. Calcite crystals (0.4 mm) also appear in veins showing characteristic twinning. Muscovite and chlorite appear as elongate clasts (0.05 mm width).

Greyschist

The greyschist in the footwall is light grey with discontinuous quartz/albite layers up to 3 cm thick. It is highly fissile and with a spaced foliation that contains irregular kink bands and chevron folds (Figure 3.5).

Figure 3.5. Representative photo of the footwall greyschist with kink banding.

Adjacent to the main trace of the Moonlight Fault the foliation dips steeply to the west (average 82/68W). To the east the foliation defines a large antiform-synform pair with wavelengths on the order of a few hundred metres (Figure 3.1). The greyschist at the sediment contact is complexly deformed and deeply weathered for up to 5 m.

3.3 Fault Zone Structure and deformation

3.3.1 Fault core

The principal slip zone is a well-defined, continuous and planar feature that has a northerly strike and dips steeply to the west (020/74 W). It is flanked by 15 - 20 cm of dark grey/black foliated gouge to the west and 20-25 cm of green foliated gouge to the east (Figure 3.6).

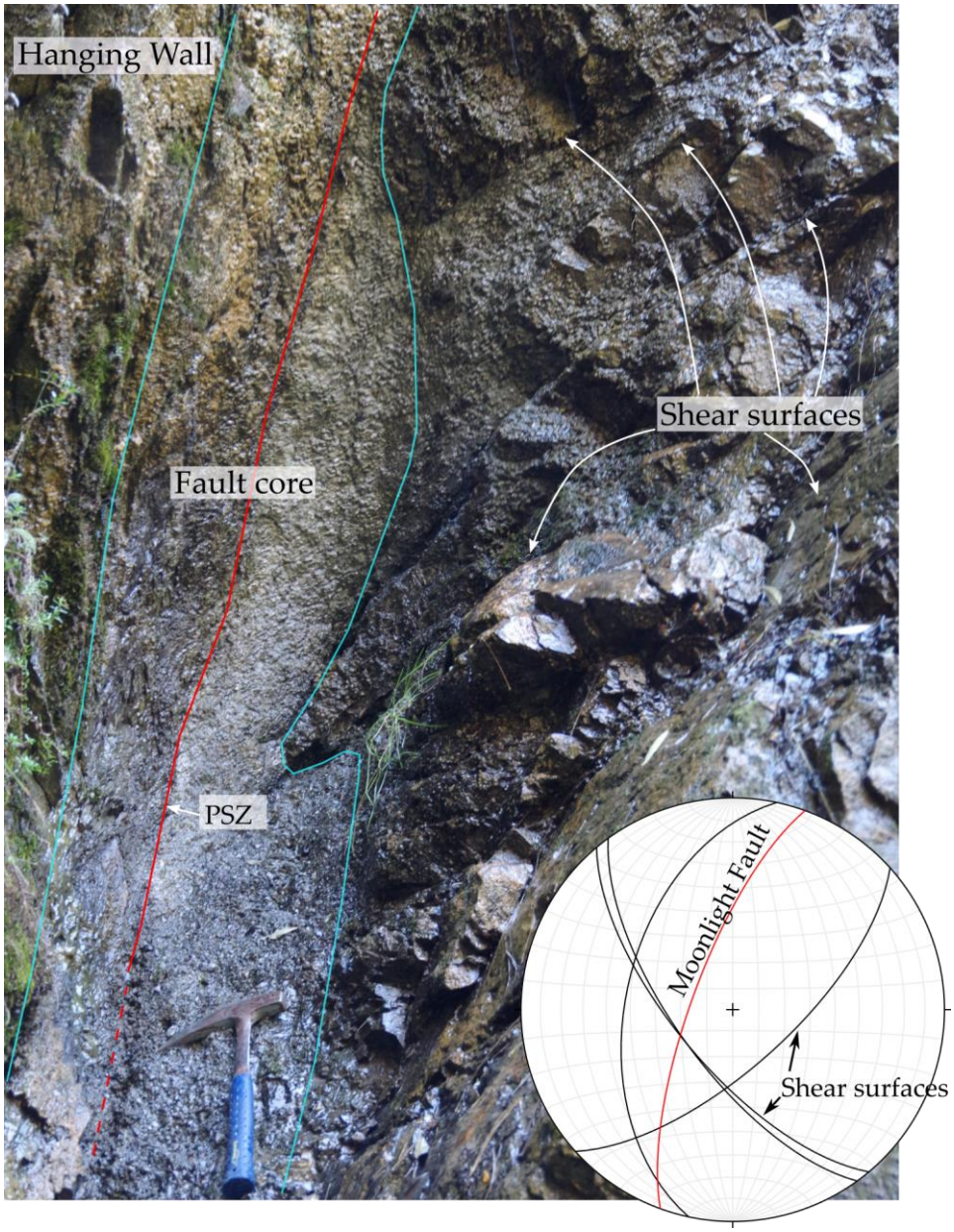

Figure 3.6. Discrete shear surfaces within the sedimentary package offsetting the margin of the fault core, but not the principle slip zone (PSZ). Equal area lower hemisphere projection showing shear surfaces (black planes) in relation to the Moonlight Fault.

3.3.2 Hanging Wall

In-situ observation of the structure of the hanging wall is limited to a few metres adjacent to the fault core. In this area, fault-related deformation is brittle in nature with pseudotachylyte and one 3 cm thick green cataclasite which cross-cut the foliation at a high angle (Figure 3.7).

One pseudotachylyte vein was present *in-situ* as a foliation parallel continuous, planar vein of up to 2 mm width, identified by its dark black aphanitic nature. Boulders of greenschist in the creek host abundant pseudotachylyte veins up to 2 cm wide, with melt pools and injection veins up to 3 cm long (Figure 3.8).

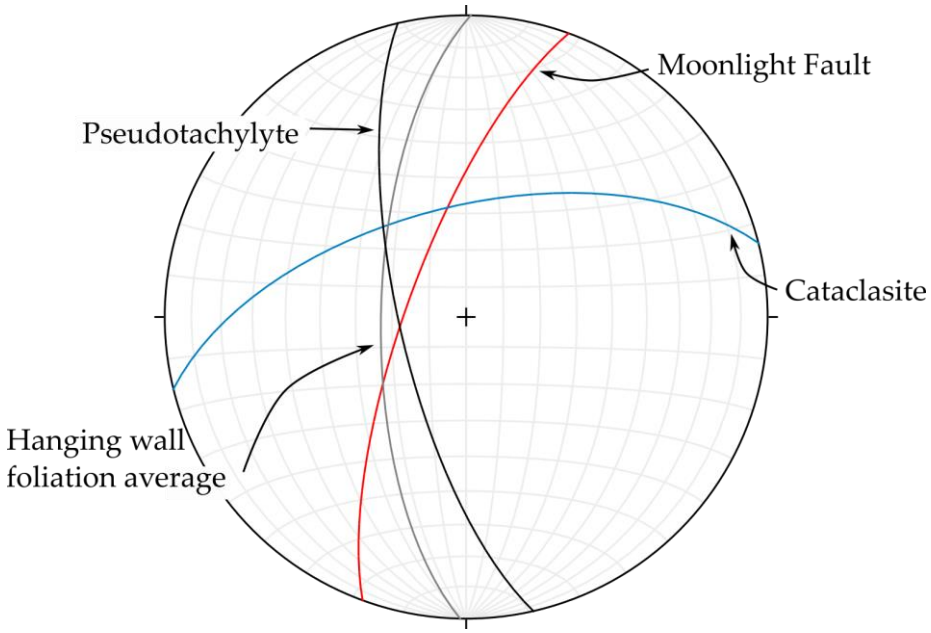

Figure 3.7. Equal area lower hemisphere projection of structural features in the hanging wall. The hanging wall foliation and pseudotachylyte lie sub-parallel to the Moonlight Fault while the cataclasite bearing fault cross cuts the foliation and pseudotachylyte.

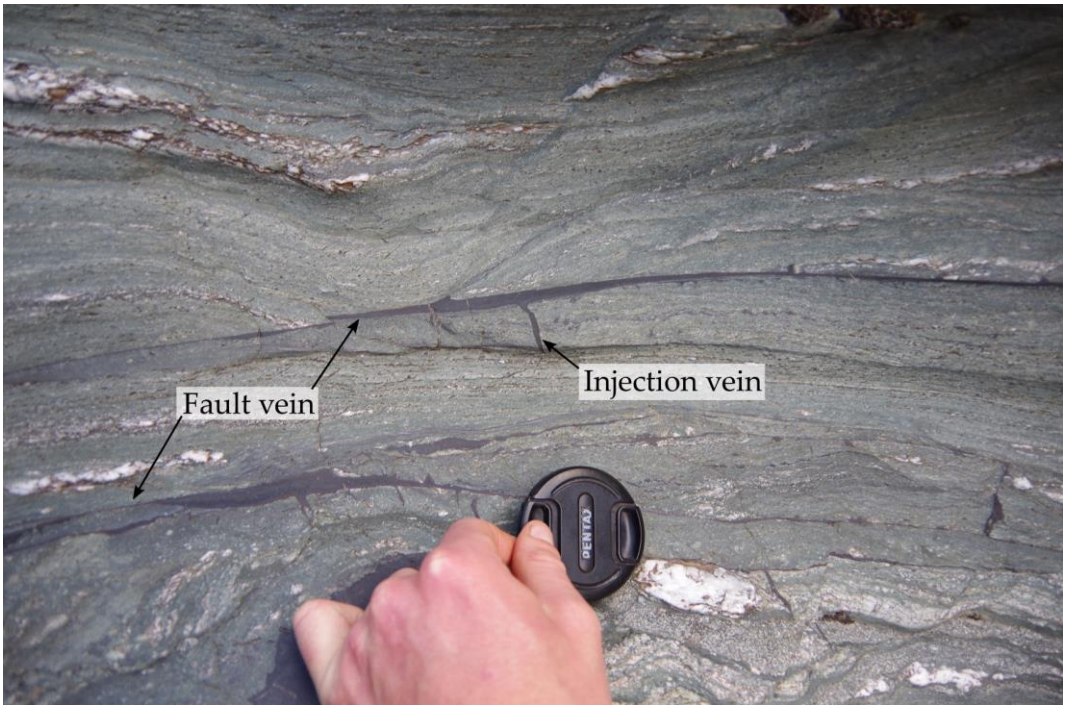

Figure 3.8. Pseudotachylyte fault and injection veins in hanging wall greenschist float.

3.3.3 Footwall

Small faults at the top of the sedimentary package

The sedimentary package is host to discrete faults that contain slickensided black slip surfaces. These faults throughout the sedimentary package have highly variable orientation (Figure 3.6). Some of these small faults enter the fault core, offsetting the eastern margin but not the principle slip surface.

Shear fractures at the base of the sedimentary package

The base of the sedimentary package is defined by well-developed slip surfaces that contain steeply-dipping slickenlines suggesting dip-slip movements (Figure 3.9). The slip surfaces were inaccessible but lie sub-parallel to the plane of the Moonlight Fault. The surface appears to have been offset by a series of regularly spaced backshears that cut across the greyschists and upwards into the sedimentary package. As a result the slip surfaces at the base of the sediments now forms a series of steps, defined by 1 – 2 m offsets. The back-shears do not appear to displace the main plane of the Moonlight Fault.

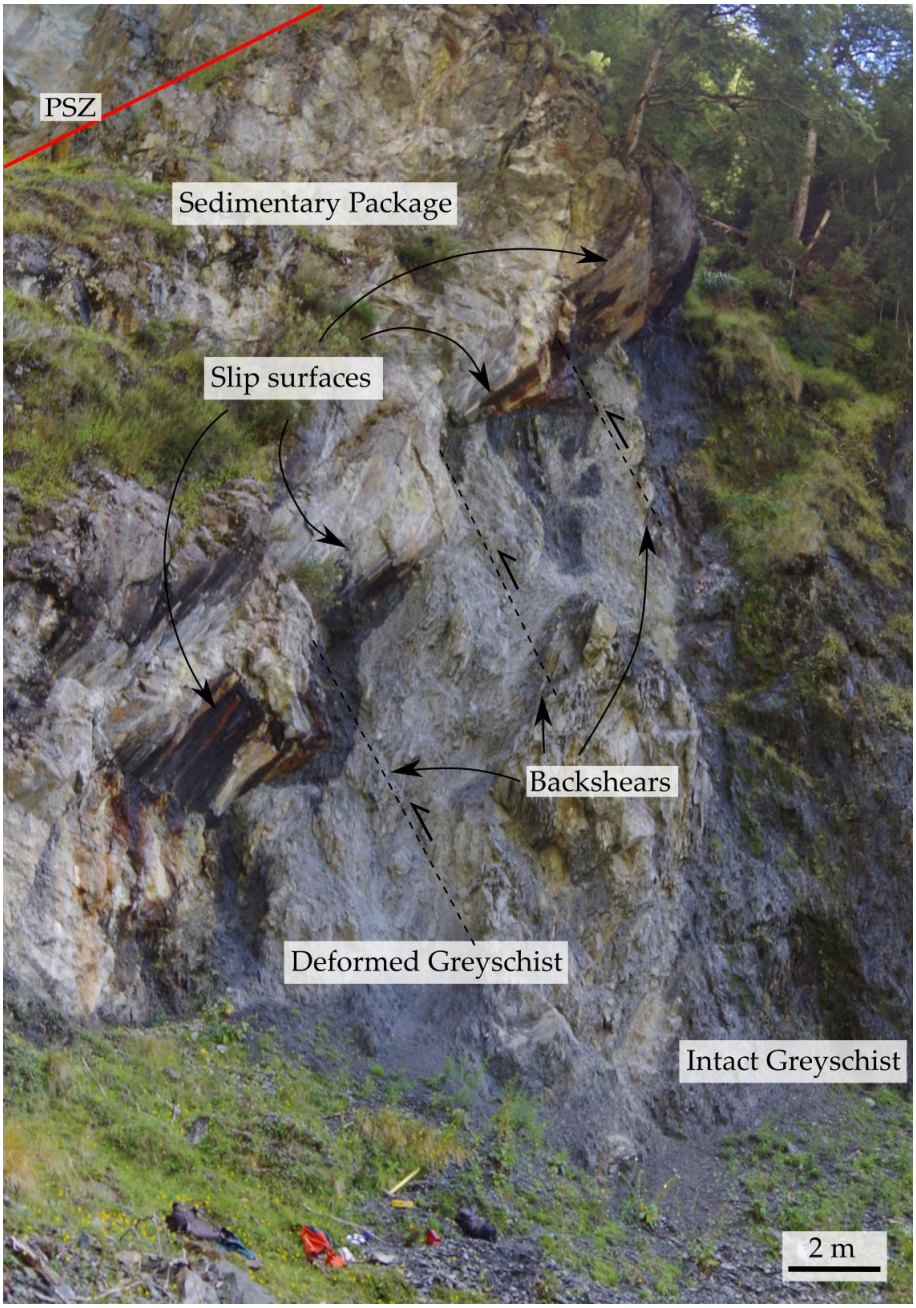

Figure 3.9. Slickensided base of sedimentary package likely offset by backshears forming a step-like appearance.

Breccia in footwall greyschists

In the easterly dipping limb of the anticline c. 200 m from the main fault trace (Figure 3.1) an up to 1 m wide well-indurated breccia is present striking NNW and dipping 44˚ E (Figure 3.10). Inherited chevron folds are preserved from the greyschist host rocks, however elsewhere a new foliation, defined by dark seams, has developed sub-parallel to the orientation of the breccia (Figure 3.10).

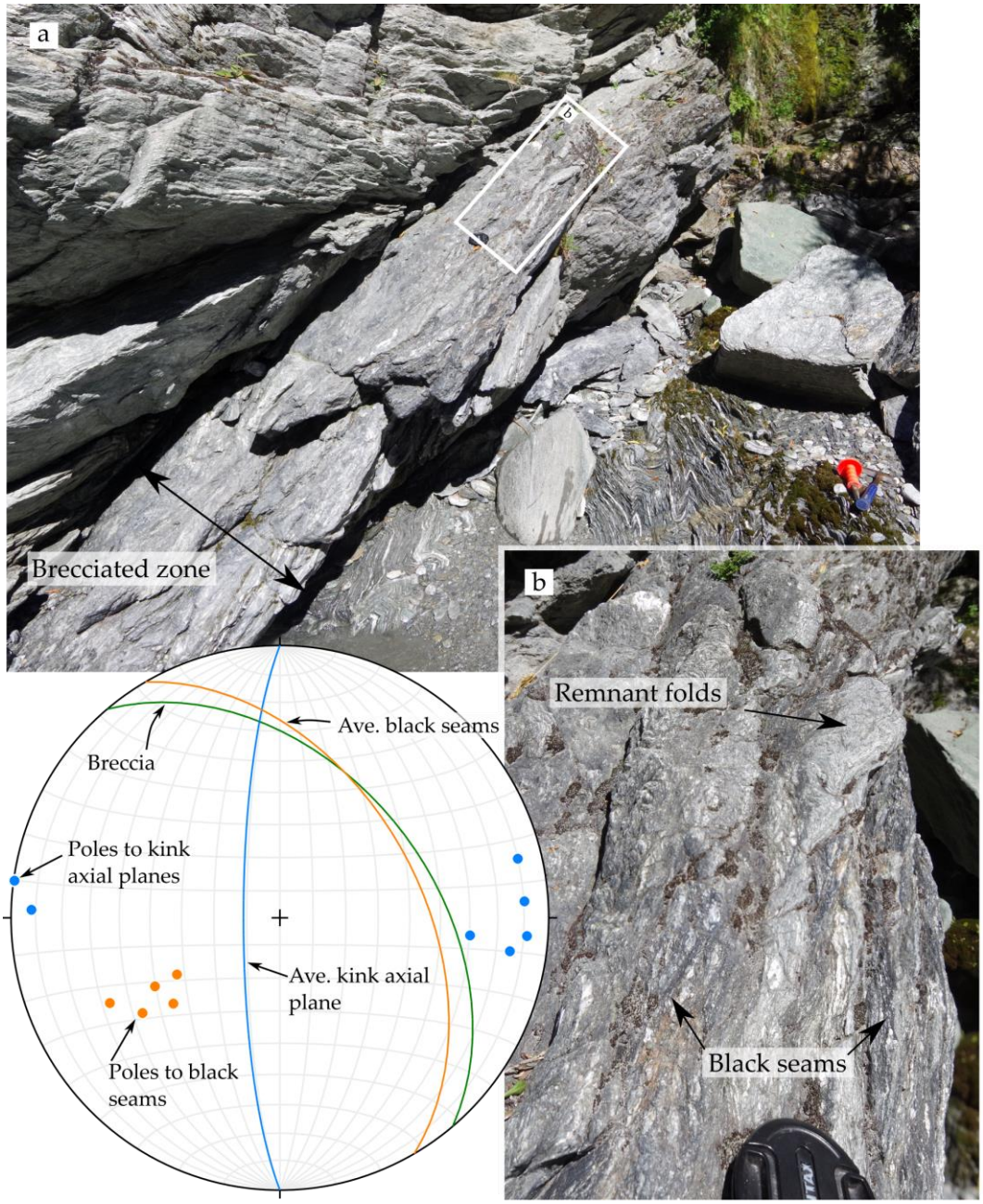

Figure 3.10. a) 1 m wide breccia crosscutting footwall greyschist. b) The breccia is host to remnant folding and a newly formed foliation defined by dark black seams. Equal area lower hemisphere projection showing the parallel nature of the black seams to the breccia orientation.

Greyschist folds

The macro scale folds with wavelengths of c. 400 m in the footwall greyschist are also represented at a smaller scale by kink bands and chevron folds forming as parasitic z-, s- and m- or w-folds in the macroscale fold limbs (Figure 3.1). The kink bands and chevron folds fold axial planes are generally north – south striking and dip sub-parallel to the macro scale fold limbs. The macro scale fold has an east vergence indicting that it may have formed during reverse movements.

3.4 Fault rock microstructures

3.4.1 Hanging Wall

Pseudotachylyte

Pseudotachylyte was observed in the hanging wall greenschist in Stony Creek, identified by its aphanitic nature and injection veins, however the sample retrieved from the field is less clear. The vein is <5 mm in width with an up to 2 mm ultracataclasite present along one side of the vein, pinching out along its length. The rest of the contact with the greenschist is highly irregular, as indicated by it wrapping around a large opaque grain (Figure 3.11). Clasts within the vein contain blurry rims and include quartz, apatite, titanite, albite, rare epidote and clasts of adjacent ultracataclasite. Quartz and albite clasts are up to 1 mm wide though are predominately <0.3 mm. Chlorite also occurs as small, randomly oriented laths up to 6 μm in length and 1-2 μm in width (Figure 3.12). Some remnant chlorite is also present as large grains that pass through quartz/albite clasts and, at times, lies in contact with the matrix. Titanite largely appears as <10 μm anhedral clasts. Iron oxides are liberally distributed throughout the vein ranging in size from sub-micron to 20 μm, a feature only associated with two pseudotachylyte samples from Downs Creek in the Matukituki Valley.

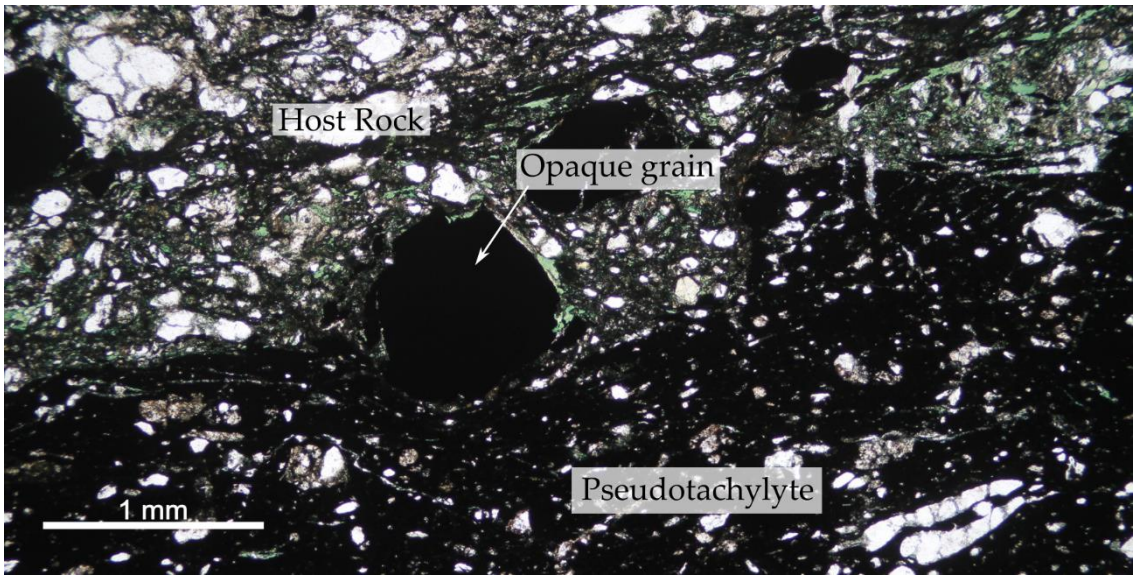

Figure 3.11. Cross-polarised photomicrograph of a pseudotachylyte vein margin wrapping around an opaque grain within the hanging wall greenschist.

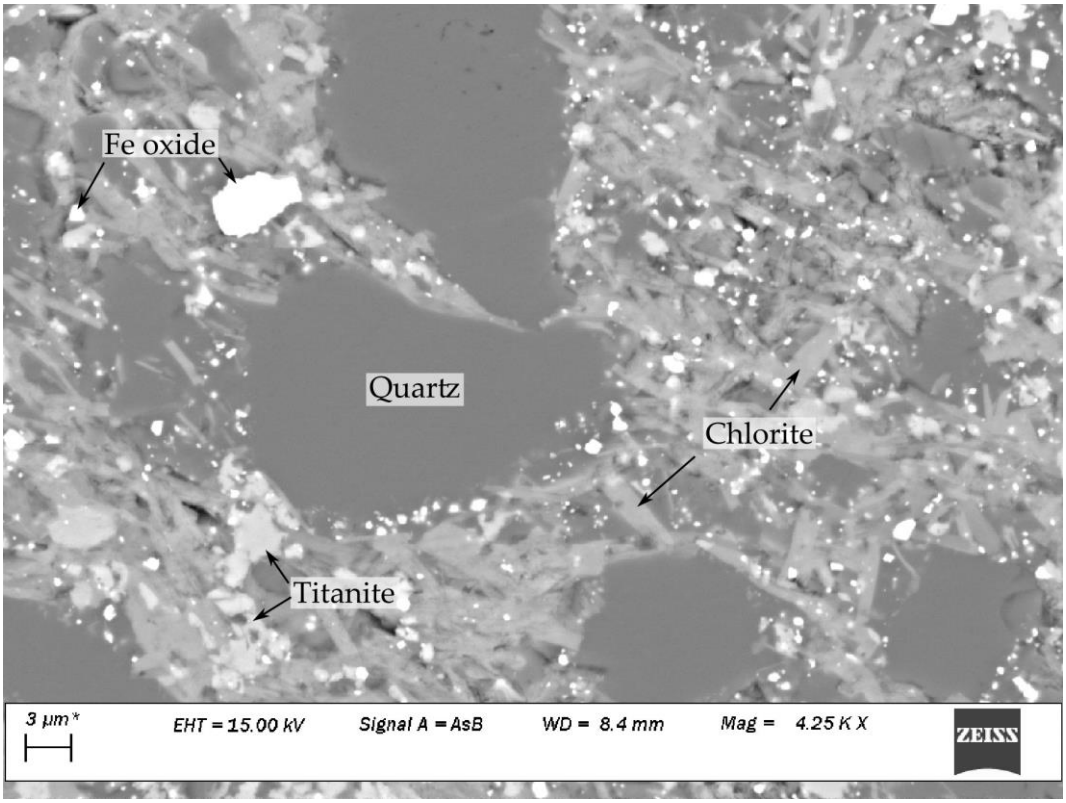

Figure 3.12. Backscatter electron image of very fine chlorite grains within the matrix of the black vein. Bright iron oxide grains are abundant. Other clasts include quartz and titanite.

3.4.2 Footwall

Black shear surfaces

The black slip surfaces on the small faults in the footwall sedimentary package are made up of an at least 0.5 mm thick ultracataclasite that lies in sharp contact with the sediments (Figure 3.13). It is clearly derived from the sedimentary package as it consists predominately of quartz and albite clasts, the primary constituents of the sediments. These clasts reach up to 150 µm in size. Also present in the ultracataclasite are small (<20µm) fragments of muscovite.

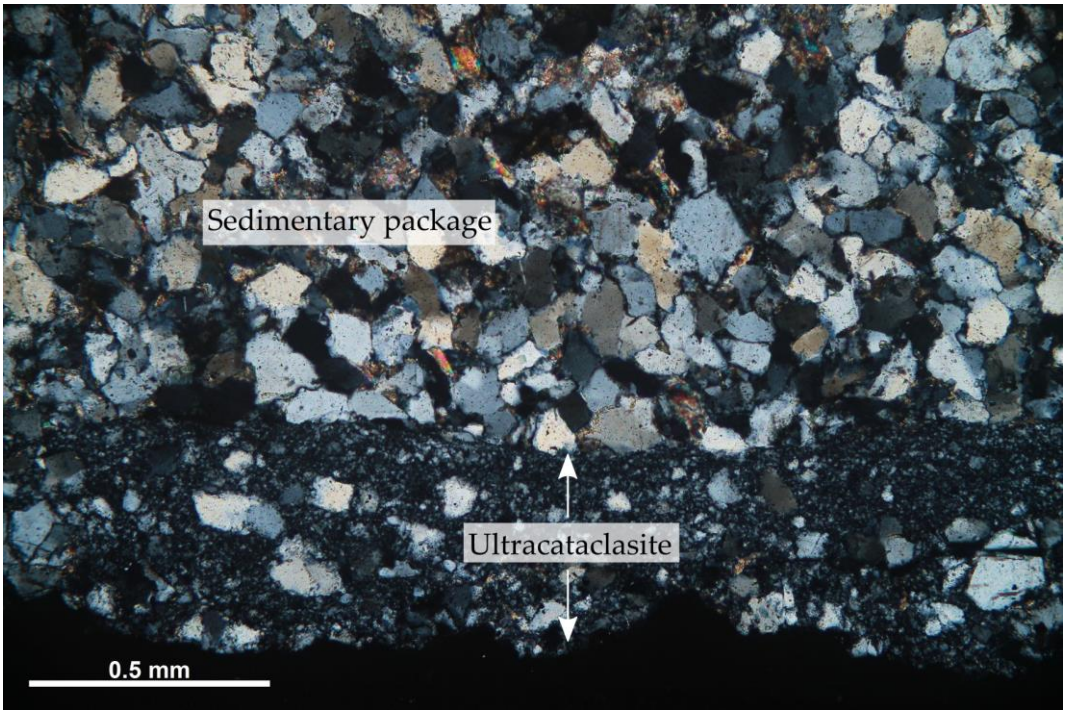

Figure 3.13. Cross-polarised photomicrograph of an up to 0.5 mm wide ultracataclasite containing comminuted quartz and albite clasts.

Breccia in footwall greyschist

This breccia consists of anastomosing seams of muscovite and chlorite which wrap around elongate polycrystalline clasts of quartz and feldspar. The polycrystalline clasts are commonly lensoidal with these shapes defining the foliation along with seams of fine grained phyllosilicates. Thin seams of dark/opaque minerals also align parallel to the foliation which SEM-EDS analysis revealed these are pyrite and titanite.

Throughout this breccia a series of up to 0.25 mm wide shears infilled with altered muscovite and chlorite, and rare calcite form oblique to the foliation. These shears regularly offset the foliation by at least a few millimetres, indicated by foliation drag and offset clasts (Figure 3.14).

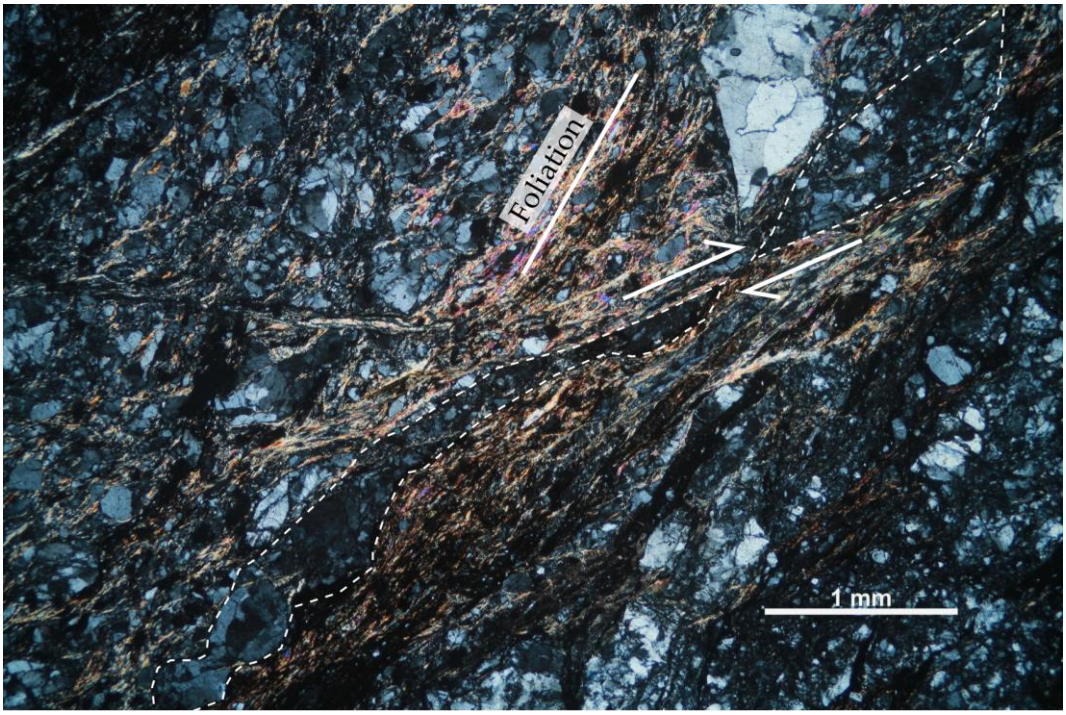

Figure 3.14. Cross-polarised photomicrograph of a polycrystalline quartz clast drawn in and offset in a shear oblique to the foliation which is defined by the alignment of phyllosilicate phases in the matrix.

4. Moonlight Creek

4.1 Overview

Outcrops of the Moonlight Fault Zone in Moonlight Creek occur 16 km northwest of Queenstown, south of Mt Gilbert. Movements on the Moonlight Fault in this area have juxtaposed fissile TZIV greyschists and more competent TZIV quartzofeldspathic gneiss in the hanging wall against bedded sedimentary rocks in the footwall which lies unconformably upon greyschist (Figure 4.1). The major fault plane is defined by a prominent 1-2 m wide gully containing black ultracataclasite and incohesive green – black gouges. In this chapter firstly the host rocks will be described followed by the structure of the fault zone and the microstructures observed in fault related rocks.

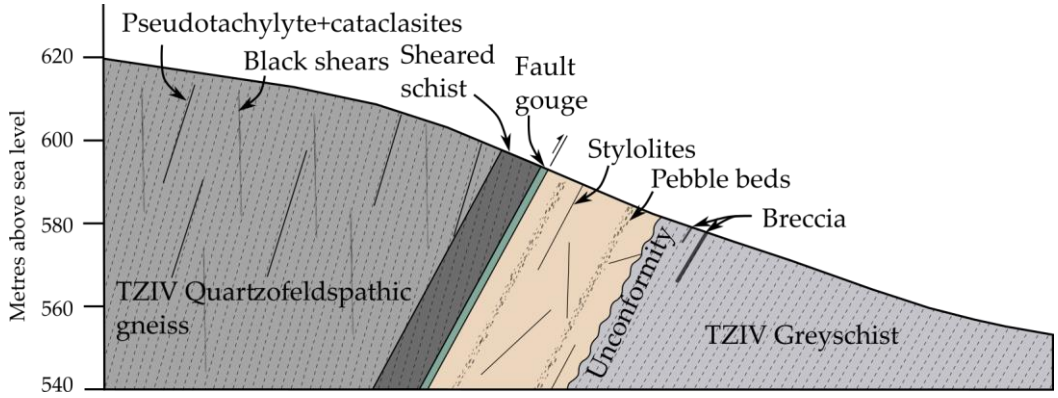

Figure 4.1. Cross section illustrating the structure and fault rock assemblages of the Moonlight Fault Zone in Moonlight Creek.

4.2 Host Rocks

4.2.1 Hanging wall

The hanging wall is predominately made up of a quartzofeldspathic gneiss with white/grey segregations of up to 1 cm, though commonly on the order of 1 - 3 mm (See Figure 4.6). Immediately adjacent to the main fault trace a c. 10 m wide zone of heavily sheared fissile greyschist is present. The foliation in these units strikes

north and dips steeply to the west (average – 002/75 W), sub-parallel to the Moonlight Fault (Figure 4.2). In the quartzofeldspathic gneiss the light segregations are made up of quartz and feldspar with the grey segregations largely made up of muscovite, chlorite and epidote. Minor rutile and apatite is also present. Chlorite (<0.2 mm wide) and muscovite (<0.1 mm wide) are elongate and aligned parallel to the foliation, with chlorite displaying blue interference colours. Epidote appears largely as elongate anhedral crystals of up to 0.3 mm aligned to the foliation.

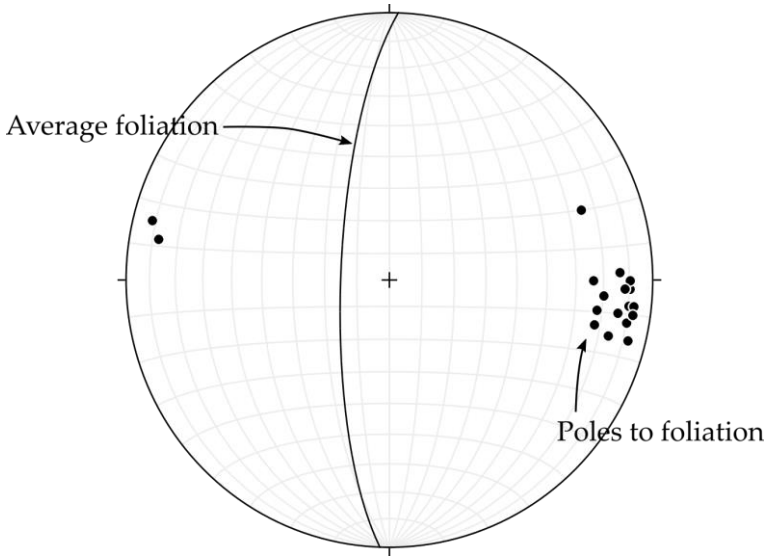

Figure 4.2 Foliation in the hanging wall quartzofeldspathic gneisses and greyschists.

4.2.2 Footwall

Sedimentary rocks

In the footwall, adjacent to the Moonlight Fault, a c. 34 m wide sedimentary package of well indurated, light grey sandstone is present. The basal (eastern) contact of the sedimentary package lies unconformably on the greyschist in the footwall which indicates a westerly younging direction. Large scale fracture surfaces lie mainly parallel to bedding in the sediments which strike north east and dip steeply to the west (030/66 W) (Figure 4.3a). This bedding is defined by occasional quartz + schist pebble beds of 15 – 40 cm thickness (Figure 4.3b). The pebbles are sub-rounded and range from <1 cm to 2 cm in size. Rare shell fragments and bioturbation were also identified.

Thin section analysis shows that the sediments are largely made up of sub-angular – rounded 1-2mm quartz and feldspar clasts set within a calcite matrix. Also present is minor epidote (<0.4 mm), chlorite and muscovite which reach up to 0.25mm.

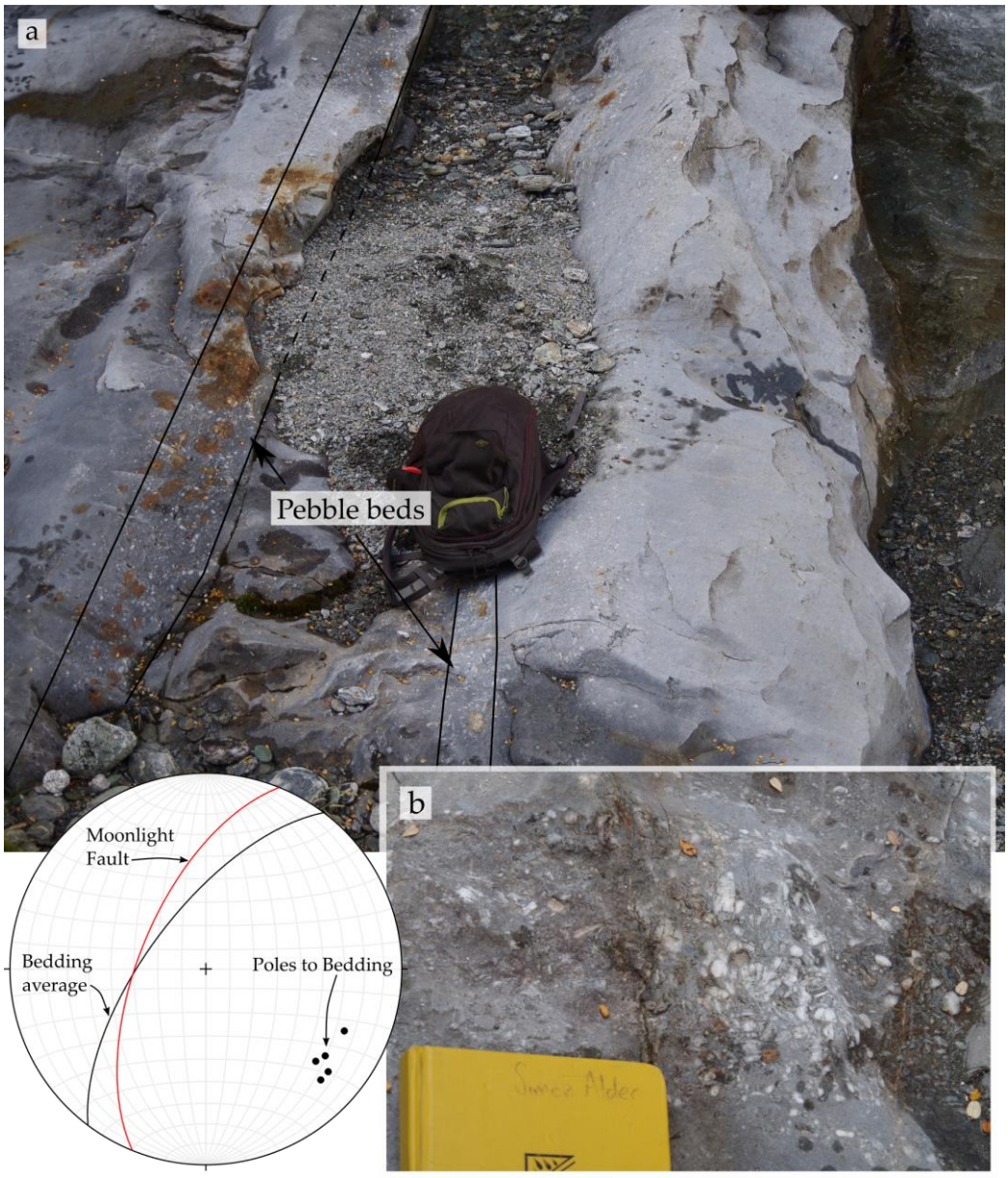

Figure 4.3. a) Outcrop photo of quartz sandstone with pebble beds. b) 20 cm quartz pebble bed within quartz sandstone. Equal area lower hemisphere projection shows the sub-parallel nature of the bedding in the quartz sandstone to the Moonlight Fault (for Moonlight fault orientation see Section 4.3.1).

Greyschist

The footwall greyschist is light grey and fissile with occasional massive greenschist layers up to 30 cm wide. The spaced foliation is steeply dipping to the west with rare kink bands whose axial planes dip steeply to the east (Figure 4.4). Deformation in the footwall is most intense in the 15 m from the sediment contact in which the greyschist is host to intensive top-east S folds.

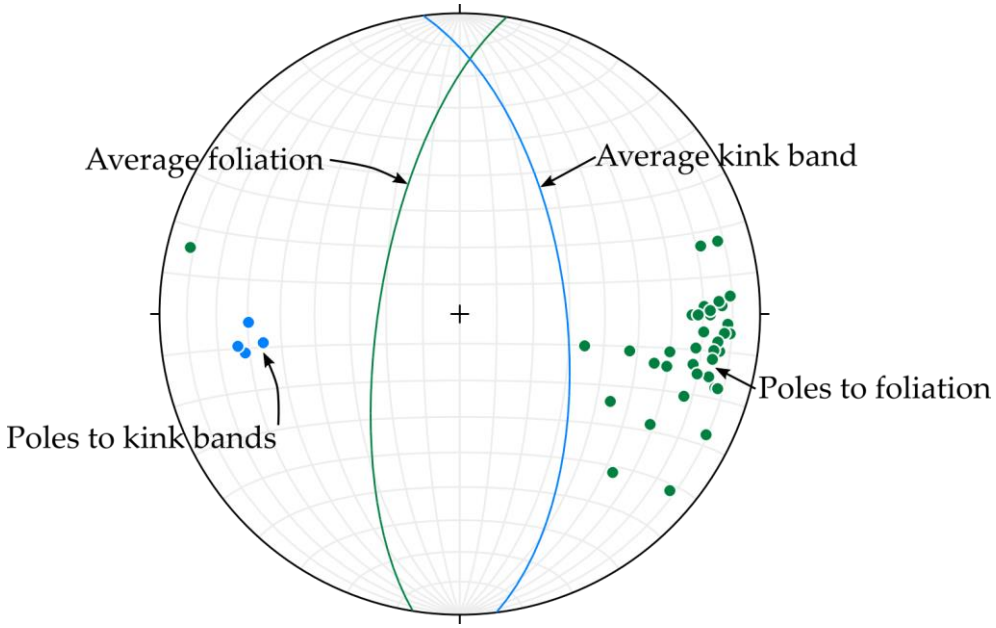

Figure 4.4. Equal area lower hemisphere projection showing the foliation and kink band axial planes in the footwall greyschist.

4.3 Fault zone structure and deformation

4.3.1 Fault core

The core of the fault zone is ~ 35 cm wide and contains black and green incohesive gouges that are intimately mixed (Figure 4.5). The gouges separate the footwall sedimentary package from the heavily sheared hanging wall greyschist that is heavily sheared. The green gouge contains a foliation that is northerly striking and steeply west dipping (009/61 W) and hosts slickenlines of highly variable orientations.

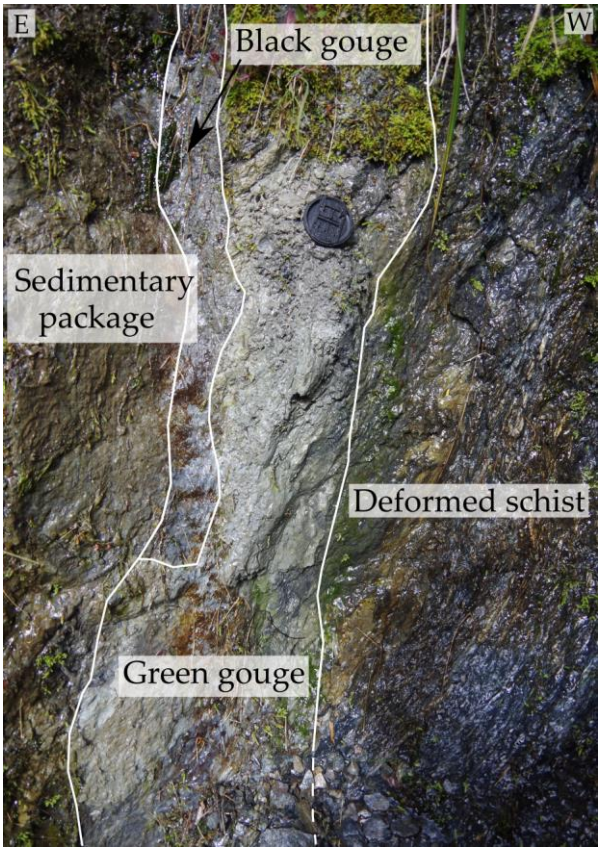

Figure 4.5. 30 cm wide zone of black and green gouge in the core of the Moonlight Fault.

4.3.2 Hanging wall

Pseudotachylyte

Pseudotachylyte veins are present in the hanging wall quartzofeldspathic gneisses as sharp, planar features that lie sub-parallel to the foliation. They are identified by their dark, aphanitic nature with melt pools and injection veins (Figure 4.6). Fault veins range from <1 mm–0.5 cm in width with melt pools reaching a thickness of 1 cm. Injection veins branch off into the host rock at high angles and are up to 4 cm in length and 3 mm in width at the point at which they emanate from the fault vein. Occasionally pseudotachylyte veins were observed grading into cataclasites or breccias. Due to their foliation parallel nature displacement on these veins could not be determined.

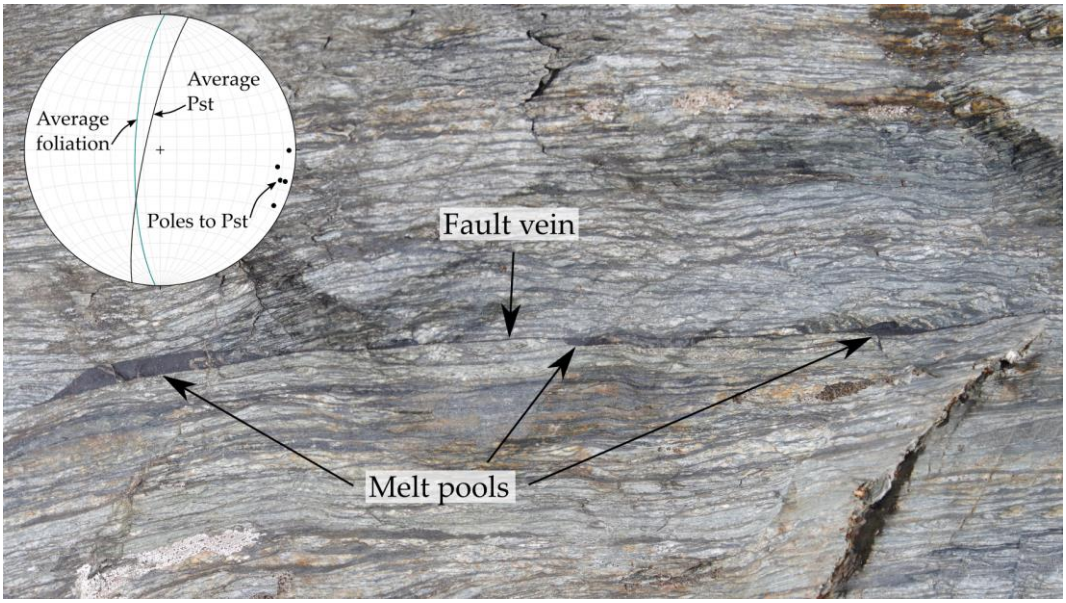

Figure 4.6. Foliation parallel pseudotachylyte vein showing multiple melt pools along its length. Equal area lower hemisphere projection shows the sub-parallel nature of the pseudotachylyte veins to the foliation.

Cataclasites

There were variable forms of cataclasite in the hanging wall, one being the along strike evolution of a pseudotachylyte vein. This 4 mm – 1.2 cm thick cataclasite was identifiable from a pseudotachylyte by it being a much lighter colour, having an observable grain size and evolving to a much more complex vein system. Also present in the hanging wall are fine-grained black shears which crosscut the foliation at low angles (Figure 4.7) and are up to 2 cm in width though are more commonly <0.5 cm. These are prevalent in outcrop with 13 present in a 20 m transect, an average of one every 1.3 m (Figure 4.8). These black shears appear coeveal with kink banding in the hanging wall as, at times the formation of these deform the other. The youngest cataclastic feature in the hanging wall is late stage small faults which offset all other previously described deformation features. At times these faults contain thin (<2 mm) green gouge. Observed offset on these faults was less than 10 cm.

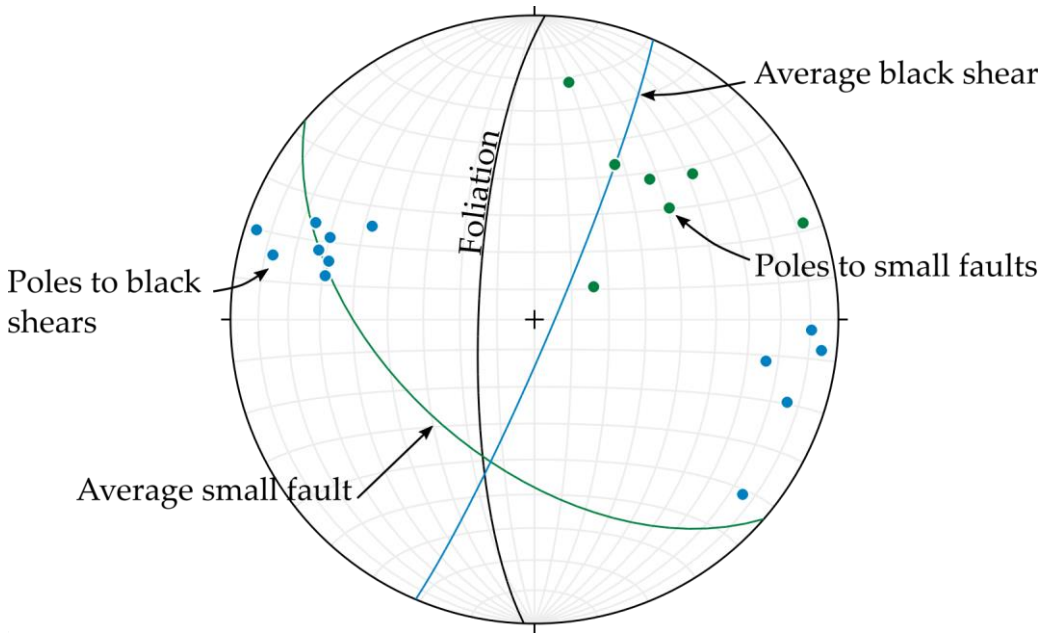

Figure 4.7. Equal area lower hemisphere projection of the cataclastic features in the hanging wall greyschist. This shows that the black shears cross-cut the foliation at low angles while the late small faults crosscut it at high angles.

4.3.3 Footwall

Sedimentary package deformation

The sedimentary package is host to abundant, very thin (<0.5 mm) fine grained black networks of variable orientation with displacements of up to a few cm's. The upper 5 m of the sedimentary package is heavily fractured while the transition from the sedimentary package into the fault core gouges is marked by either, (1) an up to 2 cm thick, cohesive dark black ultracataclasite in contact with well foliated green/black gouge of the fault core (Figure 4.9), or (2) a cohesive 40 – 100 cm wide cataclasite that is host to black layers that lie parallel to the strike of the main fault trace. The dark layers reach up to 5 cm in width, though are more commonly 1 - 2 cm. The contact between the ultracataclasite and the fault core gouge lies parallel to the Moonlight Fault trace and it is from this contact that an orientation of the Moonlight Fault was retrieved.

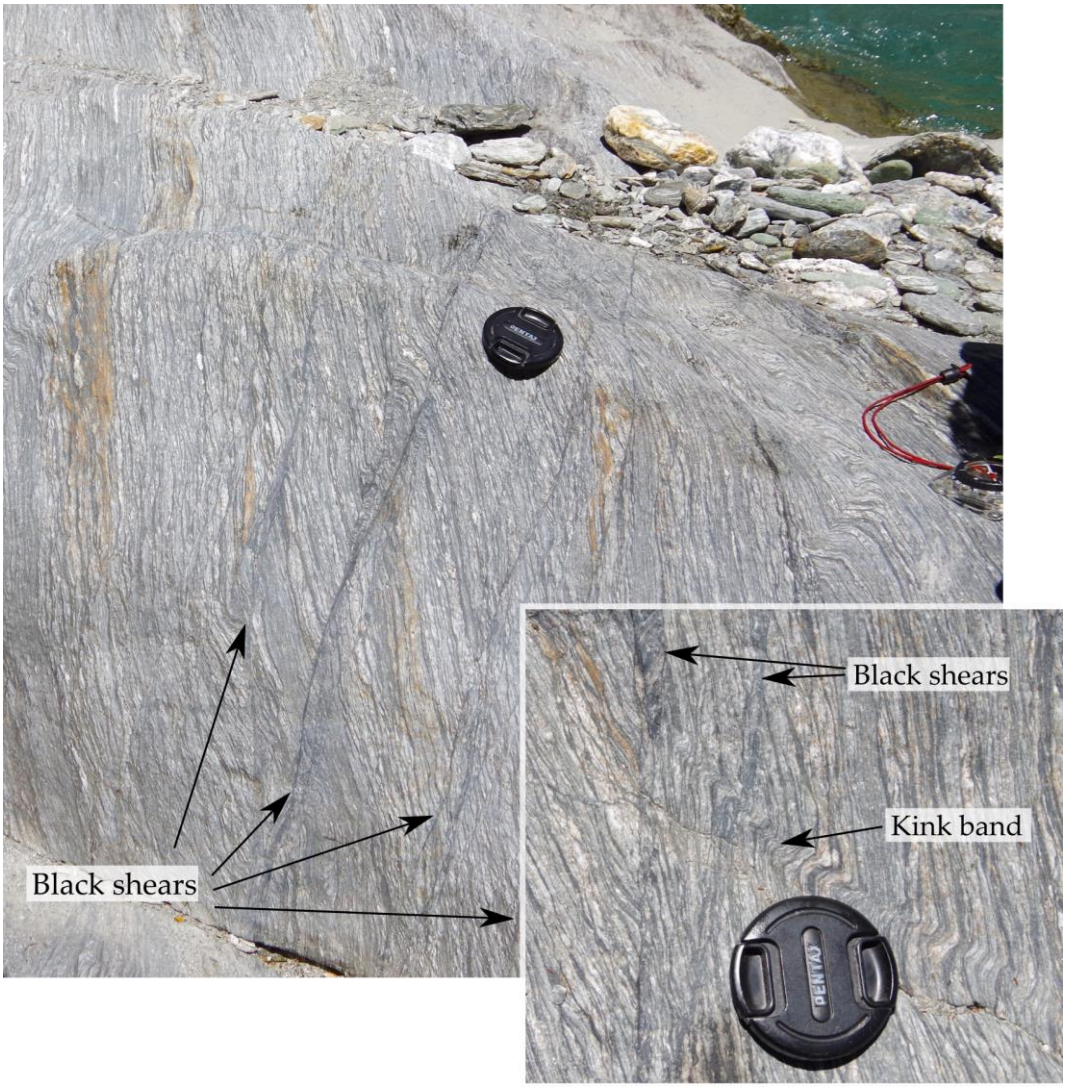

Figure 4.8. Zone of black shears crosscutting the quartzofeldspathic gneiss foliation. *Inset:* Photo showing coeveal evolution of kink bands and black shears, one black shear (right) drawn into kink band which has subsequently been offset by a later black shear (left).

Figure 4.9. Thin black layer at the top of the sedimentary package. Eroded face would lie in contact with foliated gouge of the fault core.

Breccia

There are three significant zones of brecciation in the footwall greyschists, two that lie within 10 m of the contact with the sedimentary package, 44 m from the Moonlight Fault and a third that lies c. 750 m from the Moonlight Fault. The first, 10 m east of the sedimentary package is a 40 cm wide pod which contains angular schist fragments of highly variable size, the largest reaching 6 cm. The breccia margins cross cut the schist foliation and contain slip surfaces which average 052/68 NW with slickenlines indicating near pure dip – slip movements (Figure 4.10). The greyschist adjacent to the breccia is heavily fractured and deformed tapering to the base of the brecciated zone. The eastern contact is deformed for up to 2 m, the western contact for 50 cm. The second breccia pod lies 3 m west of the previous. It is a 20 x 10 cm pod that lies within a 50 cm wide zone of intensely deformed and weathered greyschist.

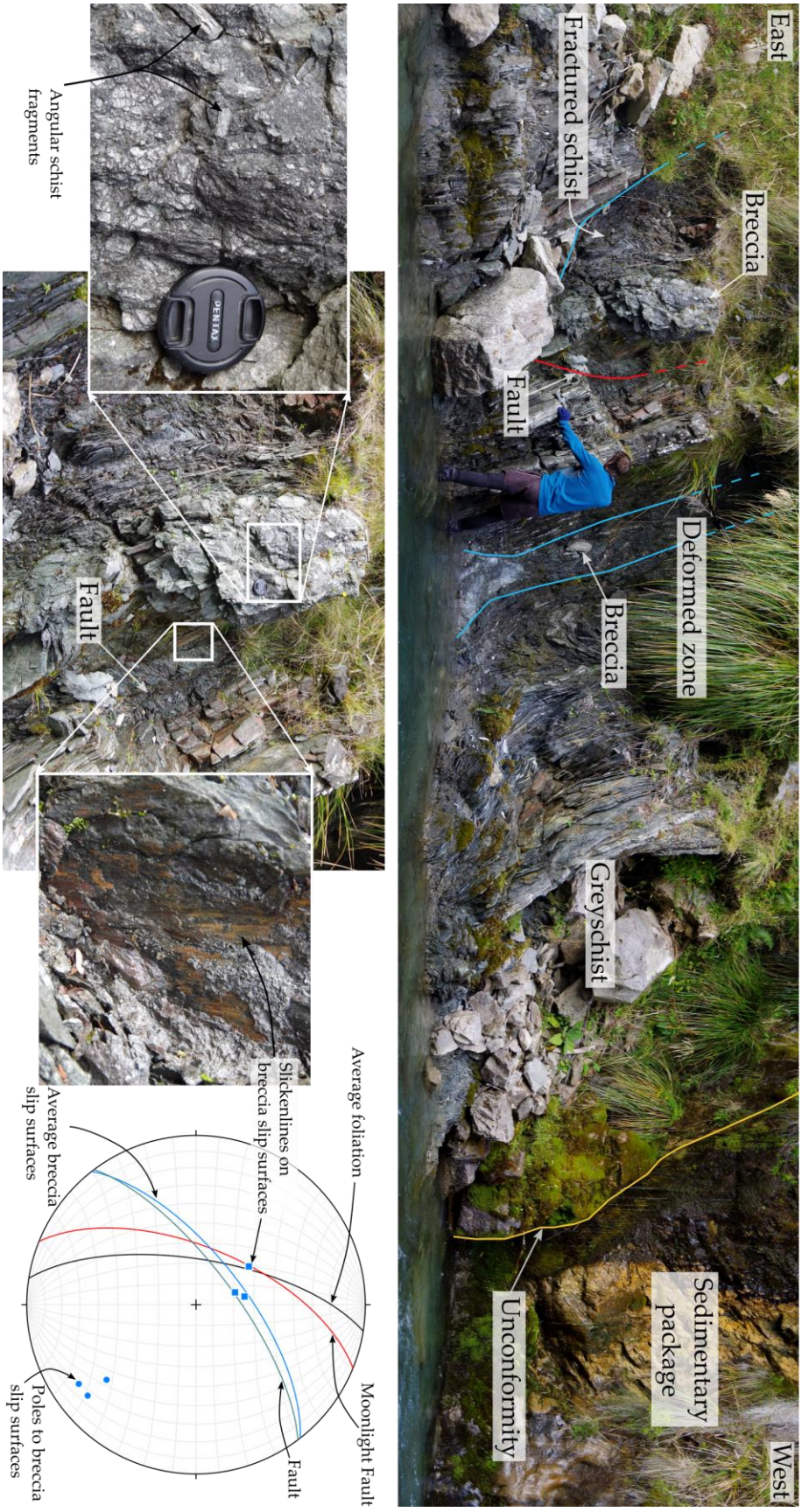

Figure 4.10. 15 m wide deformation zone in the greyschist adjacent to the sedimentary package. The deformation consists of two brecciated pods within intensely folded and fractured greyschist and one fault that juxtaposes schists with differing foliations.

The breccia that lies furthest from the Moonlight Fault, is a light grey up to 1 m wide incohesive breccia (Figure 4.11). The western margin of the breccia is marked by a prominent fault plane that strikes north and dips steeply to the west (177/73 W), sub-parallel to the surrounding greyschist foliation. Within the breccia a series of shears lie at c. 25˚ to the shear zone boundary which is consistent with them being Riedel shears (Logan et al., 1979). With the assumption that the movement direction in this breccia is perpendicular to the intersection of the main fault plane and the R-shear planes, the shear direction plunges moderately SSW (46/196). Top-to-the-east folds within the breccia and kink bands adjacent to the breccia indicate that this movement direction was also likely top-to-the-north east (Figure 4.11).

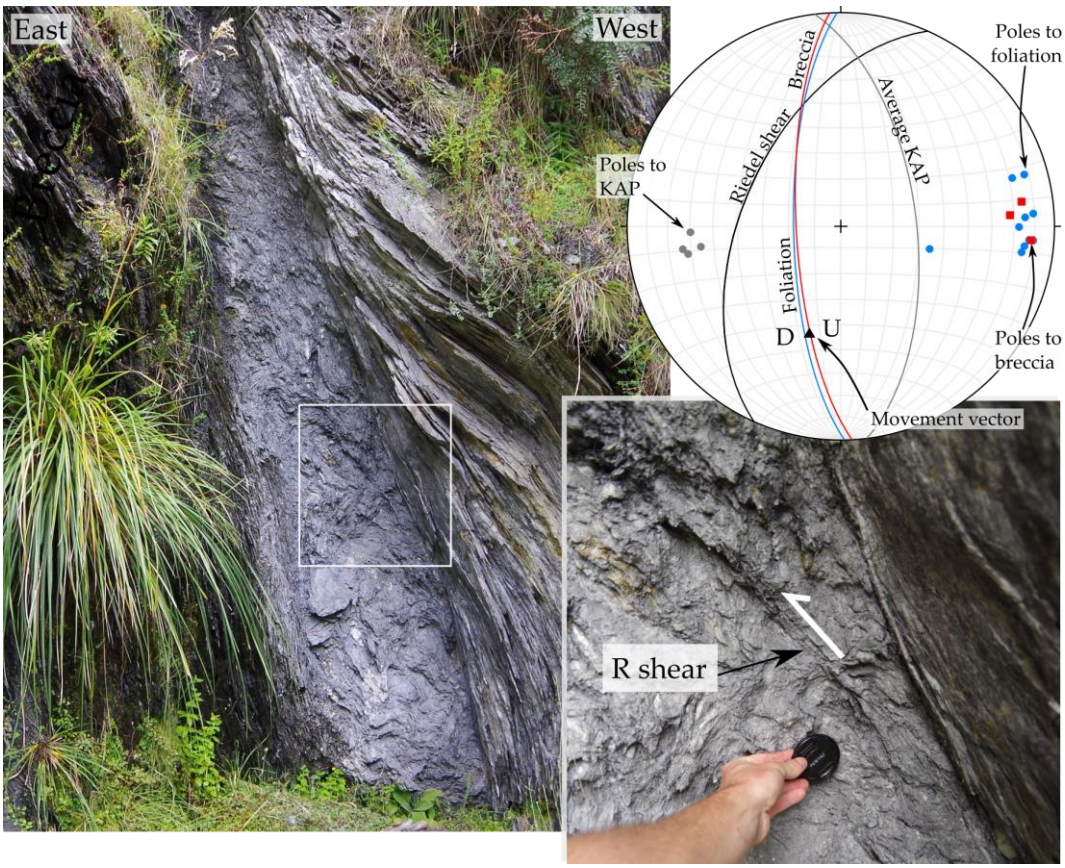

Figure 4.11. Up to 1 m wide incohesive breccia 750 m from the trace of the Moonlight Fault in the footwall. *Inset:* Reidel shear that lies c. 25º to the shear boundary. Equal area lower hemisphere projection shows the orientation of the breccia, kink axial planes (KAP), foliation and Moonlight Fault. Stereonet also shows the movement vector retrieved from the R-shear which, along with top-east verging folds adjacent to the breccia, indicates it hosted top-to-north east movement or oblique reverse movement.

4.4 Fault rock microstructures

4.4.1 Pseudotachylyte

The foliation parallel pseudotachylyte identified in the hanging wall of the MFZ in Moonlight Creek contains dual slip surfaces linked by a complex fractured zone infilled with pseudotachylyte melt (Figure 4.12). Along strike this vein merges into a single slip surface, indicating this was probably formed in one slip event.

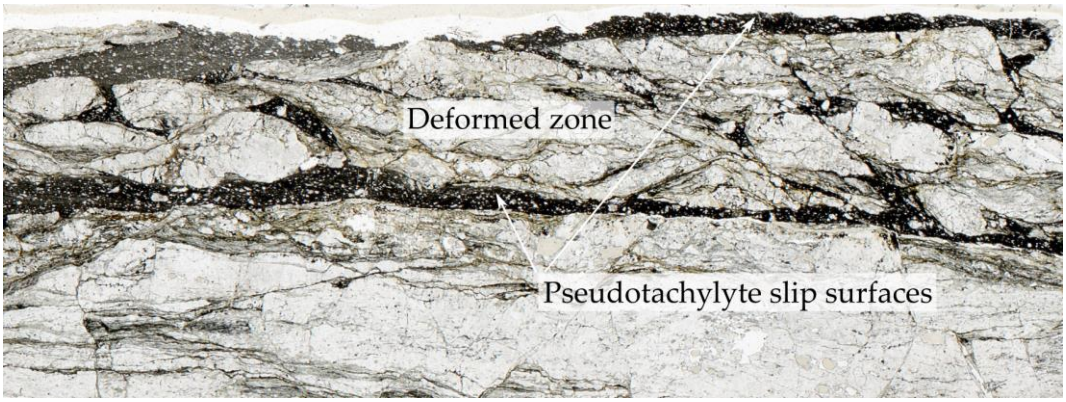

Figure 4.12. Scanned thin section displaying dual pseudotachylyte veins which bound a highly deformed zone.

The pseudotachylyte contains clasts of quartz, albite and fragments of the host rock all of which contain blurry rims. The quartz and albite clasts are commonly lensoidal, aligning to the shear boundary. Host rock fragments have become incorporated due to the complex nature of the contact.

The pseudotachylyte matrix varies from black to dark grey with the colour differences aligning parallel to the slip plane (Figure 4.13). Backscatter electron images show that the matrix consists of randomly oriented laths up to 4 μm in length and 1 μm in width (Figure 4.14). These laths are also seen to be intruding clasts, likely the cause of the blurry rims. Due to the small size of these laths, identification was not possible.

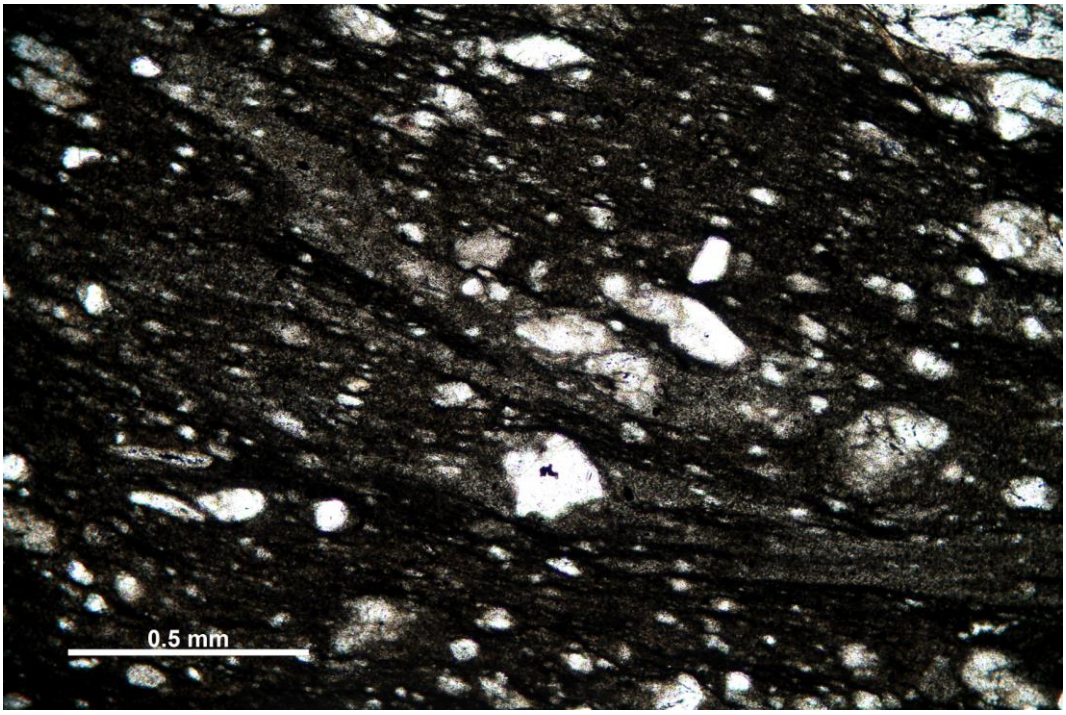

Figure 4.13. Plane-polarised photomicrograph showing colour variation within the pseudotachylyte.

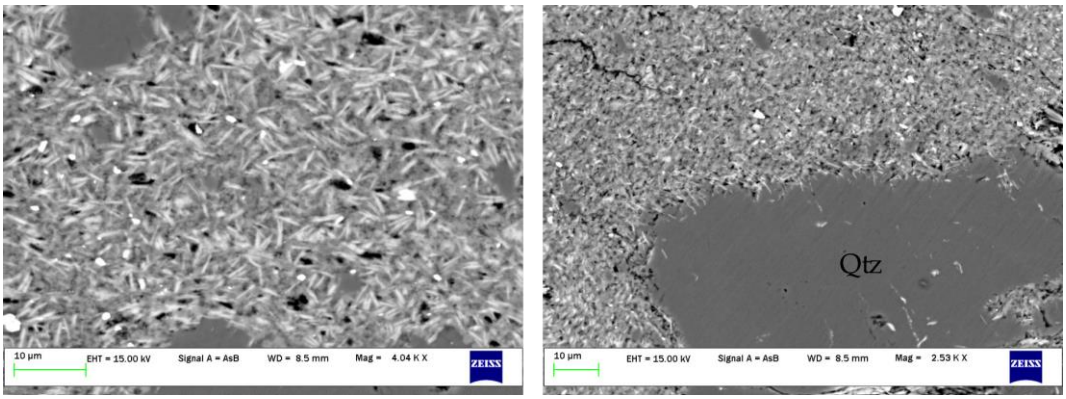

Figure 4.14. SEM backscatter electron images revealing laths in the matrix indicating that it has been through a melt phase. The image on the right shows these laths intruding the rim of a quartz grain, likely forming the blurry rims observed through optical microscopy.

4.4.2 Foliated cataclasites in the hanging wall

Cataclasites in the hanging wall is present in the form of layer-parallel ultracataclasites and cataclasites while black shears and green cataclasites lie at high angles to the foliation. All of these fault rocks contain the same mineralogy consisting of quartz, albite, muscovite/phengite, epidote with minor titanite and pyrite. With the exception of the black shears which have a gradational contact with the host rock, all other fault rocks are in sharp contact with the quartzofeldspathic gneiss. These fault rocks are variably foliated with the ultracataclasites containing

the strongest foliation. The foliation is defined by a number of features that align parallel; 1) elongate axes of phyllosilicate phases; 2) lensoidal clasts; 3) growth of chlorite and muscovite tails upon quartz and feldspar clasts which gives them an elongate form (Figure 4.15a); 4) rare clasts host to tails of an opaque mineral (likely pyrite) (Figure 4.15b); and, 5) rare seams of insoluble titanite.

The foliation parallel foliated ultracataclasite contains phyllosilicate-rich layers within it, likely inherited from the quartzofeldspathic gneiss's muscovite rich segregation bands (Figure 4.16). This ultracataclasite also contained offset albite clasts with syn-kinematic growth of phyllosilicates.

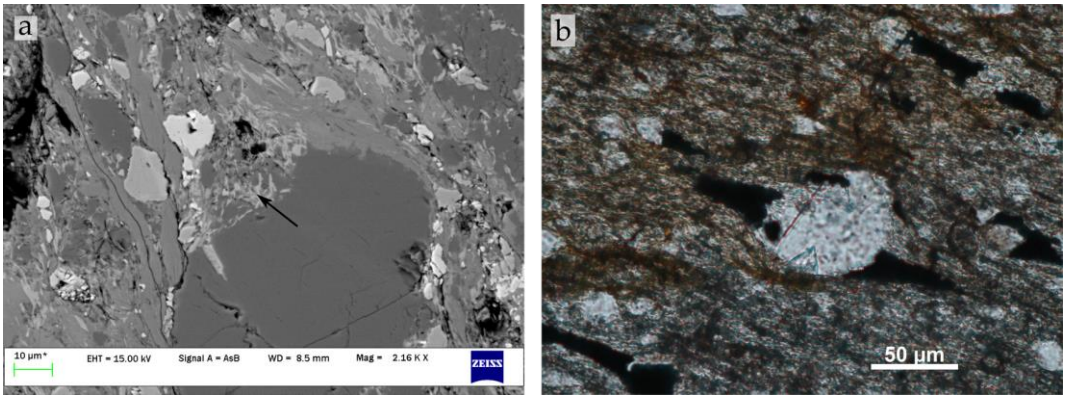

Figure 4.15. a) Electron backscatter image of newly grown chlorite (arrow) in the strain shadow of a quartz grain. b) quartz grain containing tails of opaque minerals which align parallel to the foliation.

4.4.3 Stylolites within the sedimentary package

The thin black fracture networks within the sedimentary package have an undulating form in thin section with amplitudes not exceeding 0.4 mm (Figure 4.17). Optical microscopy and SEM analysis revealed that these seams contain concentrations of epidote, chlorite, titanite and pyrite and are interpreted as stylolites related to dissolution (Heald, 1955). In outcrop the stylolites were observed as continuous features up to several metres long, although in thin section many smaller, discontinuous seams are also present with variable orientations and lengths (>0.5 mm).

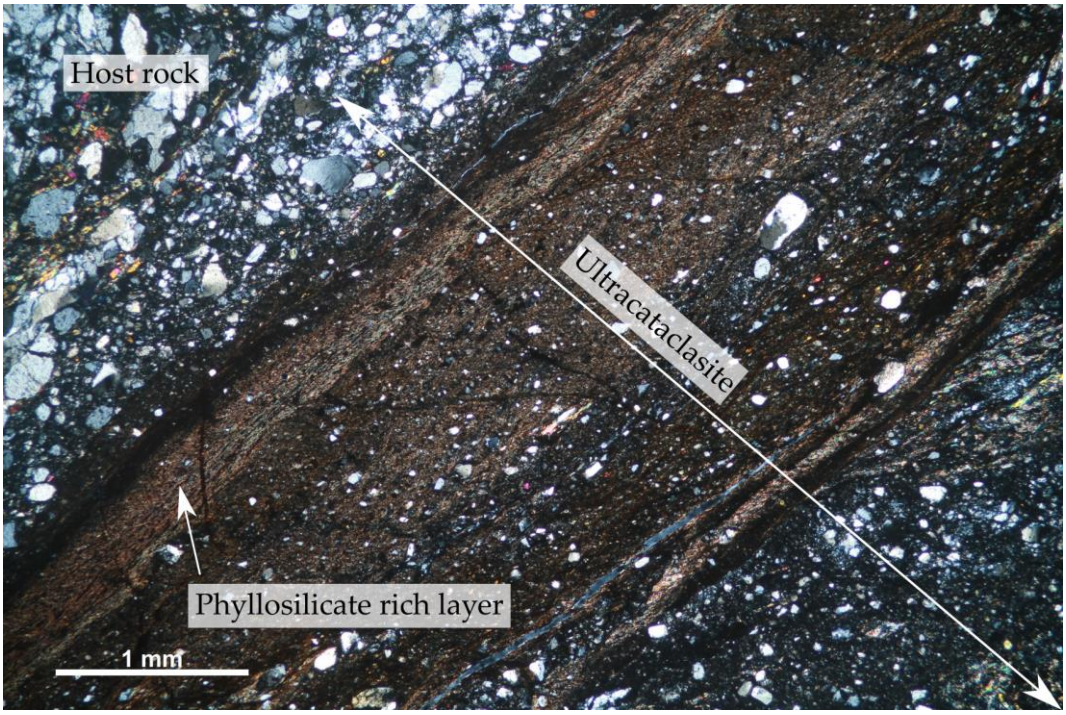

Figure 4.16. Ultracataclasite in the hanging wall with phyllosilicate-rich layers – likely inherited from the lithological banding within the quartzofeldspathic gneiss.

Figure 4.17. Plane polarised photomicrograph of a black stylolite undulating through the sedimentary package.

Where there are seams adjacent to one another the clasts between them are smaller in size than the host rock (Figure 4.18). The size of these grains is usually <0.05 mm when the host rock grain size is usually greater than 0.1 mm. Larger quartz and albite clasts that are in contact with the seams contain serrate boundaries indicating that the seam has intruded the clasts (Figure 4.18).

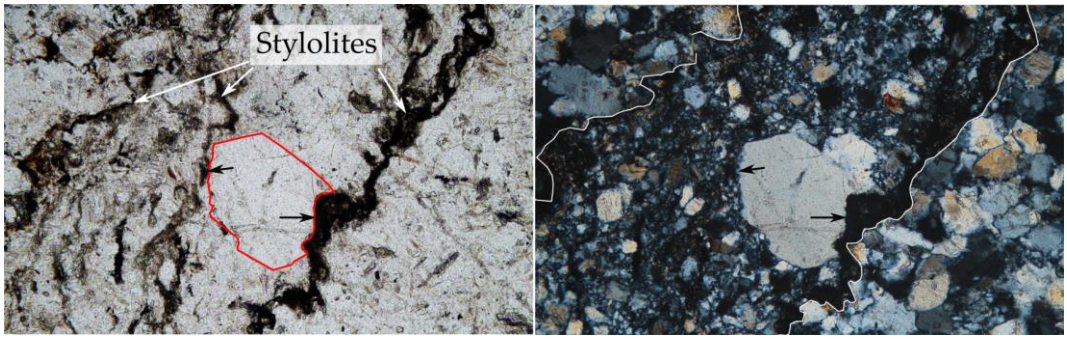

Figure 4.18. Plane-polarised (left) and cross-polarised (right) photomicrographs of the deformation associated with stylolite development. Arrows indicate location where stylolites intrude a relatively equant quartz grain forming undulatory edges. The grains in the zone between these stylolites (marked by white lines) are much smaller than those found in the host rock.

4.4.4 Fault core

The gouge within the fault core consists of quartz and albite clasts set within a fine-grained anastomosing network of phyllosilicates. The phyllosilicates are largely clay minerals likely altered from chlorite and muscovite which are rarely observed. These phyllosilicates regularly appear as tails upon predominately lensiodal, heavily fractured quartz and albite clasts (Figure 4.19). Clasts sizes reach up to 2.5 mm though are generally <0.05 mm with their long axes aligning parallel to the foliation. These features are very similar to those identified in the foliated cataclasites within the Moonlight Fault core in the Matukituki valley.

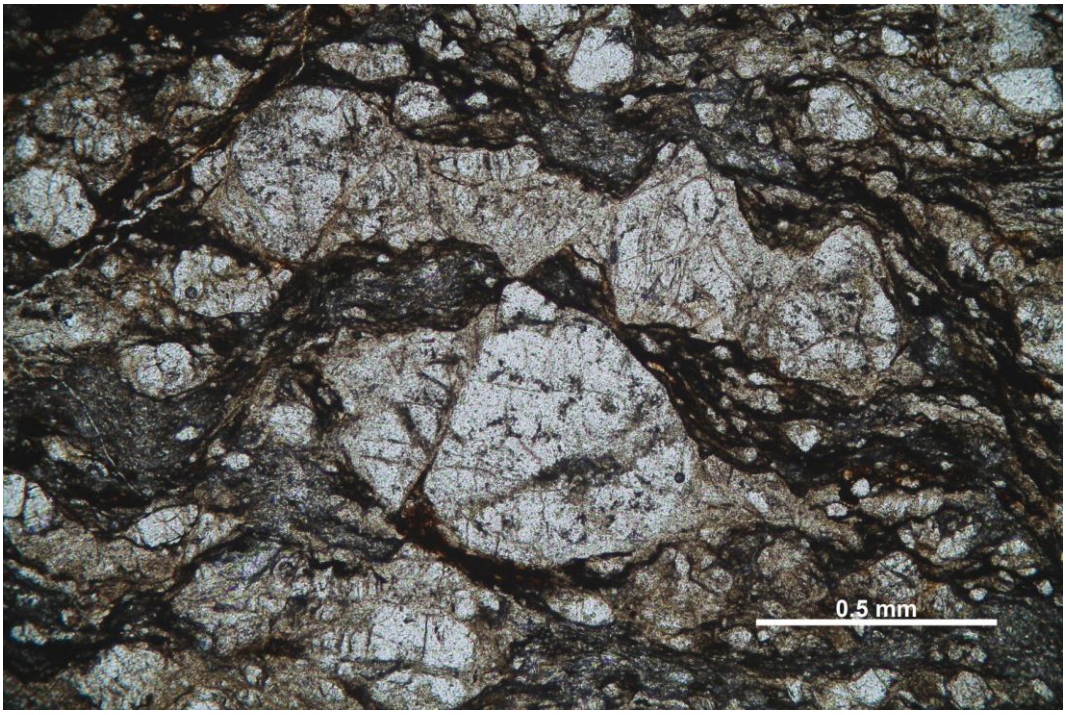

Figure 4.19. Plane-polarised photomicrograph of the fault core gouge showing that it consist of quartz and albite clasts (white) surrounded by a network of fine phyllosilicates (dark seams).

5. Twelve Mile Creek

5.1 Overview

Moonlight Fault Zone exposures are present in Twelve Mile Creek c. 10 km west of Queenstown adjacent to the Mt Crichton Loop Track. Movements upon the Moonlight Fault have juxtaposed TZIV greyschist in the hanging wall against a thin sliver of sediments in the footwall which lie unconformably upon low grade TZIIB semischist (Figure 5.1). Outcrops are easily accessible as Twelve Mile Creek flows directly along the trace of the Moonlight Fault for 800 m, exposing a cohesive black ultracataclasite and rocks of the footwall and hanging wall. In this chapter firstly the host rocks will be described followed by the structure of the fault zone and the microstructures observed in fault related rocks.

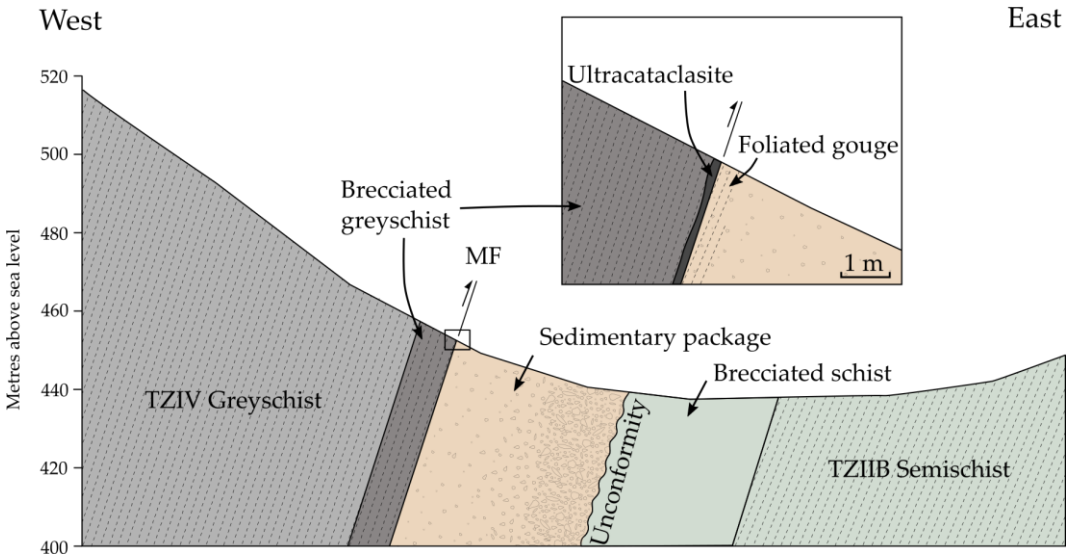

Figure 5.1. Cross section of the Moonlight Fault Zone within Twelve Mile Creek. *Inset:* details of the fault core.

5.2 Host Rocks

5.2.1 Hanging wall

The hanging wall is made up of complexly deformed intact greyschist which becomes brecciated up to 5 m from the Moonlight Fault. The intact greyschist has a northerly striking, compositionally spaced foliation which dips steeply to the west. Fold hinges have highly variable orientations but when plotted on a stereonet form a great circle that lies subparallel to the Moonlight Fault (Figure 5.2). The zone of brecciated greyschist (<5 m in width) contains no visible fold hinges and contains a foliation subparallel to the Moonlight Fault (Figure 5.2). Within this fault-related greyschist quartz boudin long axes and rare 2 – 5 cm dark green layers lie parallel to the foliation.

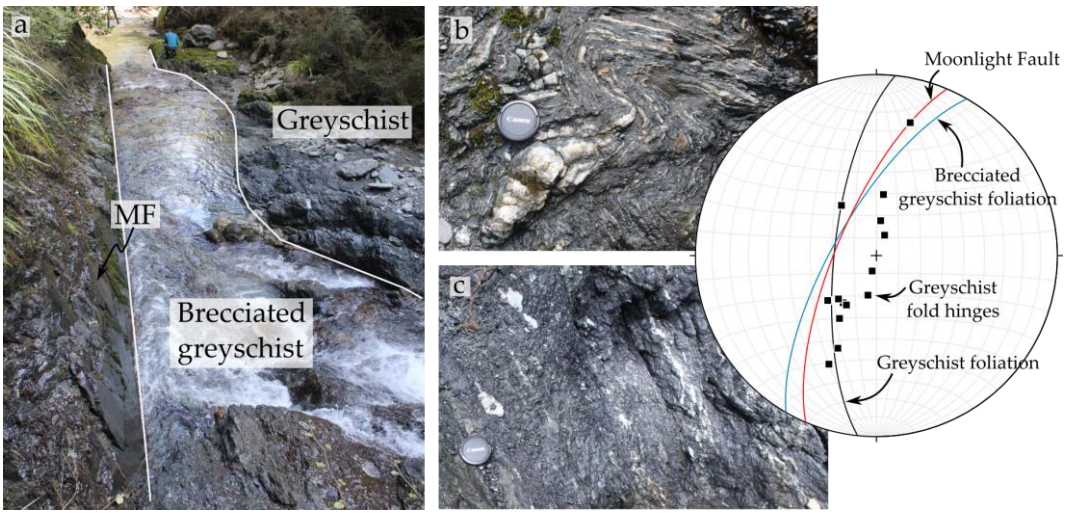

Figure 5.2. a) Photo taken along strike of the Moonlight Fault showing the spatial distribution of the brecciated greyschist and intact greyschist. b) folded intact greyschist with quartz segregations. c) brecciated greyschist with quartz boudins. Equal area lower hemisphere projection showing the sub-parallel nature of the brecciated greyschist to the Moonlight Fault. Greyschist fold hinges align along a great circle sub-parallel to the Moonlight Fault.

5.2.2 Footwall

Sedimentary package

In the footwall, adjacent to the Moonlight Fault an at least 40 m thick sedimentary package is present. This package predominately consists of a matrix-supported conglomerate that contains up to 15 cm clasts though are commonly < 4 cm. The clasts are angular to rounded low-grade schist that show no imbrication and make up c. 60% of the total volume (Figure 5.3). Adjacent to the Moonlight Fault a 5-6 m thick sandstone is present, with schist fragments making up <10% of the total rock volume and is likely part of a gradational sequence from the clast-rich conglomerates. The matrix of these units are made up of calcite and crystals derived from the schist fragments. Calcite also forms rims around the schist clasts (Figure 5.4).

Figure 5.3. Sedimentary package matrix-supported conglomerate containing schist fragments lies in contact with the brecciated schist.

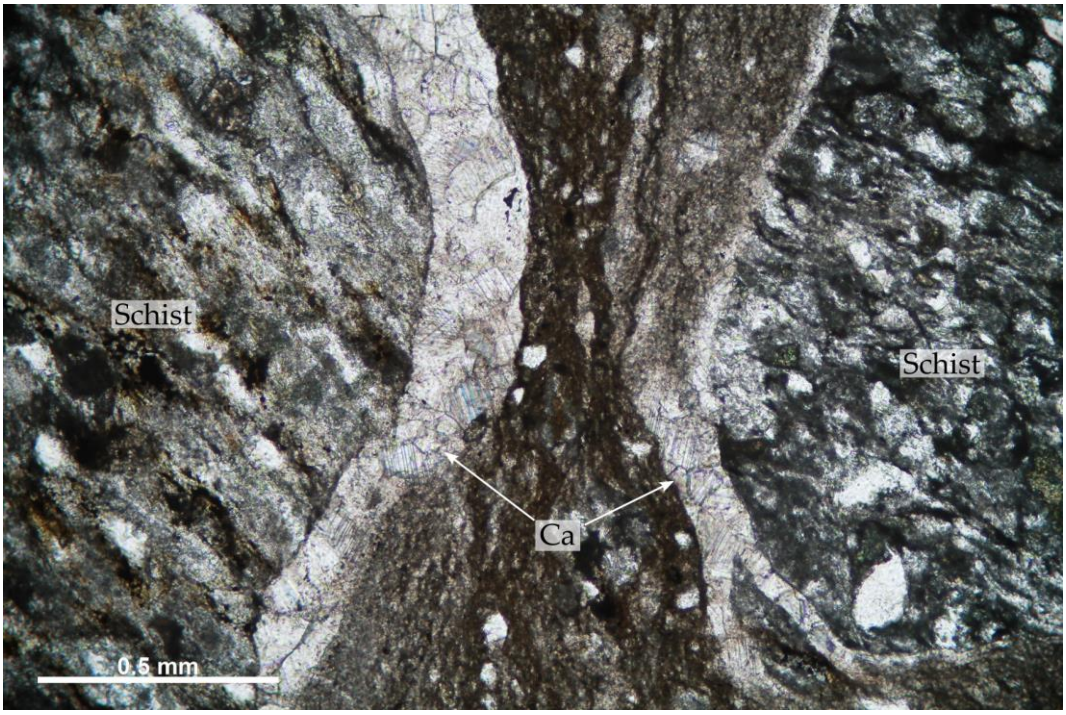

Figure 5.4. Plane-polarised photomicrograph of two schist clasts with rims of calcite within the sedimentary package.

Footwall semi-schist

The semi-schist in the footwall is predominately psammitic with occasional pelitic beds. Psammitic layers are a light grey-green with rare quartz veins and lies largely sub-parallel to the Moonlight Fault (Figure 5.5). Pelitic layers reach up to c. 30 m thick, though are more commonly <2 m. The pelitic layers are largely dark grey in colour and appear in different forms; at times as weakly foliated, relatively undeformed beds; as parallel sided slate-like blocks; and rarely, some layers are host to shear fabrics (see Section 5.3.3).

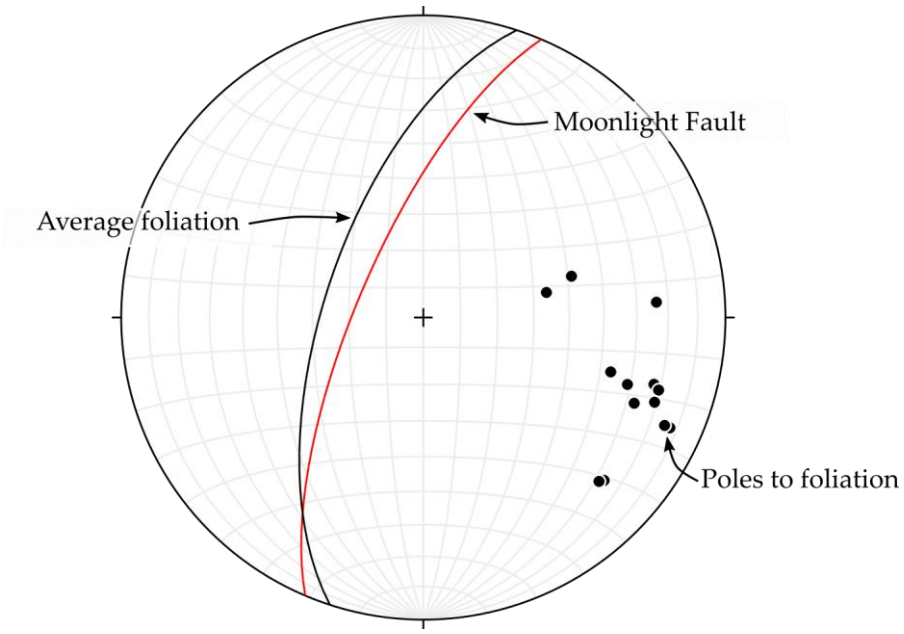

Figure 5.5. Equal area lower hemisphere projection of the foliation in the footwall semi-schists relative to the Moonlight Fault.

Brecciated schist?

Between the sedimentary package and the semi-schist a zone of dark grey and brown layers that host schist clasts and layer parallel veins are present (Figure 5.6). These units are well indurated and similar in appearance to the semi-schist that underlies it, however it contains schist fragments within it. The boundaries of the bulk layering lie at low angles to the Moonlight Fault (Figure 5.6). One of the grey layers was sampled and was found to contain angular fragments of low grade quartzofeldspathic schist. The fragments are poorly sorted and show no imbrication. It is clast supported with the matrix made up of minerals from the fragmented schist. Calcite is present, as rims around some clasts (Figure 5.7), veins within schist fragments and rare crystals in the matrix. There are lithological variations in the schist fragments with the more massive layers (at outcrop scale) containing flattened and elongate detrital quartz and albite clasts while pelitic layers are identified by their very fine grain size and strong crystal orientation.

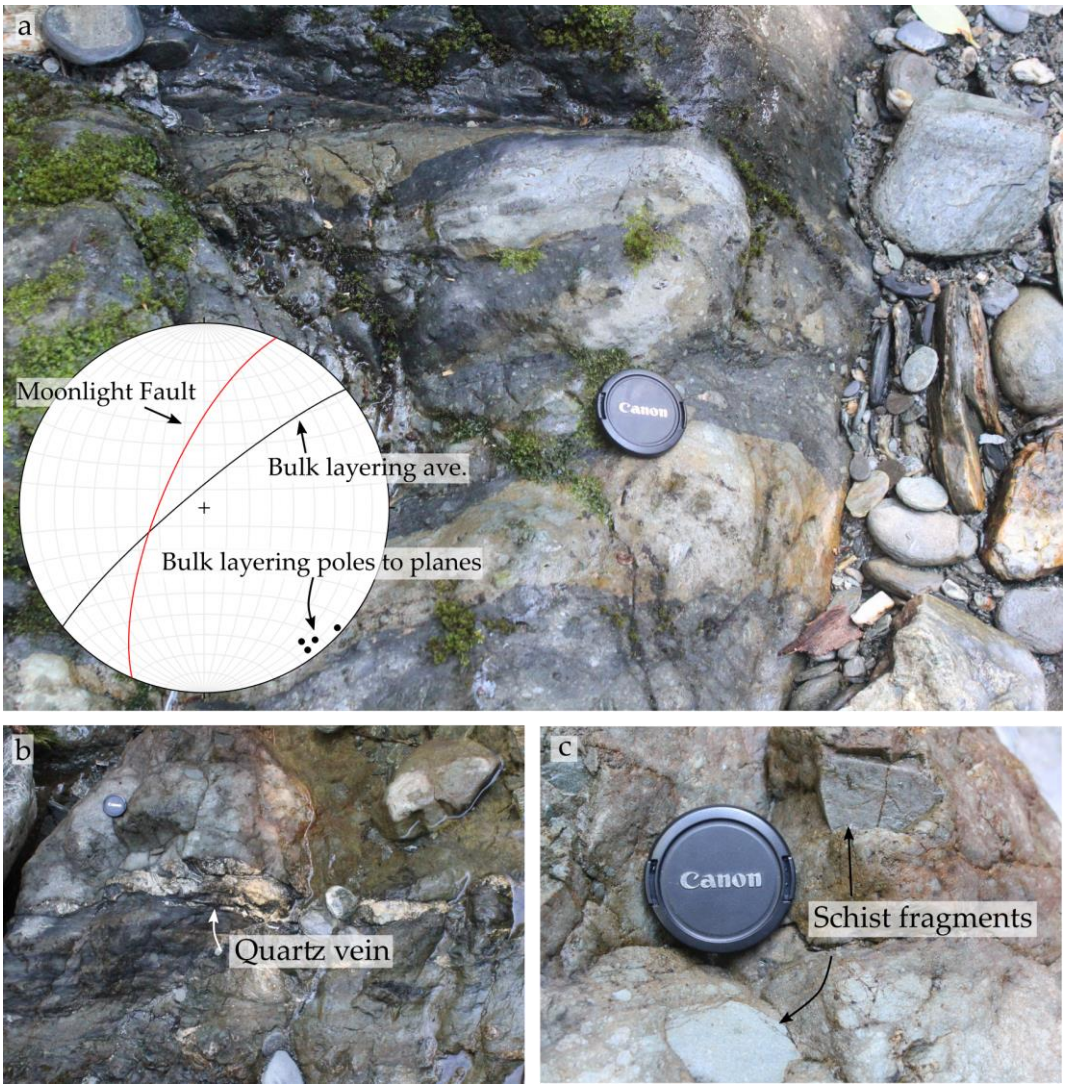

Figure 5.6. a) Photo showing outcrop of the bulk layering in the brecciated schist. Equal area lower hemisphere projection displays the orientation of these relative to the Moonlight Fault. b) quartz veining parallel to layering. c) schist fragments within one the layers.

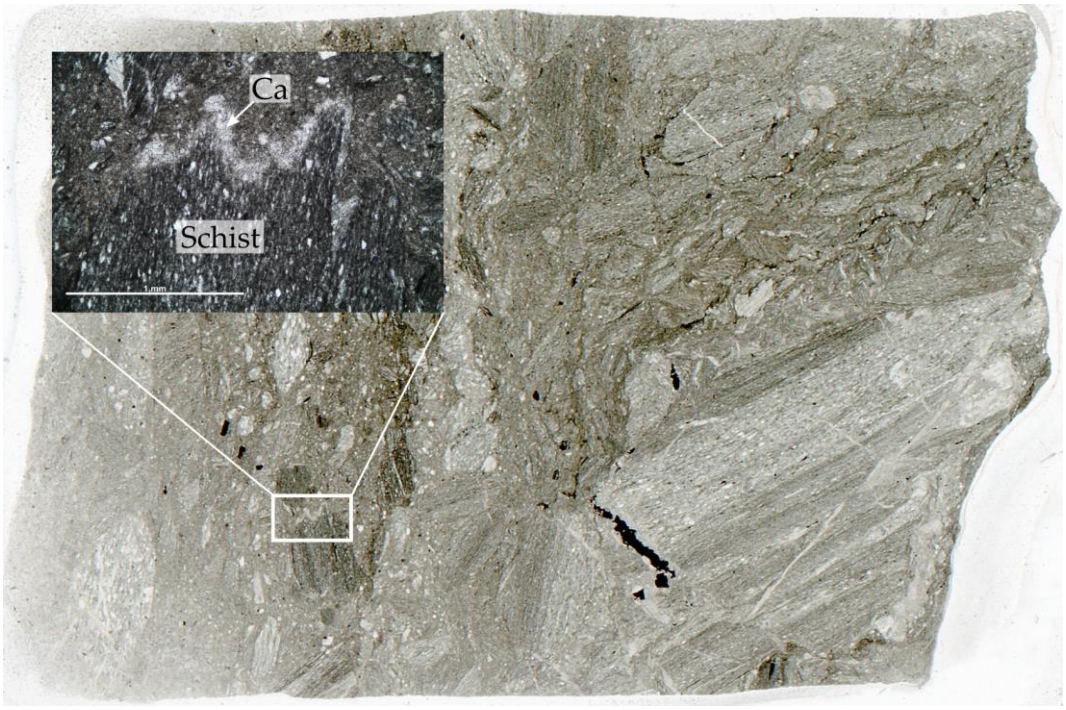

Figure 5.7. Scanned thin section of the brecciated schist. Inset shows cross-polarised photomicrograph of an angular clast rimmed by calcite.

5.3 Fault zone structure and deformation

5.3.1 Moonlight Fault ultracataclasite

The Moonlight Fault is marked by a black cohesive ultracataclasite that forms a resistant planar bench in Twelve Mile Creek (Figure 5.2). The contacts of the ultracataclasite consist of a planar surface on one side (the plane of the Moonlight Fault) with an undulating surface on the other (Figure 5.8). This undulating surface is not exclusively in contact with a particular wall of the fault. The undulating nature of the ultracataclasite causes it to 'pinch and swell' to zero thickness and 30 cm respectively, with the points of zero thickness likely an erosive feature. The ultracataclasite contains layers within it that also pinch and swell, at times appearing as an ultrafine, shiny layer upon the planar slip surface or as dark grey layers with variable fracture patterns. At times, <10 cm from the main fault plane a secondary ultracataclasite vein (up to 2 cm thick) was present in the footwall sediments (Figure 5.8). Slickenlines present on the planar slip surface were unable to be measured accurately but were steeply plunging (rake >60°).

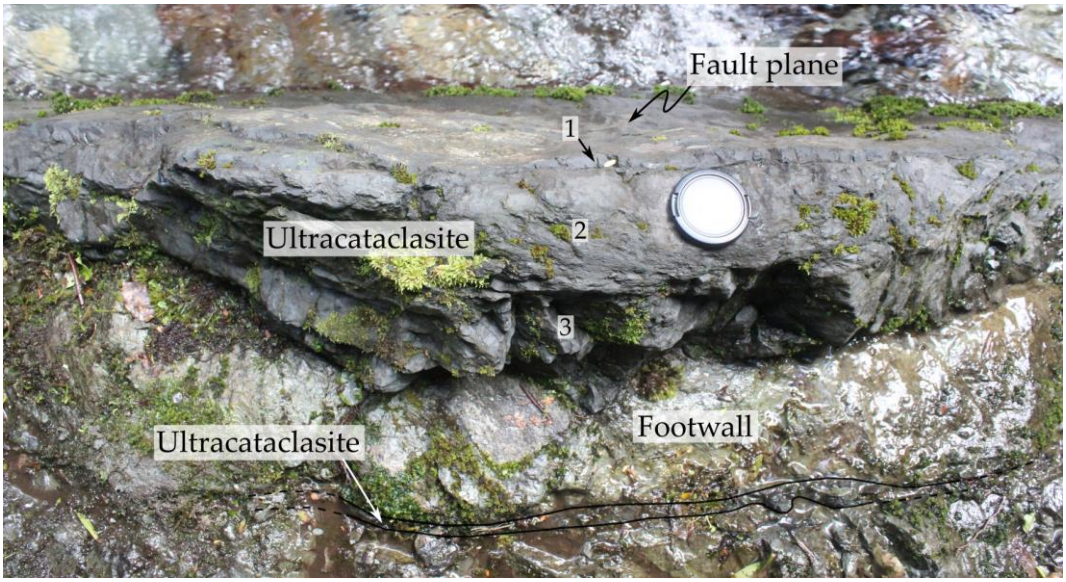

Figure 5.8. Photo looking down upon the Moonlight Fault plane showing the pinch and swell nature of the ultracataclasite. The ultracataclasite contains three distinct layers within it (1, 2 & 3) which are defined on the basis of their colour and fracture patterns.

5.3.2 Foliated fault gouge

In one location, immediately adjacent to the Moonlight Fault a <0.5 m incohesive foliated grey gouge is present. It contains subrounded schist fragments up to 6 cm in size indicating that it is derived from the sedimentary package. The foliation lies sub-parallel to the Moonlight Fault and with the schist clast long axes aligning parallel to the foliation (Figure 5.9).

5.3.3 Shear zones

The semi-schist and brecciated schist within the footwall contain sheared zones up to 1 m wide within the dark grey/argillite layers. Within these shear zones clast size decrease towards dark seams that truncate layering within the shear zone. The shear zone in the brecciated schist has elongate schist clasts aligning parallel to the black seams in the core of the shear zone (Figure 5.10).

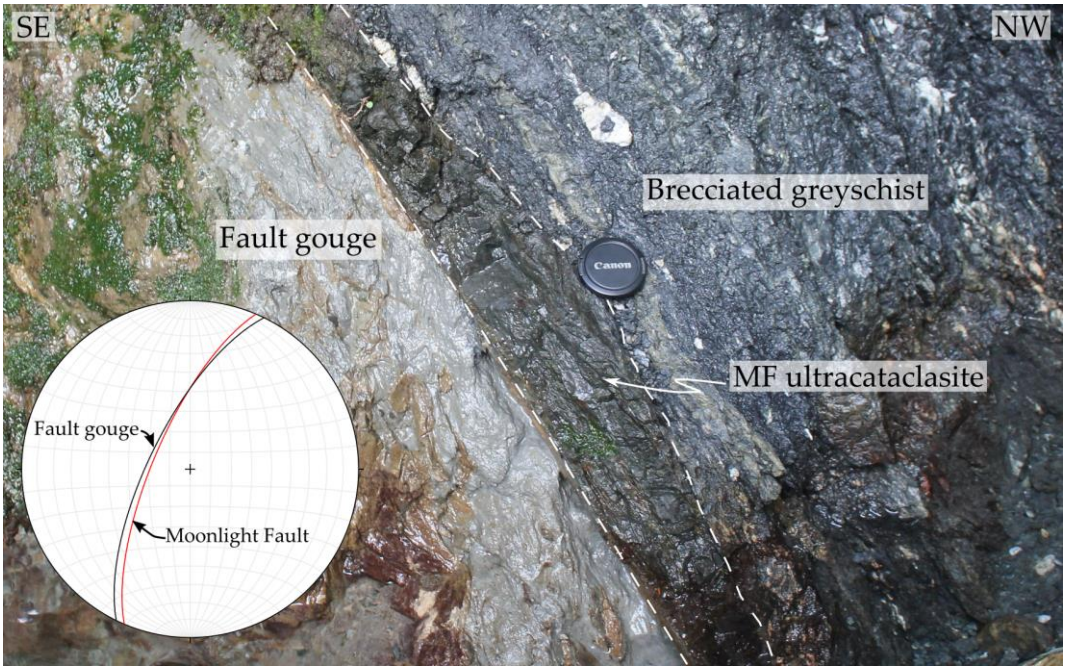

Figure 5.9. Grey fault gouge in the footwall of the Moonlight Fault is separated from brecciated greyschist in the hanging wall by an up to 10 cm thick, fault-defining ultracataclasite. Equal area lower hemisphere projection shows the parallel nature of the gouge foliation to the Moonlight Fault.

Figure 5.10. Shear zone within the brecciated schist. Black seams lie sub-parallel to the shear zone boundary.

5.4 Fault rock microstructures

5.4.1 Moonlight Fault ultracataclasite

The layering observed in outcrop in the ultracataclasite (Figure 5.8) is also observable in thin section and is defined by variations in the size and proportion of clasts (Figure 5.11). The majority of the Moonlight Fault core is an ultracataclasite (90-100% matrix) although some layers of cataclasite are present (50-90% matrix). Within the cataclastic layers clasts reach up to 0.5 mm in size and make up to 40% of the cataclasite. The proportion of clasts in the ultracataclasite varies between layers, with no clasts >0.3 mm size and the majority <0.1 mm. The layer of ultracataclasite in contact with the footwall gouge is almost entirely void of clasts (<1%), with those present <30 μm in size. Clasts in all layers are randomly oriented, sub-angular to sub rounded clasts set in a fine grained black or brown matrix.

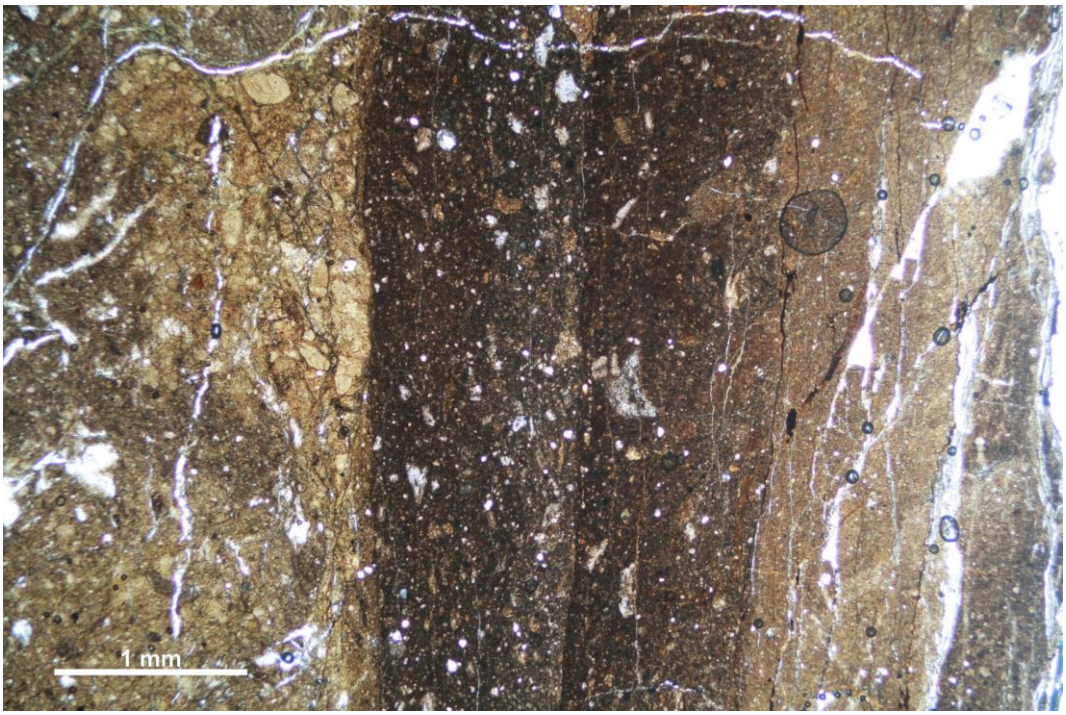

Figure 5.11. Plane-polarised photomicrograph of layering within the fault-defining ultracataclasite. The right edge of the image lies in contact with the footwall gouge. White 'veins' are cracks in the thin section.

XRD analysis revealed that the ultracataclasite predominately consists of quartz, albite and anorthite with SEM-EDS analysis identifying a number of minor phases including iron sulphide, calcite, titanite, K-feldspar and epidote. Quartz is present as individual crystals and in veins. Iron sulphide was observed as loose concentrations of crystals that reach 50 μm in width. Epidote appeared as individual rounded crystals of up to 30 μm size. Calcite appeared as individual crystals (rarely) as well as in veins. These veins contained large crystals with clear twinning and were often associated with quartz.

Contacts between the layers that are more clast-rich are largely graded over a few millimetres while the layers in contact with matrix-rich layers are sharp. These contacts lie sub-parallel to the orientation of the Moonlight Fault. Deformation in these cataclasite layers consist of brittle fractures which offset clasts and veins with movements on the order of <0.5 mm (Figure 5.12). These offsets lie perpendicular to the fault plane. The calcite+quartz veins were also folded with the crystals often highly deformed (Figure 5.12).

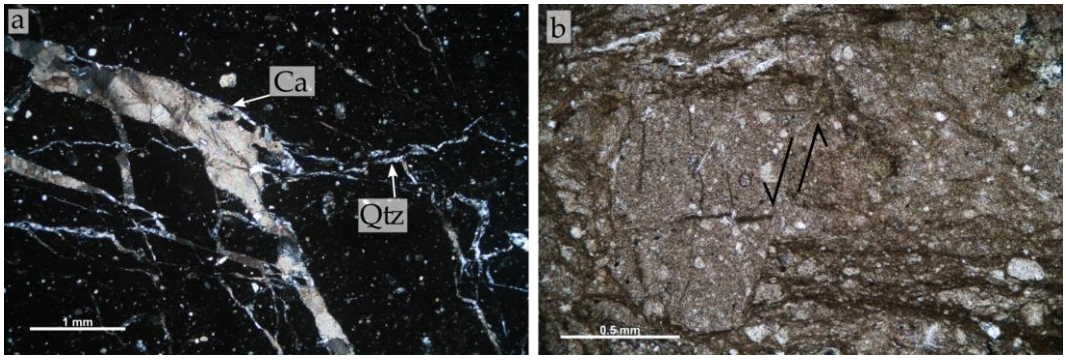

Figure 5.12. a) Complexly deformed Calcite (Ca) and quartz (Qtz) veins. b) small (<0.5 mm) brittle offsets within the ultracataclasite.

6. Discussion

This discussion will firstly investigate the exhumation history and offset of the Moonlight Fault Zone, then the deformation mechanisms active in the fault zone along strike. From these observations, frictional data from the literature will be applied to mechanical models of compressional basin inversion. The implications of this will then be discussed.

6.1 Neogene exhumation and offset

The Moonlight Fault Zone has juxtaposed TZIV green- and greyschists of the Torlesse Terrane along most of its length, with the exception of Twelve Mile Creek where Caples Terrane TZIIB semischist makes up the footwall lithology. These rocks contain a mineralogy indicating peak metamorphism at chlorite-zone, lower greenschist facies (eg. albite, quartz, chlorite, epidote, titanite). The peak metamorphism of chlorite zone schist occurred around 300˚C and 5 kbar (Essene, 1989; Mortimer, 2000) which, assuming a typical continental geotherm of 25˚/km, is c. 12 km depth.

Neogene exhumation of the region occurred due to regional uplift from oblique transpression of the Australian-Pacific plate boundary which began 5 ± 2 Ma (Norris et al., 1990) where uplift was greatest along the plate boundary (20-25 km) and decreased to the south-east (Cooper, 1980; Tippett and Kamp, 1993). Zircon fission track data retrieved from the basement rocks either side of the Moonlight Fault in the Matukituki Valley by Tippett & Kamp (1993) suggested that the area has been exhumed from around 9.5 ± 2.1 km depth. Decreasing uplift of the region southeast is also indicated by the increasing thickness of sediments along the MFZ towards Lake Wakatipu.

The clays present within fault gouge, montmorillonite in Twelve Mile Creek and kaolinite in Fan Creek (Menzies, 2014), are not stable above 150˚C (Moore and Lockner, 2007) and 300˚C (Hurst and Kunkle, 1985) respectively. Assuming a

typical continental geotherm the maximum depth of exhumation at Twelve Mile Creek is therefore 6 km and in Fan Creek, 12 km.

The Oligocene sedimentary sequences associated with normal movement on the Moonlight Fault have an estimated thickness of 2 - 4 km (Norris et al., 1978; Norris and Carter, 1982). This suggests that the basal unconformity present in several of the studied creek sections, cannot have been at more than 4 km depth before reverse reactivation of the Moonlight Fault, constraining maximum uplift to 4 km.

6.1.1 Offset along the Moonlight Fault

A structural thickness map of the Otago Schist based upon textural grade (Mortimer, 2003) reveals apparent dip-slip separation of 6 – 8 km in Twelve Mile – Fan Creek region, 5 km in the Moonlight – Stony Creeks and 3 km in the Matukituki Valley. The 3 km offset in the Matukituki Valley is corroborated by Tippett and Kamp (1993) who suggested that movement on the Moonlight Fault is unlikely to be more than 3 km, the value associated with their most probable error for zircon fission track data.

The apparent vertical offset of 6 – 8 km from Mortimer (2003) does not take into account the strike-slip component along the Moonlight Fault, made evident by juxtaposition of differing textural grades, which Norris and Carter (1982) suggested could be as great as 6 km. The observed lateral offset is c. 18 km, so replacing 6 km of strike-slip movement reduces the apparent vertical offset to 4 – 5 km. As the maximum thickness of the Bobs Cove Beds is 4 km, and that this sequence is absent from the hanging wall indicates that 4 km must be the lower limit of offset.

To summarise, reverse offset along the Moonlight Fault is likely in the range of 3 – 5 km, with greater offset closest to Lake Wakatipu. Exhumation is likely in the range of 4 - 10 km with greater exhumation towards the Alpine Fault.

6.2 Kinematics of the Moonlight Fault Zone

The Moonlight Fault is believed to have undergone post-Oligocene reverse movements, evident by the incorporation of the Bobs Cove Beds, juxtaposition of textural grades, upthrown schist foliation in the hanging wall and topographic variation across the fault (Turnbull et al., 1975; Norris et al., 1978; Craw, 1985).

Further evidence of reverse movement resultant from this study are as follows:

1) The steeply west dipping fault plane in Twelve Mile Creek are host to steeply plunging slickenlines (>60°) suggesting oblique dip slip.
2) The incohesive breccia within the footwall in Moonlight Creek believed to have formed during Moonlight Fault deformation contains Reidel shears that reveal a movement vector that indicates oblique dip-slip motion.
3) Moonlight generation folds throughout the footwall are commonly asymmetric with a top-east sense indicating reverse movements.
4) In the hanging wall slickenline measurements upon breccias in Moonlight Creek, cataclasites in the Matukituki Valley and faults in the sedimentary package in Fan Creek were all steeply plunging with offset markers indicating reverse movements.
5) Foliation parallel breccias in Fan Creek hanging wall contain microstructural evidence for top east movement (Menzies, 2014).

6.3 Fault zone deformation

6.3.1 Hanging wall deformation

Pseudotachylyte

It is widely believed that pseudotachylytes are formed by co-seismic frictional melting and are unequivocal evidence of slip at seismic rates (eg. Sibson, 1975), however friction melts have recently been produced at aseismic slip rates (Pec et al., 2012). All veins appeared to be single slip events or 'single-jerk microfaults' after Sibson (1975). As not all aphanitic rocks in the field are pseudotachylytes (Magloughlin and Spray, 1992) evidence of a prior melt phase must be clear (Sibson, 1975; Maddock, 1983; Magloughlin and Spray, 1992; Sibson and Toy, 2006). The pseudotachylytes in the Moonlight Fault hanging wall contain many features that suggest they represent a solidified melt phase, including;

1) Newly crystallised phases that are not found in the host schist (eg. microcline)

2) Amphibole spherulites and other microlitic crystals

3) Chilled margins and injection veins

4) Internal flow banding

5) Amygdules

6) Melt corroded rims of remnant clasts

The presence of ultracataclasites and reworked clasts of ultracataclasite along the margins of some fault veins indicates that cataclasis preceded frictional melting (Spray, 1992, 1995). The paucity of remnant ferromagnesium minerals (chlorite, stilpnomelane, actinolite) is a common feature in pseudotachylytes (eg. Maddock et al., 1987) which is due to the initial process of comminution selectively decreasing the grain size of these weaker minerals. This selective process influences the composition of the melt which are commonly Fe- and Mg-rich (Maddock, 1992).

The MFZ pseudotachylytes corroborate this with Mg- and Fe-rich newly crystalline phases in the form of granular, euhedral iron oxide grains (likely magnetite) and kaersutite spherulites (Mg bearing). Ilmenite microlites were also observed in some veins in association with the amphibole spherulites, a feature similar to that identified by previous authors (Sibson, 1975; Magloughlin, 2005; Lin, 2008). The newly grown ilmenite and kaeursutite are not found in the host rock and bear titanium which suggests that their growth has been facilitated by the melting of a Ti-rich phase from the host rock. The mineral that is most likely for this is titanite as it abundant in the host rocks while is very rarely found as a remnant clast within the pseudotachylyte veins. It is present in veins however as very fine grains (<2 μm) in clusters, much different to the elongate form it contains within the host rock suggesting that it has grown from the melt.

The presence or absence of certain mineral phases in pseudotachylyte can provide broad constraints on the minimum and maximum temperatures reached during pseudotachylyte formation. In the pseudotachylyte veins only quartz, albite and apatite are present as remnant host rock clasts, indicating that the other mineral phases in the greenschist were consumed by the melt. Quartz and apatite have melting temperatures of 1760^{o}C and 1500^{o}C, respectively (Robie et al., 1979)

and as these minerals are relatively unaltered (apart from corroded rims) this indicates that the maximum melt temperature did not exceed 1500°C. Albite (melting temperature of 1130°C) is highly disaggregated and contains extensive melt embayments, which suggests that the melt temperatures were at least 1130°C. The absence of remnant titanite grains in pseudotachylyte veins and the presence of newly grown Ti-rich phases suggests the former has melted, which takes place at 1384˚C (Thieblot et al., 1999). So, melt temperatures were likely >1384˚C though <1500˚C. At these temperatures it may be expected that albite be totally consumed by the melt however this would be influenced by grainsize variations and cooling rate (Maddock, 1992; Swanson, 1992; Lin, 2008).

Mixed pseudotachylyte – brittle fault veins

The mixed pseudotachylyte-brittle fault veins present in the Matukituki Valley and Moonlight Creek were both formed by brittle shearing however melt has only been produced in some regions along their length. The cause of this frictional melting may have been due to the presence of asperities along the shear surface forming areas of high shear stress and thus, heat production, forming localised areas of melt (Spray, 1992). The areas where pseudotachylyte are present have a narrow zone of deformation associated with it, indicating that the majority of the applied shear stress is taken up in the production of melt. Where no frictional melting was produced, ie. a cataclasite, the applied stress was distributed further into the wall rock forming a wider zone of deformation.

The mixed pseudotachylyte-brittle vein in the Matukituki Valley hanging wall was the only vein recognised to host amygdules, believed to be vesicles filled by a later fluid-deposited mineral phase, in this case calcite. Vesicles in pseudotachylytes develop by the exsolution of volatiles in a melt under low lithostatic pressure (Maddock et al., 1987) and are likely hydrous due to the melting of hydrous minerals such as chlorite and actinolite. Other reports of amygdule bearing pseudotachylytes in the literature indicate that they only occur at relatively shallow depths (Craddock and Magloughlin, 2005), as such, we interpret this mixed pseudotachylyte-brittle fault vein to have formed at less than 5 km depth.

Cataclasites and breccias

Catalasis in the hanging wall has formed by a combination of comminution, fracture and rotation of grains. Foliated cataclasites and ultracataclasites are present, with the foliation defined by compositional layering and grain size variations (Chester et al., 1985). Some of the ultracataclasites were present within wider cataclastic zones and bore slickenlines, indicating that shear has localised to these surfaces, increasing the degree of comminution (Engelder, 1974). Cataclasites are clearly the last deformation feature in the hanging wall as they are commonly observed cross cutting and offsetting previous deformation features.

Present in layer-parallel ultracataclasites and breccias are evidence for diffusive mass transfer (DMT). DMT processes occur by the transfer of material from zones of high stress (dissolution) to areas of low normal stress (precipitation) and are driven by chemical potential gradients assisted by the presence of fluids (Rutter, 1983; Knipe, 1989; Jefferies et al., 2006). These mechanisms are enhanced by finer grain sizes and are made evident by dissolution seams and overgrowths of chlorite upon quartz and albite clasts in layer-parallel ultracataclasites in Moonlight Creek. In Fan Creek foliation parallel breccias contain evidence for multiple cycles of DMT and alternating cataclasis. Fracturing and grain size reduction from cataclasis likely facilitated an influx of fluid (eg. Jefferies et al., 2006) which resulted in the precipitation of calcite as a cement and in conjugate fractures while also promoting the onset of DMT (Menzies, 2014). Dissolution-precipitation mechanisms are evident by the concentrations of relatively insoluble titanite which are sheared indicating a syn-tectonic origin.

Folding

In the Matukituki Valley hanging wall folds axes and lineations are sub-parallel and plunge moderately to the north-west, perpendicular to the strike of the Moonlight Fault. Lineations west of the Moonlight Fault in the Matukituki Valley plunge moderately to the west and Craw (1985) associated these with D_2 and D_3. As the lineations measured adjacent to the Moonlight Fault in this study show a slight deviation from this orientation, they may have rotated due to uplift in the hanging

wall of the Moonlight Fault and now display the overall movement direction upon the main fault (Bryant and Reed, 1969).

Within the intact greyschist in Twelve Mile Creek the orientations of the fold hinges form a plane parallel to the Moonlight Fault indicating they may be sheath folds as they form a curvilinear feature with >90˚ curvature (Ramsay and Huber, 1987; Skjernaa, 1989). Sheath folds are typically considered to represent the gradual rotation of fold hinges towards the direction of shear during progressive non-coaxial deformation (Cobbold and Quinquis, 1980). The steepest hinge lines are likely the 'point' of the sheath folds with the rotation of axes to shallower orientations representing the base of the sheath folds (Alsop and Holdsworth, 1999). If these are indeed sheath folds they indicate a shear direction that is steeply west-dipping.

Brecciation of schist

Where the hanging wall consisted of a quartzofeldspathic lithology there was a zone of brecciation or shearing up to 10 m wide adjacent to the trace of the Moonlight Fault. In these zones, any features contained within the host rocks, such as folds or continuous quartz veins, have been destroyed and a new fault-parallel foliation has formed. The orientation of the new fabric in this zone, and that it only occurs adjacent to the Moonlight Fault, indicates that it is related to movements upon the main fault plane.

6.3.2 Footwall deformation

Oligocene sediments

The sedimentary packages within the fault zone are similar to sequences described by Barry (1966) and Turnbull (1975) indicating they are basal sections of the larger Bob's Cove Beds sequence present on the shores of Lake Wakatipu. Shears within the sediments that penetrate the fault core indicate that deformation is synchronous with Moonlight Fault movement.

Also present in parts of the sedimentary sequence are stylolites, a pressure-dissolution feature which concentrates relatively insoluble minerals into serrated seams. Stylolites form roughly perpendicular to the main stress direction and are

commonly found parallel to the bedding planes due to depositional lithification and compaction (eg. Heald, 1955; Rispoli, 1981). The variety of orientations the stylolites contain suggests formation within a varying stress field (Railsback and Andrews, 1995), likely during the change from tectonic extension to compression.

Breccias

Within the footwall schist of the Moonlight Fault Zone breccias were identified up to 750 m from the main fault trace. One of the cohesive breccias was found to crosscut the macro-scale folds associated with Moonlight Fault deformation. It also contained foliation sub-parallel to the Moonlight Fault which suggests its formation was associated with Moonlight generation deformation and took up strain that was not accommodated by folding of the footwall greyschists.

6.3.3 Fault core deformation

The Moonlight Fault contains a fault core of foliated fault rocks rich in phyllosilicates as either a foliated cataclasite or foliated gouge, with the exception of Twelve Mile Creek which contains a random fabric ultracataclasite.

Foliated cataclasites are present in the Matukituki Valley and Fan Creek which in the Matukituki Valley was flanked by a 10 m wide zone of breccia that exhibits an increasing strain transition towards the Moonlight Fault. This is evident by i) progressive grain size reduction through cataclasis, ii) the increasing alignment, abundance and connectivity of fine grained phyllosilicate phases to form foliated cataclasites and, iii) the onset of dissolution – precipitation (diffusive mass transfer). The fracturing and grain scale dilatancy associated with this brecciation has allowed for the formation of fluid pathways into the fault core (Sibson, 1977). This fluid influx altered the load bearing clasts (albite+quartz) which produced fine grained aggregates of phyllosilicates (chlorite+muscovite) that align to form interconnected, anastomosing networks (Wintsch et al., 1995; Holdsworth, 2004). The observed localisation of strain into the foliated fault core suggests that these processes led to significant weakening of the fault zone (Jefferies et al., 2006).

Fault gouge in Moonlight Creek also shows the anastomosing network of phyllosilicates. Associated with the formation of the fine grained phyllosilicates and fluid influx is the onset of stress-induced diffusive mass transfer (dissolution-

precipitation) processes. Dissolution has occurred at sites of high strain and produces characteristic features such as pressure dissolution seams and sutured/indented albite clasts. Precipitation of this material occurs in low stress sites such as along the trailing edges of rigid albite and quartz clasts, which in the Moonlight Fault core by the fibrous chlorite overgrowths. The differences in composition between dissolved (e.g. albite) and precipitated (e.g. chlorite) phases indicate incongruent pressure solution (Beach, 1979).

Dissolution-precipitation features within phyllosilicate rich rocks were experimentally produced by Bos et al. (2000) and Bos and Spiers (2002). From this they produced a model of 'frictional-viscous flow' where deformation was achieved by frictional slip along phyllosilicate foliation planes accompanied by pressure solution of rigid clasts at high stress sites. The experiments on frictional-viscous flow indicates it is associated with velocity strengthening behaviour characteristic of aseismic creep (Bos and Spiers, 2002; Niemeijer and Spiers, 2005; Ikari et al., 2011).

Fault rocks within the fault core that do not contain evidence for frictional-viscous flow are present in Twelve Mile Creek as a cohesive, foliated ultracataclasite and in Fan Creek as an incohesive, random fabric fault gouge. These have formed by cataclastic flow, involving brittle fracture and comminution, with the gouge likely having formed <4 km depth (Sibson, 1977). The Twelve Mile Creek ultracataclasite has a foliation defined by grainsize variations due to the localisation of strain into fine grained regions.

Evidence for fluid within the fault core is present not only by fluid-induced DMT but also in the form of calcite and quartz veins. The veins are commonly folded and disaggregated indicating that they formed synchronously with cataclastic deformation. The dilatational quartz veins that taper away from the fault core in Fan Creek suggests large volumes of fluid has been associated with faulting (Sibson, 1981).

6.4 Along strike variation in fault zone structure

Pseudotachylyte is present in the hanging wall from the Matukituki Valley to the Moonlight Creek, a distance of c. 50 km along strike in the Moonlight Fault Zone. It was hosted in greenschist in the Matukituki Valley and Stony Creek and a competent quartzofeldspathic gneiss in Moonlight Creek. Pseudotachylyte was not observed in hanging wall of the Fan and Twelve Mile Creeks which contain fissile greyschists. Pseudotachylyte has been found to occur largely in crystalline rocks which typically have low porosities and high competence (Sibson and Toy, 2006). It may be that the fissility of the host rocks in Twelve Mile and Fan Creeks did not allow for the accumulation of elastic strain energy required to produce melt. Instead deformation in the fissile greyschists is accommodated by foliation-parallel breccias which are the along strike equivalent of the pseudotachylytes.

Of the pseudotachylyte fault veins observed in the Matukituki Valley 85% were either parallel or sub-parallel to the foliation, while elsewhere along strike all veins lay sub-parallel. This suggests that the foliation in the hanging wall greenschist represented a strong anisotropy allowing for preferential failure along the foliation. The field observations are consistent with other reports of natural pseudotachylyte (eg. Sibson, 1975) and also experimental work by Paterson and Wong (2005) who demonstrated that the brittle shear strength parallel to the foliation is half of the brittle shear strength perpendicular to foliation. This would allow for preferential failure parallel to the foliation.

Deformation in the footwall of the Moonlight Fault has been accommodated predominately by folding on various scales. Folding associated with movement on the Moonlight Fault has previously been studied by Barry (1966) and Craw (1985) on a regional scale, the latter terming this deformation phase D_4. Regional folding in the footwall during D_4 formed the Shotover Antiform which strikes sub-parallel to the trace of the Moonlight Fault with a fold axes shallowly plunging to the south. Kink, chevron and macro-scale folds recorded in the field areas all contain a similar orientation to the Shotover Antiform indicating they are likely related to D_4 deformation. In Twelve Mile Creek no folding was observed in the footwall and

deformation was limited to pelitic layers host to shear fabrics that lie sub-parallel to the Moonlight Fault, implying they formed during D_4 movements.

Foliated cataclasites and foliated gouge are present within the Moonlight Fault core from the Matukituki Valley to Fan Creek, a distance of approximately 53 km. Evidence of diffusive mass transfer mechanisms within these fault rocks suggests they experienced widespread aseismic creep.

6.5 Frictional strength measurements

Fault zones that contain foliated phyllosilicate-rich fault cores have been shown to reduce the strength of mature faults compared to standard values of friction for the crust (eg. Wintsch et al., 1995; Holdsworth, 2004). The coefficients of friction for a variety of minerals have been experimentally derived by a number of authors (eg. Byerlee, 1978; Morrow et al., 2000; Moore and Lockner, 2004) and have found that phyllosilicate phases in particular can have much lower friction coefficients than the values outlined by Byerlee (1978). This is due to platy minerals becoming preferentially oriented parallel to shear planes, where shear can occur along weak interlayer bonds. In dry conditions they largely retain friction coefficients similar to those summarised by Byerlee (1978), however under saturated conditions these values can be much less. Water adsorbs to the surface of the sheet structures due to a surface charge attraction forming a thin film between platy grains even under high effective normal stress coefficient (Morrow et al., 2000; Moore and Lockner, 2004). This provides a low-resistance slip interface which substantially reduces the frictional strength of the material as shear is concentrated into the water films that separate phyllosilicate sheets.

Due to the presence of fluid-induced DMT processes it seems reasonable to suggest that when active the Moonlight Fault contained a water-saturated fault core with high proportions of chlorite and muscovite. Experimentally derived friction values for these two minerals under saturated conditions are displayed in Table 6.1 with variations due to varying conditions of experiments. These values must be treated as the upper limit of friction as the experiments have been completed on powdered samples which Collettini et al. (2009) has shown have higher friction values that intact wafers.

The summation of these authors shows that coefficients of friction for muscovite and chlorite decrease in the presence of fluid (eg. Moore and Lockner, 2004) and slightly increase with temperature (Mariani et al., 2006; Van Diggelen et al., 2010; den Hartog et al., 2013). The effect of sliding velocity on friction has been found to be independent (Mariani et al., 2006; Van Diggelen et al., 2010) and dependant (Ikari et al., 2009). This difference may be attributed to the purity of the samples as Van Diggelen et al. (2010) and Mariani et al. (2006) used pure gouges while Ikari et al. (2009) experiments contained 46% weak phase. Niemeijer and Spiers (2005) also found that with increasing purity of muscovite-halite gouges the more likely the strength was independent of sliding velocity.

Some authors indicate an increase in friction coefficient with an increase in effective normal stress (Behnsen and Faulkner, 2012) while others have found that it stays consistent (Kopf and Brown, 2003; Ikari et al., 2009). (Behnsen and Faulkner, 2012) attributed this to water loss which would lead to a reduction in pore space which increases mineral-mineral contacts creating more 'dry' friction interfaces. However in a confined environment no water loss would occur thus, no increase of friction would be expected.

Also included for comparison in Table 1 are friction coefficients for natural gouge from the Alpine Fault, New Zealand which contain proportions of muscovite/illite and chlorite slightly less than that of the foliated cataclasites in the Moonlight Fault. These gouge samples were experimentally deformed as wafers in their natural state. Fault gouge from Gaunt Creek was tested by Boulton et al. (2012) and Barth et al. (2013) under the same conditions with the exception of the effective normal stress which showed that an increase in effective normal stress resulted in an increase in friction coefficient. The foliated cataclasites in the Moonlight Fault core contain a higher proportion of phyllosilicates to framework silicates, and as it has been shown that friction coefficient decreases with increasing gouge purity (Niemeijer and Spiers, 2005; den Hartog et al., 2013) they may contain lower values of friction, at the same experimental conditions, than the Alpine Fault gouges.

Ideally, for modelling failure along a fault (see Section 6.6) the friction coefficient for muscovite and chlorite used would be that closest to represent the temperatures and pressures they deformed at within the Moonlight Fault (ie. 5 – 10

km). Although higher friction values are given for muscovite at higher temperatures (ie. μ = 0.56 at 300˚C)(Van Diggelen et al., 2010), the value for chlorite and the effective normal stresses within the compressive tectonic setting of the Moonlight Fault are unknown. So for this case, the friction coefficients used will be those retrieved from low temperature experiments while also allowing for easier comparison to previous work.

Despite the differences, all reported friction coefficients at room temperature for muscovite lie within the range of μ = 0.312 – 0.619 with an average of μ = 0.38, while chlorite values lie between μ = 0.18 – 0.38 with an average of μ = 0.32.

Table 6.1. Experimentally-measured friction coefficients for natural gouge, muscovite, chlorite and crustal rock under varying conditions.

	Friction coefficient (μ)	*Saturation*	*Effective normal stress (MPa)*	*Displacement (mm)*	*Axial displacement velocity (μm/s^{-1})*	*Mineral %*	*Temp (°C)*
Natural Gouge							
Boulton et al. (2012)	0.31	Y	31	-	1 - 300	Musc/illite - 32 Chl – 9	Room
Barth et al. (2013)	0.28	Y	6	-	1 - 300	Musc/illite - 32 Chl – 9	Room
Barth et al. (2013)	0.37	Y	31	-	1 - 300	Musc/illite - 35 Chl - 39	Room
Muscovite							
Moore and Lockner (2004)	0.42	Y	100	5	0.5	100	Room
Morrow et al. (2000)	0.42	Y	100	5	0.5	100	Room
Behnsen and Faulkner (2012)	0.38	Y	100	0.4	0.5	100	Room
den Hartog et al. (2013)	0.4 - 0.84	Y	170	<40	1 - 100	65	100 - 600
den Hartog et al. (2013)	0.3 - 0.67	Y	170	<40	1 - 100	100	100 - 600
Scruggs and Tullis (1998)	0.35 - 0.43	Room Humidity	25	6 - 331	1 - 10	100	Room
Van Diggelen et al. (2010)	0.56	Y	20 - 100	<70	0.03 - 3.7	90	300
Van Diggelen et al. (2010)	0.38	Y	20 - 100	<70	0.03 - 3.7	90	Room
Mariani et al. (2006)	0.25 - 5	Y	34 - 190		0.0003 - 0.61	100	400 - 700
Niemeijer and Spiers (2005)	0.312	Y - Brine	1 – 9	40	<1	100	Room
Niemeijer and Spiers (2005)	0.486 – 0.619	Y – Brine	1 - 5	32 - 60	<1 – 10	20	Room
Chlorite							
Moore and Lockner (2004)	0.38	y	100	5	0.5	100	Room
Morrow et al. (2000)	0.38	Y	100	5	0.5	100	Room
Ikari et al. (2009)	0.27 - 0.32	Y	12 - 59	<36	0.5 - 300	46	Room
Brown et al. (2003)	0.26	Y	2 - 30	<23	0.01 - 100	-	Room
Kopf and Brown (2003)	0.18 - 0.26	Y	2 - 30	<23	0.01 - 100	-	Room
Behnsen and Faulkner (2012)	0.32	Y	100	0.7	0.5	95	Room
Crustal rock (Westerly Granite)							
Beeler et al. (1996)	0.6 - 0.8	Room humidity	25	10-100	0.5	-	Room

6.6 Mechanics of inversion

In this section, field and microstructural observations from the Moonlight Fault are combined with published values of frictional strength (Table 6.1) to explore possible reactivation scenarios during compressional basin inversion.

Anderson (1905) showed that faults form when the crust fails in accordance with the Coloumb criterion (inclusive of fluid pressure, P_f after Sibson, 1990b):

$$\tau = C + \mu_i \sigma_n' = C + \mu_i (\sigma_n - P_f) \qquad (1)$$

Where τ and σ_n are, respectively, the shear and normal stresses acting upon the fault plane; μ_i, the coefficient of internal friction and C, cohesive strength are rock material properties. Jaeger and Cook (1979) found that the coefficient of internal friction (μ_i) lies between 0.5 – 1, so that brittle faults should form at $32^\circ > \Theta_i > 22^\circ$ to the maximum compressive stress (σ_1) where $\theta_i = 45° - \Phi/2$ (and $\phi = \tan^{-1} \mu_i$) (Figure 6.1). Therefore within an extensional 'Andersonian' regime where $\sigma_1 = \sigma_v$, the overburden stress is vertical, normal faults should form with initial dips of 58° – 68° (see Chapter 1, Figure 1.1).

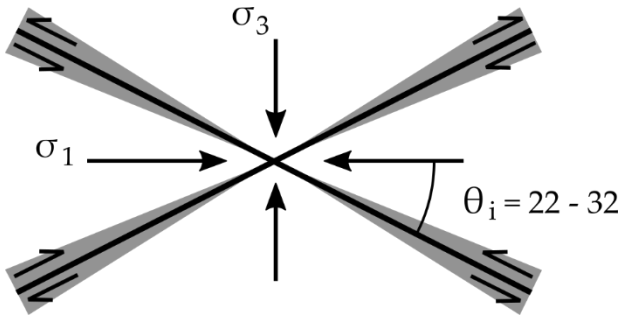

Figure 6.1. Expected attitudes of faults forming in intact homogeneous, isotropic crust relative to the maximum compressive stress.

However this theory is based upon the initiation of faults within intact crust and does not account for reactivation of pre-existing faults. The conditions for fault reactivation remove cohesion from (1) as it is assumed to be negligible thus the reactivation criterion can be represented as:

$$\tau = \mu_s \sigma_n' = \mu_s (\sigma_n - P_f) \qquad (2)$$

where μ_s is the static coefficient of friction (Sibson, 1985) and can be represented in Figure 6.2.

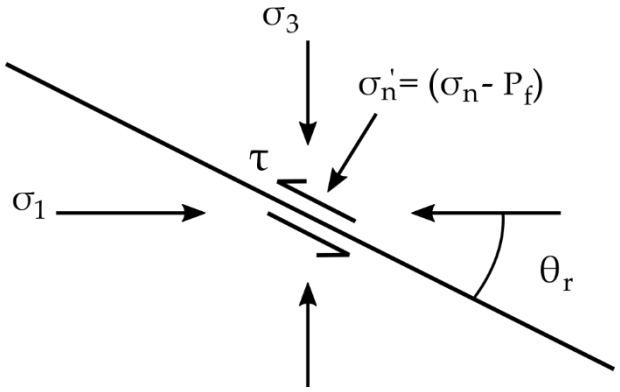

Figure 6.2. Resolved stress components affecting the stability of a cohesionless fault plane. See text for details.

When the poles to the existing faults lie within the $\sigma_1/\ \sigma_3$ plane (σ_2 is contained within the fault plane) the reactivation criterion, that is, the relative ease of reactivation over a range orientations (θ_r), can be viewed in a 2-dimensional case in terms of the ratio of effective stresses as:

$$\frac{\sigma_1'}{\sigma_3'} = \frac{(\sigma_1 - P_f)}{(\sigma_3 - P_f)} = \frac{(1 + \mu_s cot\theta_r)}{(1 - \mu_s tan\theta_r)} \qquad (3)$$

The level of fluid pressure at a depth (z) is defined in terms of the pore-fluid factor, $\lambda_v = P_f/\rho gz$, where p is the average rock density and g is gravitational acceleration. The magnitude of differential stress required for reactivation of a fault with dip (δ) for particular values of ρ, μ_s, z and λ_v can then be rewritten as:

$$(\sigma_1 - \sigma_3) = \frac{\mu_s(tan\delta + cot\delta)}{(1 - \mu_s tan\delta)} \rho gz(1 - \lambda_v) \qquad (4)$$

The optimum angle for reactivation occurs when the differential stress (σ_1'/σ_3') required for reshear is at a minimum, which is when, $\theta_r^* = 0.5\ tan^{-1}(1/\mu_s)$. With increasing deviation from this, reactivation becomes progressively more difficult as a higher differential stress is required and at $\theta_r = 2\theta_r^*$ frictional lockup takes place, which when considering Byerlee-type friction (μ_s = 0.6 – 0.8), occurs at 50^0 - 59^0. However, from a compilation of intracontinental reverse faults Sibson and Xie (1998) found that the apparent frictional lock-up angle takes place at c. 59^o, consist with the lower end of Byerlee-type friction, ie. μ = 0.6. So for existing normal

faults (ie. dip c. 60°) that now lie within a compressional regime during basin inversion would lie close to the lockup angle.

Equation 4 allows for the differential stress to be plotted against fault dip (δ) for a particular depth, friction coefficient and various values of the pore-fluid factor (Sibson, 1990b). For application of differential stress required for failure to the Moonlight Fault with a friction coefficient of 0.6, Figure 6.3 is plotted for a depth of 7.5 km, the average assumed depth of exhumation (5 – 10 km). Also plotted is the value for the shear strength of intact rock approximated by assuming a composite Griffith-Coulomb failure envelope normalised to rock tensile strength (T) with a cohesive strength (C = 2T) and coefficient of internal friction (μ_i = 0.75)(Sibson, 1998). The T = 10 MPa corresponds to rock of moderate competence (Lockner, 1995).

So in Figure 6.3 reactivation will occur when a fault lies within the 'reshear field'. For a particular pore fluid factor (λ_v) the differential stress required for reshear increases away from the optimal reactivation angle and if it crosses into the T = 10 MPa field, new, optimally oriented faults are easier to form in the surrounding rock than reactivation of the steeply-dipping fault (Sibson and Xie, 1998; Sibson, 2009). However, with an increasing pore fluid factor, the possible dip range for reshear increases to the lock-up angle. Beyond this is a field defined as 'severe misorientation' where failure upon a fault can only occur if $\sigma_3' < 0$, or the fluid pressure becomes supralithostatic ($P_f > \sigma_3$). The potential dip range for the Moonlight Fault is also included, consisting of expected dip values of reactivated normal faults (58°) and the current dip measured in the field (66° – 74°). This range, for μ_s = 0.6, lies predominantly in the field of severe misorientation indicating that for failure to occur on the Moonlight Fault supralithostatic fluid pressures would be needed.

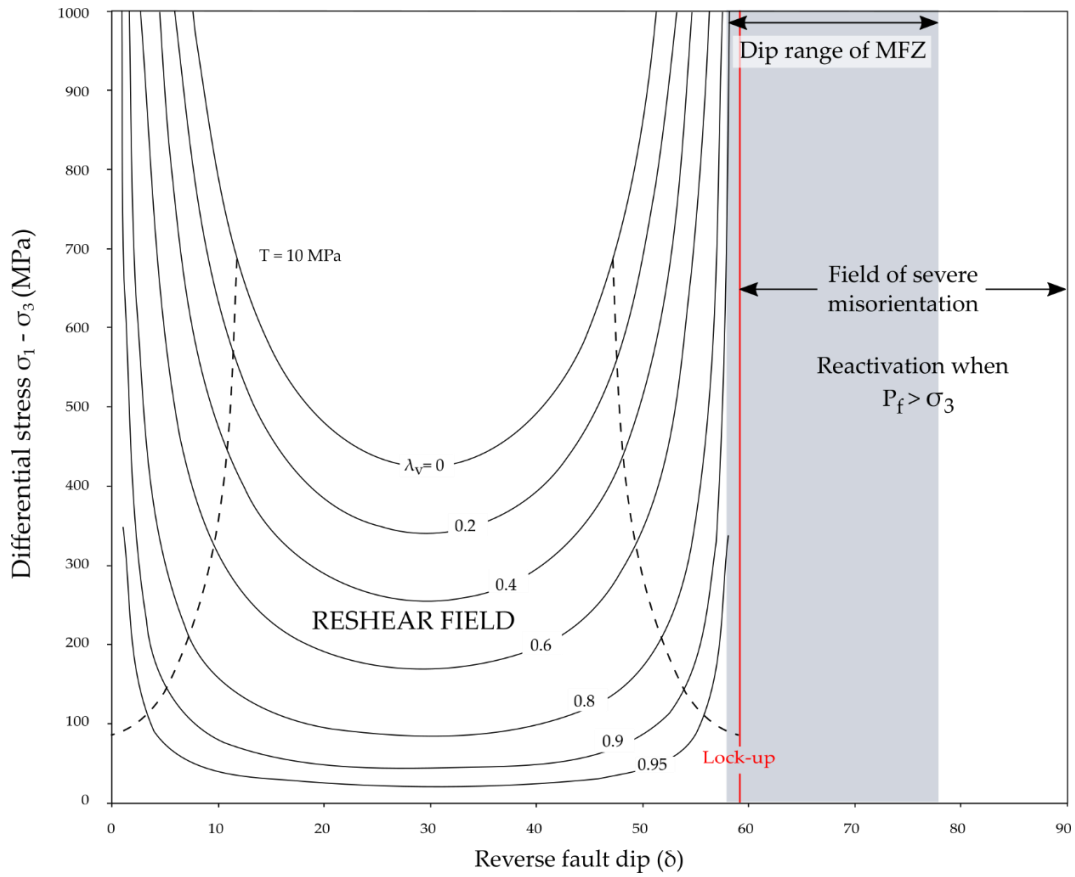

Figure 6.3. Plot of the differential stress required for reshear on normal faults with varying dip (δ) under compressional inversion. Valid for a friction coefficient of 0.6 at a depth of 7.5 km with varying λ_v. Shear strength of intact rock with T = 10 MPa calculated on assumption of $\mu_i = 0.75$ and a cohesive strength, C = 2T, for varying pore fluid factor, λ_v.

However, the lockup angle of 59˚ only holds when using a friction coefficient of 0.6. As discussed in the previous section, the chlorite and muscovite-rich cataclasites in the fault core of the Moonlight Fault contain a friction coefficient of 0.35, taken as the average value of those shown in Table 6.1. Figure 6.4 indicates that for a friction coefficient of 0.35, depth of 7.5 km, and hydrostatic fluid pressure (λ_v = 0.4) the angle of fault dip possible for reactivation increases to 65˚. With increasing pore fluid pressure, the possible dip range for reshear increases to the lock-up angle, 71˚. The potential dip range for the Moonlight Fault straddles the fields of reshear and severe misorientation, which shows that the lower friction coefficient has increased the dip range possible for reactivation. The implications of this will be discussed in the following section.

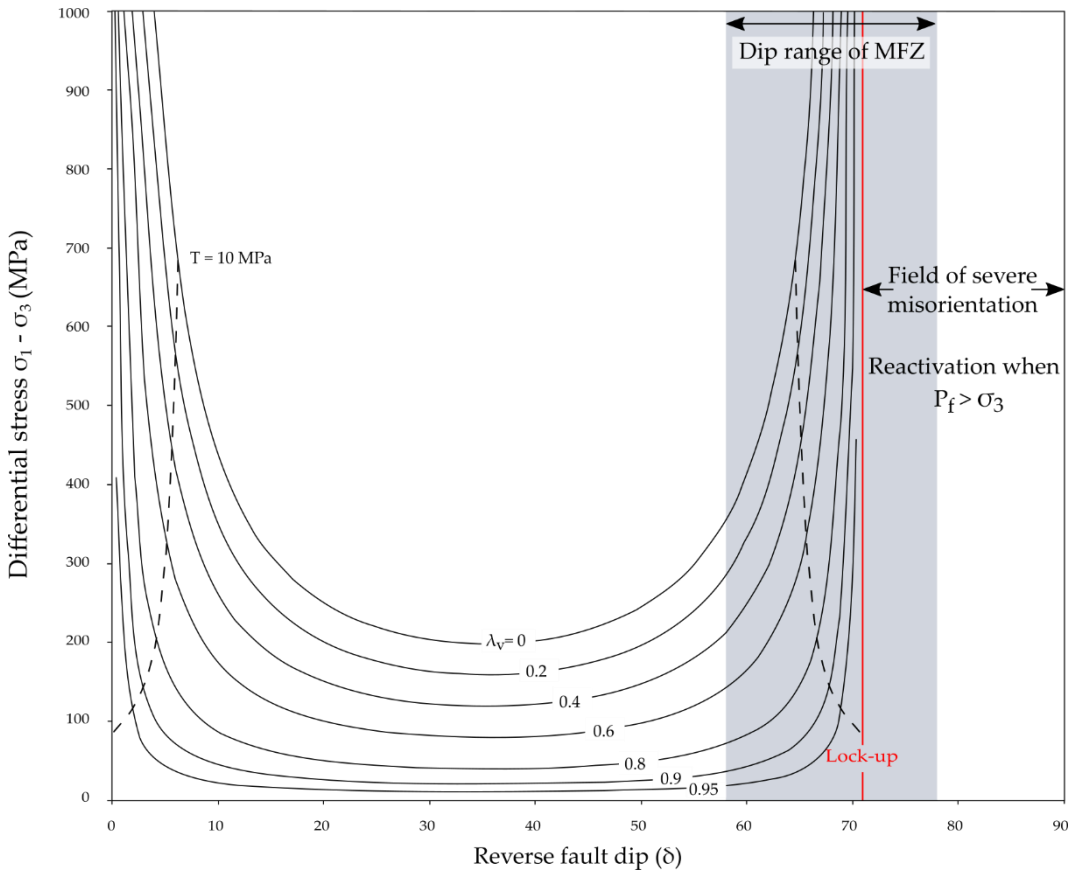

Figure 6.4. Plot of the differential stress required for reshear on normal faults with varying dip (δ) under compressional inversion. Valid for a friction coefficient of 0.35 at a depth of 7.5 km with varying λ_v. Shear strength of intact rock with T = 10 MPa calculated on assumption of $\mu_i = 0.75$ and a cohesive strength, C = 2T, for varying λ_v.

6.7 Implications

6.7.1 Failure along the Moonlight Fault Zone

The low friction coefficients that the foliated cataclasites and gouges present within the Moonlight Fault core allow for normal fault reactivation with dips up to 70˚. For faults that dip at the expected attitude of normal faults (58˚), the differential stress required for reshear drops significantly and can be reactivated at hydrostatic or only slightly supra-hydrostatic values of the pore fluid factor. The Moonlight Fault dip range (66˚ - 77˚) lies in the both the field of reshear and severe misorientation. For portions of the fault that lie in the field of reshear, ie. dip 66˚ - 70˚, failure can only occur in the presence of increased fluid pressure (from hydrostatic) with a pore fluid factor of at least 0.7. However, this indicates that supra-lithostatic pore fluid factors are not required for reverse reactivation of high-angle reverse faults.

Areas of the Moonlight Fault that dip >71˚, such as in Fan Creek (77˚) and Stony Creek (74˚), lie within the field of severe misorientation indicating that in these areas supra-lithostatic fluid pressures were necessary for reactivation. Within Fan Creek dilatational quartz veins tapering away from the fault core suggest that failure was accommodated by localised supralithostatic fluid pressures. No evidence for fluid overpressure was present in Stony Creek however, which suggests that the fault may have steepened post-failure, or that the friction coefficient is lower than that used for the modelling purposes, which would increase the lock-up angle placing the Moonlight Fault in Stony Creek within the reshear field.

Observation of the Moonlight Fault in Twelve Mile Creek revealed that the fault core consisted of an ultracataclasite, with no observed evidence of interconnected phyllosilicates, as found in other creek sections. As the depth of exhumation in this region is limited to 4 km, it may be that the pressure and/or temperature is not great enough for frictional-viscous deformation to occur. A compilation of fault zones bearing similar fault rocks to the MFZ by Wallis et al. (2015) has found that the lower limit of these fault rocks is currently at c. 5 km.

The purely friction based model presented here is used to compare current models of normal fault reactivation to the Moonlight Fault. However there is microstructural evidence for frictional-viscous flow within the fault core and this mechanism incorporates more than just frictional sliding on phyllosilicate foliae. Models of F-V flow on mixed halite-muscovite gouges by Niemeijer and Spiers (2005) based upon models by Bos and Spiers (2002) revealed that F-V flow also incorporates pressure solution, dilatational cataclasis and plastic flow within the phyllosilicate foliae. Although frictional slip is one of the main factors controlling fault strength (along with plastic flow) the purely friction model applied is a limitation of this work. Future work could be to factor in these elements to more accurately model failure upon the Moonlight Fault such as Wallis et al. (2015) has done for the Karakorum Fault Zone in the Himalayas.

6.7.2 Basin inversion

Sedimentary basin inversion and fault reactivation has been investigated by analytical, analogue and numerical models to determine deformation patterns resulting from inversion and also to address the conditions which allow reactivation of high-angle normal faults under compression (cf. Bonini et al., 2012). Previous modelling of fault reactivation has largely considered high fluid pressure conditions, specifically fluid overpressure, as a key factor controlling reverse-slip, although it has been mentioned that 'weak' fault rocks may be a possible explanation for reactivation (eg. Etheridge, 1986; Sibson, 1995). 'Weak fault' models have been explored using sandbox experiments with weak layers including glass microbeads, clay and silicon putty and have found evidence for fault reactivation during basin inversion (eg. Panien et al., 2005; Marques and Nogueira, 2008). Until now there has been no field based exploration of the friction contained within fault cores in relation to basin inversion, however faults bearing low-friction, phyllosilicate-rich fault cores, such as the Median Tectonic Line in Japan (Jefferies et al., 2006) and Zuccale Fault in Italy have also been found to be the reason for failure in unoptimal orientations (eg. Holdsworth, 2004; Collettini et al., 2009). This thesis has shown that the presence of a low-friction, phyllosilicate-rich fault core can explain movement upon reactivated normal faults that lie at high-angles to the compression direction during basin inversion.

7. Conclusions

Previous research on the mechanics of fault reactivation during basin inversion has not incorporated detailed field and microstructural observations. The Moonlight Fault Zone provides the opportunity to do so and this study has provided some of the first field- and microstructural-based constraints on the structure and fault rock assemblages of a major, basin-bounding normal fault that was reactivated as a high-angle reverse fault.

Field research along 70 km of the Moonlight Fault has revealed reverse movements formed a variety of fault rock assemblages in response to the wall rock composition. The schistosity of hanging wall host rocks has exerted a strong anisotropic control on the formation of layer parallel breccias and pseudotachylytes along its length, the latter of which is present over a distance of 50 km. The footwall consists mainly of greyschist where deformation was primarily achieved through folds ranging from kink bands to macro-scale.

The fault core contains foliated cataclasites and gouges which consist of interconnected networks of chlorite and muscovite. Deformation within the phyllosilicate rich fault core has occurred by a combination of frictional slip along phyllosilicate seams and dissolution-precipitation creep.

Comparison of these phyllosilicate-rich fault cores to frictional strength measurements from previous work indicates that the Moonlight Fault core contained friction coefficients between 0.32 – 0.38, much less than the 0.6 – 0.85 of Byerlee-type friction. Application to reactivation models indicates that these friction coefficients increase the lock-up angle of faults, allowing for typical normal faults with dips of 60˚ to be reactivated as high-angle reverse faults at relatively low differential stresses and only slight – moderately suprahydrostatic fluid pressures. This also suggests that failure on the Moonlight Fault was largely accommodated due to the presence of these low-friction fault cores, while areas that dip greater than the lock-up angle contained evidence for supralithostatic fluid pressures. As

high-angle reverse faults are a common feature in compressional basins, faults bearing foliated and phyllosilicate-rich fault rocks may be a regular occurrence.

References

Adams, C. J. (1981) Migration of late Cenozoic volcanism in the South Island of New Zealand and the Campbell Plateau. *Nature,* 294**,** 153-155.

Adams, C. J., Campbell, H. J. & Griffin, W. L. (2009a) Tracing the Caples Terrane through New Zealand using detrital zircon age patterns and radiogenic isotope signatures. *New Zealand Journal of Geology and Geophysics,* 52**,** 223-245.

Adams, C. J. & Gabites, J. E. (1985) Age of metamorphism and uplift in the Haast Schist Group at Haast Pass, Lake Wanaka and Lake Hawea, South Island, New Zealand. *New Zealand Journal of Geology and Geophysics,* 28**,** 85-96.

Adams, C. J. & Graham, I. J. (1997) Age of metamorphism of Otago Schist in eastern Otago and determination of protoliths from initial strontium isotope characteristics. *New Zealand Journal of Geology and Geophysics,* 40**,** 275-286.

Adams, C. J. & Kelley, S. (1998) Provenance of Permian-Triassic and Ordovician metagraywacke terranes in New Zealand: Evidence from 40Ar/39Ar dating of detrital micas. *Geological Society of America Bulletin,* 110**,** 422-432.

Adams, C. J., Mortimer, N., Campbell, H. J. & Griffin, W. L. (2009b) Age and isotopic characterisation of metasedimentary rocks from the Torlesse Supergroup and Waipapa Group in the central North Island, New Zealand. *New Zealand Journal of Geology and Geophysics,* 52**,** 149-170.

Adams, C. J. & Robinson, P. (1993) Potassium-argon age studies of metamorphism/uplift/cooling in Haast Schist coastal sections south of Dunedin, Otago, New Zealand. *New Zealand Journal of Geology and Geophysics,* 36**,** 317-325.

Alsop, G. I. & Holdsworth, R. E. (1999) Vergence and facing patterns in large-scale sheath folds. *Journal of Structural Geology,* 21**,** 1335-1349.

Anderson, E. M. (1905) The dynamics of faulting. *Transactions of the Edinburgh Geological Society,* 8**,** 387-402.

Andrews, P. B., Speden, I. G. & Bradshaw, J. D. (1976) Lithological and paleontological content of the Carboniferous-Jurassic Canterbury Suite, South Island, New Zealand. *New Zealand Journal of Geology and Geophysics,* 19**,** 791-819.

Barber, A. & Craw, D. (2002) Lithology, geochemistry, and structure of Moke Creek sulphide deposit host rocks, Otago Schist, New Zealand. *New Zealand Journal of Geology and Geophysics,* 45**,** 193-205.

Barry, J. (1966) Structural analysis in the middle Shotover valley, northwest Otago. *Unpublished MSc thesis*, University of Otago.

Barth, N. C., Boulton, C., Carpenter, B. M., Batt, G. E. & Toy, V. G. (2013) Slip localization on the southern Alpine Fault, New Zealand. *Tectonics,* 32**,** 620-640.

Beach, A. (1979) Pressure solution as a metamorphic process in deformed terrigenous sedimentary rocks. *Lithos,* 12**,** 51-58.

Beeler, N., Tullis, T., Blanpied, M. & Weeks, J. (1996) Frictional behavior of large displacement experimental faults. *Journal of Geophysical Research: Solid Earth (1978–2012),* 101**,** 8697-8715.

Behnsen, J. & Faulkner, D. R. (2012) The effect of mineralogy and effective normal stress on frictional strength of sheet silicates. *Journal of Structural Geology,* 42**,** 49-61.

Bishop, D. G. (1972) Progressive Metamorphism from Prehnite-Pumpellyite to Greenschist Facies in the Dansey Pass Area, Otago, New Zealand. *Geological Society of America Bulletin,* 83**,** 3177-3198.

Bishop, D. G., Bradshaw, J. D. & Landis, C. A. (1985) Provisional terrane map of South Island, New Zealand. *In:* HOWELL, D. G. (ed.) *Tectonostratigraphic terranes.* Houston, Texas: Circum-Pacific Council for Energy and Mineral Resources.

Bishop, D. G., Bradshaw, J. D., Landis, C. A. & Turnbull, I. M. (1976) Lithostratigraphy and structure of the Caples terrane of the Humboldt Mountains, New Zealand. *New Zealand Journal of Geology and Geophysics,* 19**,** 827-848.

Bonini, M., Sani, F. & Antonielli, B. (2012) Basin inversion and contractional reactivation of inherited normal faults: A review based on previous and new experimental models. *Tectonophysics,* 522–523**,** 55-88.

Bos, B., Peach, C. J. & Spiers, C. J. (2000) Frictional-viscous flow of simulated fault gouge caused by the combined effects of phyllosilicates and pressure solution. *Tectonophysics,* 327**,** 173-194.

Bos, B. & Spiers, C. J. (2002) Frictional-viscous flow of phyllosilicate-bearing fault rock: Microphysical model and implications for crustal strength profiles. *Journal of Geophysical Research: Solid Earth,* 107**,** Online Only.

Boulton, C., Carpenter, B., Toy, V. & Marone, C. (2012) Physical properties of surface outcrop cataclastic fault rocks, Alpine Fault, New Zealand. *Geochemistry, Geophysics, Geosystems,* 13.

Bradshaw, J. D. (1989) Cretaceous geotectonic patterns in the New Zealand Region. *Tectonics,* 8**,** 803-820.

Brown, K. M., Kopf, A., Underwood, M. B. & Weinberger, J. L. (2003) Compositional and fluid pressure controls on the state of stress on the Nankai subduction thrust: A weak plate boundary. *Earth and Planetary Science Letters,* 214**,** 589-603.

Bryant, B. & Reed, J. C. (1969) Significance of lineation and minor folds near major thrust faults in the southern Appalachians and the British and Norwegian Caledonides. *Geological Magazine,* 106**,** 412-429.

Buchanan, P. G. & Mcclay, K. R. (1992) Experiments on basin inversion above reactivated domino faults. *Marine and Petroleum Geology,* 9**,** 486-500.

Byerlee, J. (1978) Friction of rocks. *Pure and Applied Geophysics,* 116**,** 615-626.

Chester, F. M., Friedman, M. & Logan, J. M. (1985) Foliated cataclasites. *Tectonophysics,* 111**,** 139-146.

Cobbold, P. R. & Quinquis, H. (1980) Development of sheath folds in shear regimes. *Journal of Structural Geology,* 2**,** 119-126.

Collettini, C. & Sibson, R. H. (2001) Normal faults, normal friction? *Geology,* 29**,** 927-930.

Collettini, C., Viti, C., Smith, S. a. F. & Holdsworth, R. E. (2009) Development of interconnected talc networks and weakening of continental low-angle normal faults. *Geology,* 37**,** 567-570.

Cooper, A. F. (1980) Retrograde alteration of chromian kyanite in metachert and amphibolite whiteschist from the Southern Alps, New Zealand, with implications for uplift on the Alpine Fault. *Contributions to Mineralogy and Petrology,* 75**,** 153-164.

Cooper, M., Williams, G., De Graciansky, P., Murphy, R., Needham, T., De Paor, D., Stoneley, R., Todd, S., Turner, J. & Ziegler, P. (1989) Inversion tectonics—a discussion. *Geological Society, London, Special Publications,* 44**,** 335-347.

Craddock, J. P. & Magloughlin, J. F. (2005) Calcite strains, kinematic indicators, and magnetic flow fabric of a Proterozoic pseudotachylyte swarm, Minnesota River valley, USA. *Tectonophysics,* 402**,** 153-168.

Craw, D. (1984) Lithologic variations in Otago Schist, Mt Aspiring area, northwest Otago, New Zealand. *New Zealand Journal of Geology and Geophysics,* 27**,** 151-166.

Craw, D. (1985) Structure of Schist in the Mt Aspiring Region, Northwestern Otago, New-Zealand. *New Zealand Journal of Geology and Geophysics,* 28**,** 55-75.

De Graciansky, P., Dardeau, G., Lemoine, M. & Tricart, P. (1989) The inverted margin of the French Alps and foreland basin inversion. *Geological Society, London, Special Publications,* 44**,** 87-104.

Den Hartog, S. a. M., Niemeijer, A. R. & Spiers, C. J. (2013) Friction on subduction megathrust faults: Beyond the illite–muscovite transition. *Earth and Planetary Science Letters,* 373**,** 8-19.

Engelder, J. T. (1974) Cataclasis and the Generation of Fault Gouge. *Geological Society of America Bulletin,* 85**,** 1515-1522.

Essene, E. J. (1989) The current status of thermobarometry in metamorphic rocks. *Geological Society, London, Special Publications,* 43**,** 1-44.

Etheridge, M. (1986) On the reactivation of extensional fault systems. *Philosophical Transactions of the Royal Society of London A: Mathematical, Physical and Engineering Sciences,* 317**,** 179-194.

Fitzharris, B. B. (1965) Geology of the Elmtree Creek area, Southland. University of Otago.

Forster, M. A. & Lister, G. S. (2003) Cretaceous metamorphic core complexes in the Otago Schist, New Zealand. *Australian Journal of Earth Sciences,* 50**,** 181-198.

Frost, C. D. & Coombs, D. S. (1989) Nd isotope character of New Zealand sediments; implications for terrane concepts and crustal evolution. *American Journal of Science,* 289**,** 744-770.

Gray, D. R. & Foster, D. A. (2004) 40Ar/39Ar thermochronologic constraints on deformation, metamorphism and cooling/exhumation of a Mesozoic accretionary wedge, Otago Schist, New Zealand. *Tectonophysics,* 385**,** 181-210.

Grindley, G. W. (1963) Structure of the alpine schists of South Westland, Southern Alps, New Zealand. *New Zealand Journal of Geology and Geophysics,* 6**,** 872-930.

Hacket, J. R. (1864) Report on Limestone at Lake Wakatipu. Otago Provincial Government Gazette.

Heald, M. T. (1955) Stylolites in Sandstones. *The Journal of Geology,* 63**,** 101-114.

Holdsworth, R. E. (2004) Weak Faults--Rotten Cores. *Science,* 303**,** 181-182.

Hurst, V. J. & Kunkle, A. C. (1985) Dehydroxylation, rehydroxylation, and stability of kaolinite. *Clays Clay Miner,* 33**,** 1-14.

Hutton, C. O. (1939) The Bob's Cove beds and the Moonlight Thrust-Fault. *Transactions and Proceedings of the Royal Society of N.Z.,* 69**,** 73-88.

Ikari, M. J., Marone, C. & Saffer, D. M. (2011) On the relation between fault strength and frictional stability. *Geology,* 39**,** 83-86.

Ikari, M. J., Saffer, D. M. & Marone, C. (2009) Frictional and hydrologic properties of clay-rich fault gouge. *Journal of Geophysical Research: Solid Earth,* 114**,** n/a-n/a.

Jefferies, S. P., Holdsworth, R. E., Shimamoto, T., Takagi, H., Lloyd, G. E. & Spiers, C. J. (2006) Origin and mechanical significance of foliated cataclastic rocks in the cores of crustal-scale faults: Examples from the Median Tectonic Line, Japan. *Journal of Geophysical Research: Solid Earth,* 111**,** Online Only.

Jugum, D., Norris, R. H. & Palin, J. M. (2013) Late Jurassic detrital zircons from the Haast Schist and their implications for New Zealand terrane assembly and metamorphism. *New Zealand Journal of Geology and Geophysics,* 56**,** 223-228.

Knipe, R. (1989) Deformation mechanisms—recognition from natural tectonites. *Journal of Structural Geology,* 11**,** 127-146.

Kopf, A. & Brown, K. M. (2003) Friction experiments on saturated sediments and their implications for the stress state of the Nankai and Barbados subduction thrusts. *Marine Geology,* 202**,** 193-210.

Korsch, R. J. & Wellman, H. W. (1988) The Geological Evolution of New Zealand and the New Zealand Region. *In:* NAIRN, A. M., STEHLI, F. & UYEDA, S. (eds.) *The Ocean Basins and Margins.* Springer US.

Lin, A. (2008) *Fossil Earthquakes: The formation and preservation of pseudotachylytes,* Berlin, Springer Berlin Heidelberg.

Little, T. A., Mortimer, N. & Mcwilliams, M. (1999) An episodic Cretaceous cooling model for the Otago-Marlborough Schist, New Zealand, based on 40Ar/39Ar white mica ages. *New Zealand Journal of Geology and Geophysics,* 42**,** 305-325.

Lockner, D. A. (1995) Rock failure. *Rock physics and phase relations: A handbook of physical constants,* 3**,** 127-147.

Macgregor, D. S. (1995) Hydrocarbon habitat and classification of inverted rift basins. *Geological Society, London, Special Publications,* 88**,** 83-93.

Mackinnon, T. C. (1983) Origin of the Torlesse terrane and coeval rocks, South Island, New Zealand. *Geological Society of America Bulletin,* 94**,** 967-985.

Maddock, R. H. (1983) Melt origin of fault-generated pseudotachylytes demonstrated by textures. *Geology,* 11**,** 105-108.

Maddock, R. H. (1992) Effects of lithology, cataclasis and melting on the composition of fault-generated pseudotachylytes in Lewisian gneiss, Scotland. *Tectonophysics,* 204**,** 261-278.

Maddock, R. H., Grocott, J. & Van Nes, M. (1987) Vesicles, amygdales and similar structures in fault-generated pseudotachylytes. *Lithos,* 20**,** 419-432.

Magloughlin, J. F. (2005) Immiscible sulfide droplets in pseudotachylyte: Evidence for high temperature (> 1200 °C) melts. *Tectonophysics,* 402**,** 81-91.

Magloughlin, J. F. & Spray, J. G. (1992) Frictional melting processes and products in geological materials: introduction and discussion. *Tectonophysics,* 204**,** 197-204.

Mariani, E., Brodie, K. H. & Rutter, E. H. (2006) Experimental deformation of muscovite shear zones at high temperatures under hydrothermal

conditions and the strength of phyllosilicate-bearing faults in nature. *Journal of Structural Geology,* 28**,** 1569-1587.

Marques, F. O. & Nogueira, C. R. (2008) Normal fault inversion by orthogonal compression: Sandbox experiments with weak faults. *Journal of Structural Geology,* 30**,** 761-766.

Mckay, A. (1881) The district west and north of Lake Wakatipu. Wellington: NZ Geological Survey Reports of Geological Explorations 1879-1880.

Menzies, T. (2014) Structure, mineralisation and fluid flow in the Moonlight Fault Zone, Fan Creek, Queenstown*. Unpublished BSc (Hons)*, University of Otago.

Moore, D. E. & Lockner, D. A. (2004) Crystallographic controls on the frictional behavior of dry and water-saturated sheet structure minerals. *Journal of Geophysical Research: Solid Earth,* 109**,** Online Only.

Moore, D. E. & Lockner, D. A. (2007) Friction of the smectite clay montmorillonite. *The Seismogenic Zone of Subduction Thrust Faults***,** 317-345.

Morrow, C. A., Moore, D. E. & Lockner, D. A. (2000) The effect of mineral bond strength and adsorbed water on fault gouge frictional strength. *Geophysical Research Letters,* 27**,** 815-818.

Mortimer, N. (1993a) Jurassic tectonic history of the Otago Schist, New Zealand. *Tectonics,* 12**,** 237-244.

Mortimer, N. (1994) Origin of the Torlesse Terrane and Coeval Rocks, North Island, New Zealand. *International Geology Review,* 36**,** 891-910.

Mortimer, N. (2000) Metamorphic discontinuities in orogenic belts: example of the garnet–biotite–albite zone in the Otago Schist, New Zealand. *International Journal of Earth Sciences,* 89**,** 295-306.

Mortimer, N. (2003) A provisional structural thickness map of the Otago Schist, New Zealand. *American Journal of Science,* 303**,** 603-621.

Mortimer, N. & Roser, B. P. (1992) Geochemical evidence for the position of the Caples–Torlesse boundary in the Otago Schist, New Zealand. *Journal of the Geological Society,* 149**,** 967-977.

Niemeijer, A. R. & Spiers, C. J. (2005) Influence of phyllosilicates on fault strength in the brittle-ductile transition: insights from rock analogue experiments. *Geological Society, London, Special Publications,* 245**,** 303-327.

Norris, R. J. & Bishop, D. G. (1990a) Deformed conglomerates and textural zones in the Otago Schists, South Island, New Zealand. *Tectonophysics,* 174**,** 331-349.

Norris, R. J. & Carter, R. M. (1982) Fault-bounded blocks and their role in localising sedimentation and deformation adjacent to the alpine fault, southern New Zealand. *Tectonophysics,* 87**,** 11-23.

Norris, R. J., Carter, R. M. & Turnbull, I. M. (1978) Cainozoic sedimentation in basins adjacent to a major continental transform boundary in southern New Zealand. *Journal of the Geological Society,* 135**,** 191-205.

Norris, R. J. & Craw, D. (1987) Aspiring terrane: An oceanic assemblage from New Zealand and its implications for terrane accretion in the southwest Pacific. *Terrane Accretion and Orogenic Belts.* Washington, DC: AGU.

Norris, R. J., Koons, P. O. & Cooper, A. F. (1990) Australasian tectonics The obliquely-convergent plate boundary in the South Island of New Zealand: implications for ancient collision zones. *Journal of Structural Geology,* 12**,** 715-725.

Norris, R. J., Koons, P. O. & Cooper, A. F. (1990b) The obliquely-convergent plate boundary in the South Island of New Zealand: implications for ancient collision zones. *Journal of Structural Geology,* 12**,** 715-725.

Panien, M., Schreurs, G. & Pfiffner, A. (2005) Sandbox experiments on basin inversion: testing the influence of basin orientation and basin fill. *Journal of Structural Geology,* 27**,** 433-445.

Park, J. (1909) The Geology of the Queenstown Subdivision. *Bulletin N.Z. Geological Survey,* 7.

Paterson, M. S. & Wong, T. F. (2005) *Experimental Rock Deformation: the Brittle Field,* Berlin, Springer.

Pec, M., Stünitz, H., Heilbronner, R., Drury, M. & De Capitani, C. (2012) Origin of pseudotachylites in slow creep experiments. *Earth and Planetary Science Letters,* 355**,** 299-310.

Pickard, A. L., Adams, C. J. & Barley, M. E. (2000) Australian provenance for Upper Permian to Cretaceous rocks forming accretionary complexes on the New Zealand sector of the Gondwanaland margin. *Australian Journal of Earth Sciences,* 47**,** 987-1007.

Railsback, L. B. & Andrews, L. M. (1995) Tectonic stylolites in the 'undeformed' Cumberland Plateau of southern Tennessee. *Journal of Structural Geology,* 17**,** 911-915.

Ramsay, J. G. & Huber, M. I. (1987) *The techniques of modern structural geology: Folds and fractures*, Academic press.

Rattenbury, M. S., Jongens, R. & Cox, S. C. (2010) *Geology of the Wakatipu Area*, 1:250000. Lower Hutt, New Zealand: Institute of Geological & Nuclear Sciences Ltd.

Rispoli, R. (1981) Stress fields about strike-slip faults inferred from stylolites and tension gashes. *Tectonophysics,* 75**,** T29-T36.

Robie, R. A., Hemingway, B. S. & Fisher, J. R. (1979) Thermodynamic properties of minerals and related substances at 298.15 K and 1 Bar (105 Pascals) pressure and at higher temperatures. *US Geological Survey Bulletin,* 1452.

Roser, B. P. & Korsch, R. J. (1999) Geochemical characterization, evolution and source of a Mesozoic accretionary wedge: the Torlesse terrane, New Zealand. *Geological Magazine,* 136**,** 493-512.

Rutter, E. H. (1983) Pressure solution in nature, theory and experiment. *Journal of the Geological Society,* 140**,** 725-740.

Scholz, C. H., Rynn, J. M. W., Weed, R. W. & Frohlich, C. (1973) Detailed Seismicity of the Alpine Fault Zone and Fiordland Region, New Zealand. *Geological Society of America Bulletin,* 84**,** 3297-3316.

Scruggs, V. J. & Tullis, T. E. (1998) Correlation between velocity dependence of friction and strain localization in large displacement experiments on feldspar, muscovite and biotite gouge. *Tectonophysics,* 295**,** 15-40.

Sibson, R. H. (1975) Generation of Pseudotachylyte by Ancient Seismic Faulting. *Geophysical Journal International,* 43**,** 775-794.

Sibson, R. H. (1977) Fault rocks and fault mechanisms. *Journal of the Geological Society,* 133**,** 191-213.

Sibson, R. H. (1981) Fluid Flow Accompanying Faulting: Field Evidence and Models. *In:* SIMPSON, D. W. & RICHARDS, P. G. (eds.) *Earthquake Prediction: An International Reviw.* American Geophysical Union.

Sibson, R. H. (1985) A note on fault reactivation. *Journal of Structural Geology,* 7**,** 751-754.

Sibson, R. H. (1990a) Conditions for fault-valve behaviour. *Geological Society, London, Special Publications,* 54**,** 15-28.

Sibson, R. H. (1990b) Rupture nucleation on unfavorably oriented faults. *Bulletin of the Seismological Society of America,* 80**,** 1580-1604.

Sibson, R. H. (1995) Selective fault reactivation during basin inversion: potential for fluid redistribution through fault-valve action. *Geological Society, London, Special Publications,* 88**,** 3-19.

Sibson, R. H. (1998) Brittle failure mode plots for compressional and extensional tectonic regimes. *Journal of Structural Geology,* 20**,** 655-660.

Sibson, R. H. (2009) Rupturing in overpressured crust during compressional inversion—the case from NE Honshu, Japan. *Tectonophysics,* 473**,** 404-416.

Sibson, R. H., Robert, F. & Poulsen, K. H. (1988) High-angle reverse faults, fluid-pressure cycling, and mesothermal gold-quartz deposits. *Geology,* 16**,** 551-555.

Sibson, R. H. & Toy, V. G. (2006) The habitat of fault-generated pseudotachylyte: Presence vs. absence of friction-melt. *Earthquakes: Radiated Energy and the Physics of Faulting.* Washington, DC: AGU.

Sibson, R. H. & Xie, G. (1998) Dip range for intracontinental reverse fault ruptures: Truth not stranger than friction? *Bulletin of the Seismological Society of America,* 88**,** 1014-1022.

Skjernaa, L. (1989) Tubular folds and sheath folds: definitions and conceptual models for their development, with examples from the Grapesvare area, northern Sweden. *Journal of Structural Geology,* 11**,** 689-703.

Spray, J. G. (1992) A physical basis for the frictional melting of some rock-forming minerals. *Tectonophysics,* 204**,** 205-221.

Spray, J. G. (1995) Pseudotachylyte controversy: Fact or friction? *Geology,* 23**,** 1119-1122.

Swanson, M. T. (1992) Fault structure, wear mechanisms and rupture processes in pseudotachylyte generation. *Tectonophysics,* 204**,** 223-242.

Thieblot, L., Tequi, C. & Richet, P. (1999) High-temperature heat capacity of grossular (Ca3Al2Si3O12), enstatite (MgSiO3), and titanite (CaTiSiO5). *Am. Mineral,* 84**,** 848-855.

Tippett, J. M. & Kamp, P. J. J. (1993) The role of faulting in rock uplift in the Southern Alps, New Zealand. *New Zealand Journal of Geology and Geophysics,* 36**,** 497-504.

Turnbull, I. M. (1969) Stratigraphy, structure and metamorphism in the Bobs Cove: Moke Creek: Queenstown area, Lake Wakatipu*. Unpublished BSc (Hons)* University of Otago.

Turnbull, I. M. (1980) Structure and interpretation of the Caples terrane of the Thomson Mountains, northern Southland, New Zealand. *New Zealand Journal of Geology and Geophysics,* 23**,** 43-62.

Turnbull, I. M., Barry, J. M., Carter, R. M. & Norris, R. J. (1975) The Bobs Cove Beds and their relationship to the Moonlight Fault Zone. *Journal of the Royal Society of New Zealand,* 5**,** 355-394.

Turnbull, I. M., Mortimer, N. & Craw, D. (2001) Textural zones in the Haast Schist—a reappraisal. *New Zealand Journal of Geology and Geophysics,* 44**,** 171-183.

Turner, J. P. & Williams, G. A. (2004) Sedimentary basin inversion and intra-plate shortening. *Earth-Science Reviews,* 65**,** 277-304.

Van Diggelen, E. W. E., De Bresser, J. H. P., Peach, C. J. & Spiers, C. J. (2010) High shear strain behaviour of synthetic muscovite fault gouges under hydrothermal conditions. *Journal of Structural Geology,* 32**,** 1685-1700.

Wallis, D., Lloyd, G. E., Phillips, R. J., Parsons, A. J. & Walshaw, R. D. (2015) Low effective fault strength due to frictional-viscous flow in phyllonites, Karakoram Fault Zone, NW India. *Journal of Structural Geology,* 77**,** 45-61.

Wandres, A. M., Bradshaw, J. D., Weaver, S., Maas, R., Ireland, T. & Eby, N. (2004a) Provenance analysis using conglomerate clast lithologies: a case study from the Pahau terrane of New Zealand. *Sedimentary Geology,* 167**,** 57-89.

Wandres, A. M., Bradshaw, J. D., Weaver, S., Maas, R., Ireland, T. & Eby, N. (2004b) Provenance of the sedimentary Rakaia sub-terrane, Torlesse Terrane, South Island, New Zealand: the use of igneous clast compositions to define the source. *Sedimentary Geology,* 168**,** 193-226.

White, S. R. (2002) The Siberia Fault Zone, northwest Otago, and kinematics of mid-Cenozoic plate boundary deformation in southern New Zealand. *New Zealand Journal of Geology and Geophysics,* 45**,** 271-287.

Wintsch, R. P., Christoffersen, R. & Kronenberg, A. K. (1995) Fluid-rock reaction weakening of fault zones. *Journal of Geophysical Research: Solid Earth,* 100**,** 13021-13032.

Wood, B. L. (1966) *Sheet 24-Invercargill: Geological Map of New Zealand, 1:250,000*. Wellington: NZ Department of Scientific and Industrial Research.

Woodcock, N. H. & Mort, K. (2008) Classification of fault breccias and related fault rocks. *Geological Magazine,* 145**,** 435-440.

Appendix

A. Field access

Matukituki Valley

From the Raspberry Creek carpark follow the 4WD track up through the shelter belt. From here the fault trace outcrops just below 700 m elevation up the valley wall, halfway between Big and Downs Creeks.

Stony Creek

Moke Lake – ***4WD*** track to Moke Creek crossing at Darky's Terrac – Cross Moonlight Creek to Moonlight Lodge (Old Siphon) – 4WD track over Murphy's Saddle to Stony Creek (ends at .610). Travel up at creek level until impassable waterfall, climb bank on true right and traverse hillside until possible to drop into creek again at base of gorge, the location of the Moonlight Fault.

Moonlight Creek

Moke Lake – ***4WD*** track to Moke Creek crossing at Darky's Terrace – Butchers Hut – Lower terrace on Sheepyard Terrace – Follow 4WD track down to Moonlight Creek – 1-1.5hr easy walk up (and in) creek to outcrop at (NZTopo50 map ref) CB10 518 174. Good campsites near large bend in river (CB11 525 175). To reach fault trace requires wading/clamber through river on true right under cliffs (sedimentary package), fine under normal flow, impassable if high. To reach outcrop in the hanging wall on the true right has two options. One requires a (waist-deep) wade through river just above pool (after initial wade/scramble), possible at normal flow, though only linked with a partner. The second, safer, route is to cross the creek below the pool and climb ~100 m beside cliffs to a narrow ledge which allows access to top of cliffs then down (fault) gully back to creek.

Twelve Mile Creek

Access is via the Mt Crichton Loop Track. Entering Twelve Mile Creek at the confluence of Maori Gully, the fault plane is easily located 40 m upstream on true right.

B. Scanning electron microscopy

Scanning Electron Microscopy (SEM) and quantitative Energy-Dispersive X-ray Spectroscopy (EDS) was used on carbon coated thin sections at the University of Otago on a Zeiss Sigma VP FED SEM. SEM imaging was completed in backscatter mode (BSE) with an AsB detector. An aperture size of 120 μm was used at working distance of 6-8 mm and EHT of 15 kV. EDS data was analysed using Aztec by Oxford Instruments.

C. X-ray diffraction

University of Otago

Methods

X-ray diffraction was used to analyse powdered fault rock assemblages not identifiable by optical microscopy or SEM-EDS. This was completed at the University of Otago on a PANalytical X'Pert-Pro MPD PW3040/60 XRD. Samples were first powdered by hand with the exception of DC8_1 which was powdered by a micronizing mill. All samples were placed in a standard slide mount and run for 25 minutes from a start position (˚2Θ) of 3.0072 to 79.9912 with a step size and step of 0.008 and 4.96 (s), respectively. Scans were completed at a temperature of 25˚C with tension at 40 kV, current of 30 mA.

CSIRO report

CSIRO LAND AND WATER
www.csiro.au

XRD Report – Quantitative XRD Analysis of Bulk and Clay Fractions of Samples for University of Otago

Mark D Raven and Peter G Self

Report No: D3302

November 2015

Simon Alder

Commercial-in-confidence

Citation

Raven, M.D. and Self, P.G. (2015) XRD Report – Quantitative XRD Analysis of Bulk and Clay Fractions of Samples for University of Otago. CSIRO, Australia.

Introduction

Two samples were submitted by Simon Alder from University of Otago, NZ for bulk and clay fraction quantitative mineralogy by X-ray diffraction (XRD) analysis.

Sample Preparation

Approximately 1.5g of the as-received samples were ground for 10 minutes in a McCrone micronizing mill under ethanol. The resulting slurries were oven dried at 60°C then thoroughly mixed in an agate mortar and pestle before being lightly back pressed into stainless steel sample holders for X-ray diffraction analysis.

Particle size separation

Approximately 8g of the as received samples were dispersed using a 1wt.% sodium hexametaphosphate – 1wt.% sodium carbonate solution. From this dispersion the <2μm and >2μm size fractions were collected by repeated ultrasonification and centrifugation. At the completion of each ultrasonification-centrifugation step, the supernatant from the centrifugation was collected in 1 litre beakers.

The collected <2μm fractions were recovered by flocculation using excess NaCl and centrifugation. The recovered materials were twice washed with acetic acid solution (approximately 0.2M) to remove carbonates, twice washed with $CaCl_2$ solution (approximately 0.2M) and once washed with ethanol. High speed centrifugation was used to collect the samples after each wash. After the ethanol wash the samples were dried in an oven set to 60°C.

Approximately 50mg of the <2μm fractions were dispersed in deionised water and deposited onto 25mm diameter Durapore filter membranes (0.22μm pore size) under suction. The oriented samples were washed three times with 1M $MgCl_2$, then washed three times with deionized water. After the water has completely passed through the clay, 4 drops of liquid glycerol was added and allowed to fully pass through the membrane. The filters were removed from the suction plate and placed onto tissue paper to remove any excess glycerol before being mounted onto 25mm diameter aluminium disks using double sided tape for XRD analysis.

X-ray Diffraction Analysis

XRD patterns were recorded with a PANalytical X'Pert Pro Multi-purpose Diffractometer using Fe filtered Co K radiation, automatic divergence slit, 2° anti-scatter slit and fast X'Celerator Si strip detector. The bulk diffraction patterns were recorded from 4 to 80° (3 to 33° for the oriented samples) in steps of 0.017° 2 theta with a 0.5 second counting time per step for an overall counting time of approximately 35 minutes.

Qualitative analysis was performed on the XRD data using in-house XPLOT and HighScore Plus (from PANalytical) search/match software. Quantitative analysis was performed on the XRD data using the commercial package TOPAS from Bruker. The results are normalised to 100%, and hence do not include estimates of unidentified or amorphous materials.

Cation exchange capacity of <2µm fraction by Ba exchange and XRF analysis

Approximately 10mg of the <2µm fractions and the bulk micronized samples treated with acetic acid (to remove carbonate species) were dispersed in deionized water and deposited onto 25mm diameter Durapore filter membranes (0.22µm pore size) under suction. The oriented samples were washed three times with 1M $BaCl_2$, then washed three times with deionized water and allowed to partly air dry before mounting onto 25mm diameter aluminium disks using double sided tape. To avoid the samples peeling off the filter membranes during drying, a piece of 10µm Mylar film was placed over the samples before placing into a vacuum oven at room temperature overnight. This was to ensure any moisture was removed before placing the sample into the XRF instrument that also runs under vacuum.

XRF analysis was performed on the samples with a PANalytical Axios Advanced wavelength dispersive X ray fluorescence spectrometer operating at 4kW using an in-house developed thin film technique. The calibration was determined from standard clays of known CEC with corrections for sample thickness from the fixed amount of copper present in the aluminium disks, residual chlorine and overlap/interference lines from potassium.

Results

Particle size data is shown in Table 1. Quantitative XRD analysis results are shown in Table 2 for the bulk micronized, calcium saturated samples and for the separated <2µm fractions.

Cation exchange capacity measurements are shown in Table 2.

XRD patterns for the bulk and <2µm fractions are shown in Figures 1 to 6.

Table C.1. Particle size data

CSIRO ID	Client ID	<2µm Wt.%	>2µm Wt.%	Loss Wt.%
43907	**DC17.1**	24.0	74.8	1.2
43908	**DC18.1**	16.6	82.2	1.2

Table C.2. Quantitative XRD analysis of bulk and <2µm fractions

CSIRO ID	Client ID	Quartz Wt.%	Albite Wt.%	Chlorite Wt.%	Muscovite 2M1 Wt.%	Titanite (Sphene) Wt.%
Bulk						
43907	**DC17.1**	23.4	14.7	7.0	54.9	
43908	**DC18.1**	13.1	9.8	71.7		5.4
<2µm fraction						
43907	**DC17.1**	2.8	2.4	11.9	82.8	
43908	**DC18.1**	1.9	0.7	96.2		1.2

Table C.3. Cation exchange capacity of bulk and <2µm fractions

CSIRO ID	Client ID	CEC cmol/kg	Uncertainty cmol/kg
Bulk			
43907	**DC17.1**	0.8	0.1
43908	**DC18.1**	0.8	0.1
<2µm fraction			
43907	**DC17.1**	22	1
43908	**DC18.1**	7.8	0.5

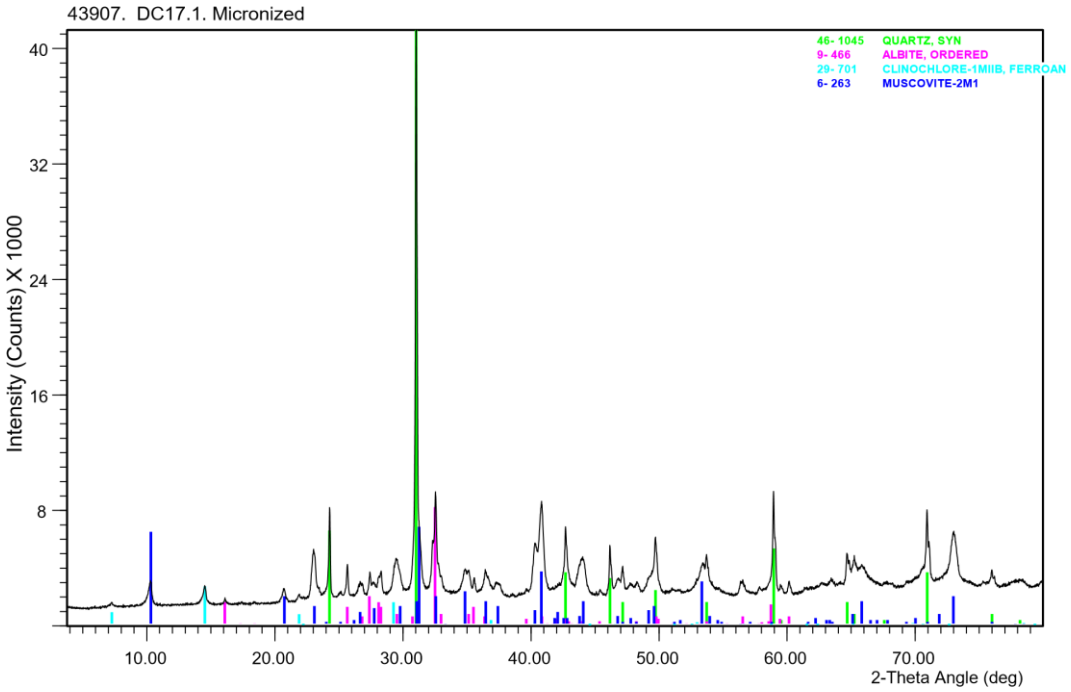

Figure C.1. XRD pattern of micronized bulk sample DC17.1 (Co Kα radiation)

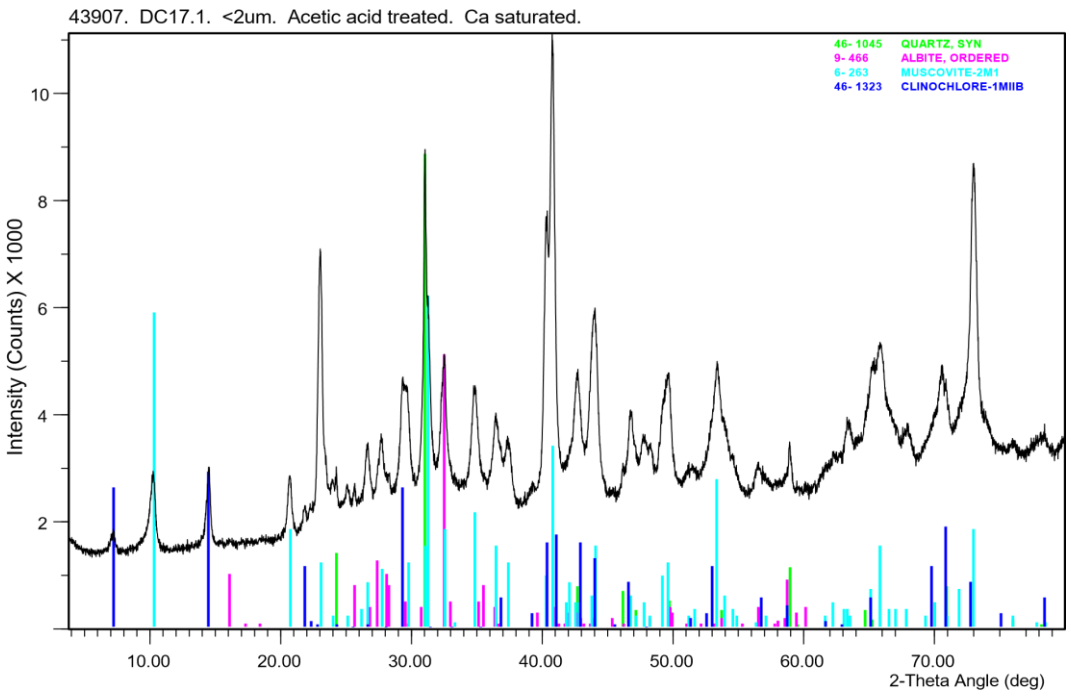

Figure C.2. XRD pattern of Ca saturated <2μm fraction of sample DC17.1 (Co Kα radiation)

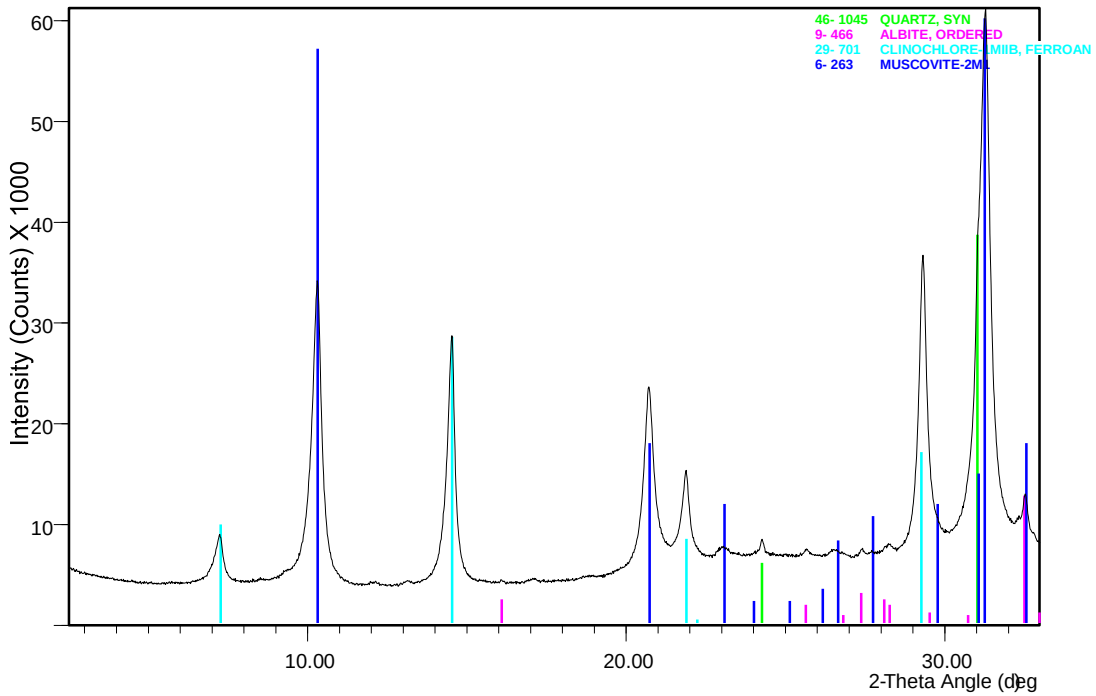

Figure C.3. XRD pattern of oriented Mg saturated and glycerolated <2µm fraction of sample DC17.1 (Co Kα radiation).

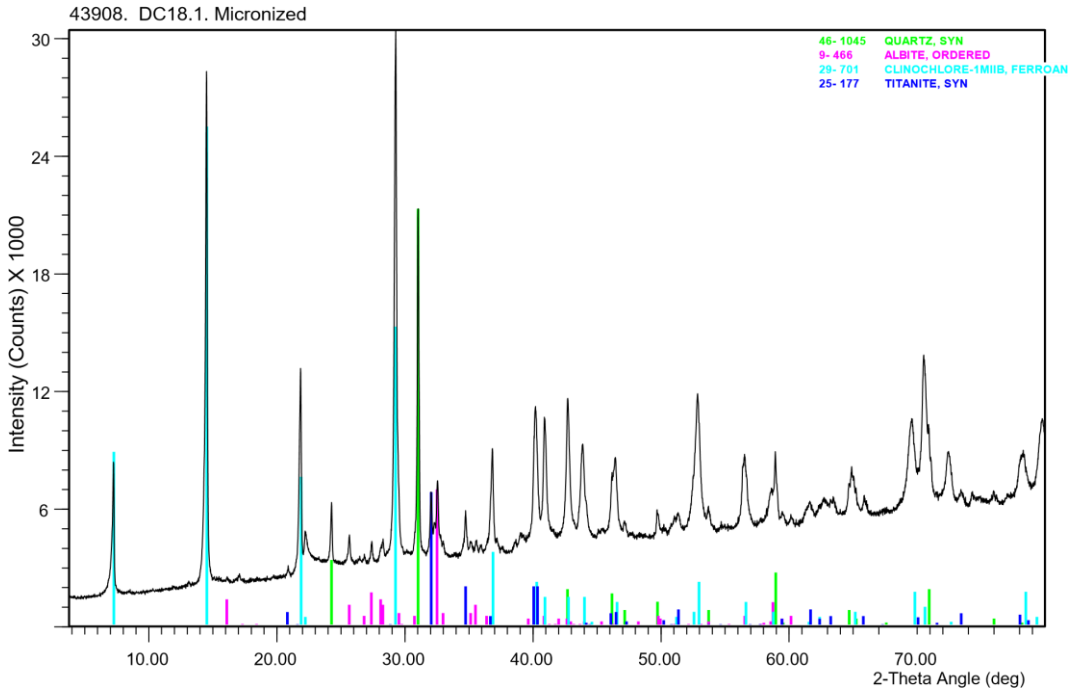

Figure C.4. XRD pattern of micronized bulk sample DC18.1 (Co Kα radiation).

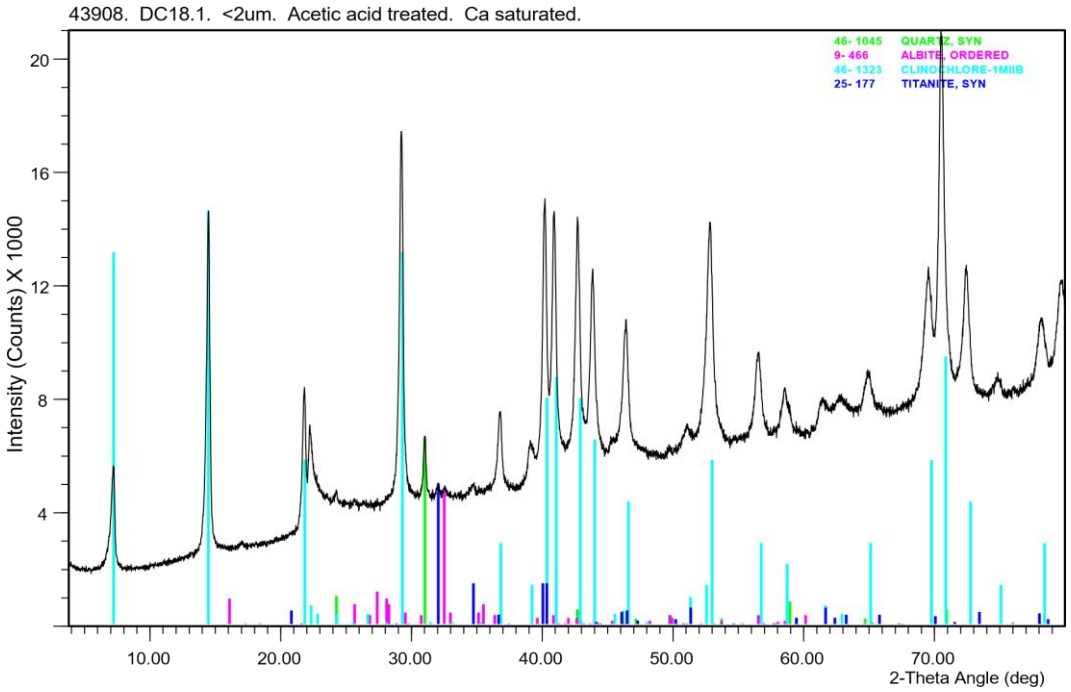

Figure C.5. XRD pattern of Ca saturated <2μm fraction of sample DC18.1 (Co Kα radiation).

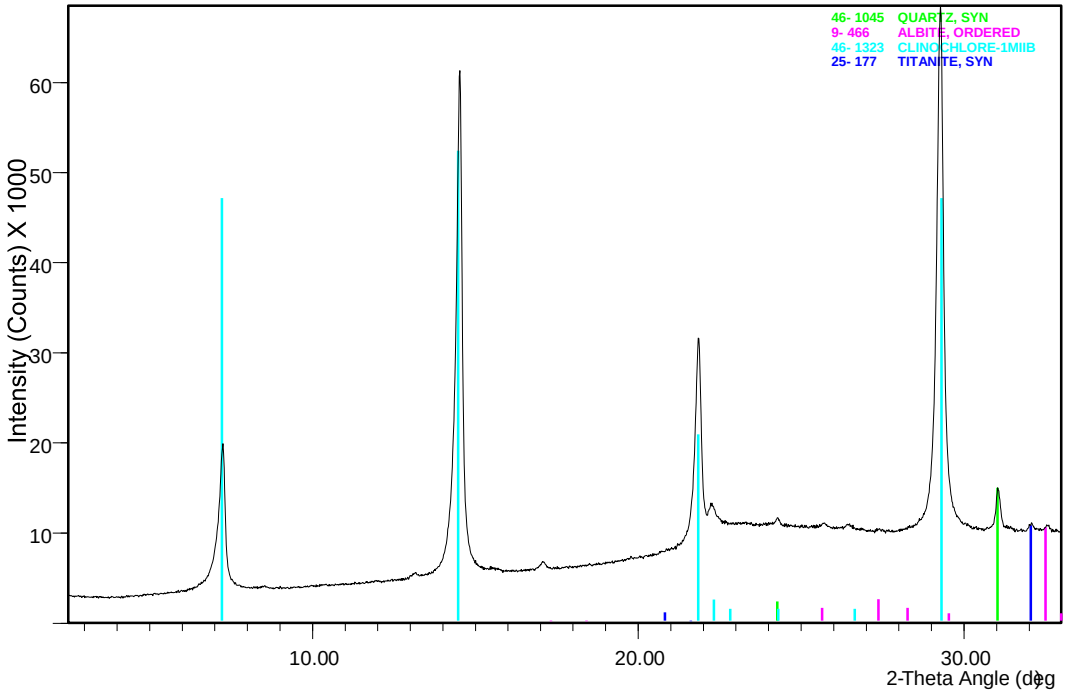

Figure C.6. XRD pattern of oriented Mg saturated and glycerolated <2μm fraction of sample DC18.1 (Co Kα radiation).

CONTACT US

t 1300 363 400
+61 3 9545 2176

e enquiries@csiro.au

w www.csiro.au

FOR FURTHER INFORMATION

CSIRO Land and Water
Mark Raven

t +61 8 8303 8497

e mark.raven@csiro.au

w www.csiro.au

YOUR CSIRO

Australia is founding its future on science and innovation. Its national science agency, CSIRO, is a powerhouse of ideas, technologies and skills for building prosperity, growth, health and sustainability. It serves governments, industries, business and communities across the nation